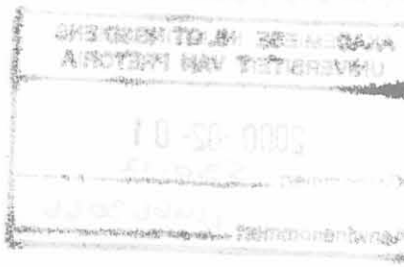

Coupled cluster analysis of model non–adiabatic Hamiltonians

by

David Michael van der Walt

Submitted in partial fulfillment of the requirements for the degree

Philosophiae Doctor (Physics)

in the Faculty of Science

University of Pretoria

Pretoria

April 1999

Abstract

Coupled cluster analysis of model non–adiabatic Hamiltonians

by

David Michael van der Walt

Submitted in partial fulfillment of the requirements for the degree

Philosophiae Doctor (Physics)

in the Faculty of Science

University of Pretoria

Pretoria

April 1999

Supervisor: Prof. R. M. Carter

Co–supervisor: Dr N. J. Davidson

In this thesis, we undertake a theoretical many–body investigation into the ground and first excited states of a class of model non–adiabatic Hamiltonians describing the interaction of a two–level fermionic system with one or more modes of a quantized bosonic field. These models are of topical interest in quantum optics, solid state physics and quantum chemistry, and we focus here in particular on the Rabi Hamiltonian (or Jaynes–Cummings model without the rotating wave approximation) in quantum optics, and the linear $E \otimes e$ Jahn–Teller and pseudo Jahn–Teller systems in quantum chemistry.

Due to their simplicity, these Hamiltonians exhibit interesting symmetries, allowing them to serve as useful testing grounds for quantum many–

body techniques. Here we analyze these models by means of the the coupled cluster method (CCM). The CCM has an impressive record as a powerful and versatile *ab initio* method, having been successfully applied in nuclear physics, quantum chemistry, lattice gauge and continuum field theories, and spin and electron lattice models. For comparison, we also present results for our model Hamiltonians obtained via a variety of other many–body methods. In particular, we present an excellent variational calculation for the Rabi Hamiltonian in which the importance of the incorporation of the correct symmetry in the variational ansatz is highlighted, as well as an elegant operator method useful in the analysis of the linear $E \otimes e$ Jahn–Teller and pseudo Jahn–Teller models.

The CCM analysis of the class of Hamiltonians considered here displays a critical dependence on the choice of the model state and corresponding creation operators which characterize the method. For certain physically reasonable choices, we present a formal demonstration of an essential incompleteness, to any finite order, in the CCM ansatz for the ground–state wave function of the system. As a result, the CCM results for these systems strongly suggest a phase transition which does not in fact exist. We also show that, for certain other choices of the model state and creation operators, the CCM breaks down as a result of the non–Hermiticity of the method.

This breakdown of the CCM is closely related to the marked change in character of the ground state of the systems considered here. Using a model state which mimics this change in character, excellent CCM results for these systems can be obtained; in particular, we present a simple yet extremely accurate CCM calculation for the linear $E \otimes e$ Jahn–Teller and pseudo Jahn–

Teller models. The dependence of the CCM results for the Hamiltonians considered here on the choice of the model state and creation operators is of considerable importance, given that the CCM formalism does not *a priori* specify this choice beyond the overall symmetry requirements of the Hamiltonian. The results demonstrate that the gross physical properties of the exact solution need to be reproduced by the model state if even qualitatively correct behaviour is to be obtained from a CCM calculation.

Samevatting

Gekoppelde–bondel–analise van model nie–adiabatiese Hamilton operatore

deur

David Michael van der Walt

Voorgelê ter gedeeltelike vervulling van die vereistes vir die graad

Philosophiae Doctor (Fisika)

in die Fakulteit Natuurwetenskappe

Universiteit van Pretoria

Pretoria

April 1999

Promotor: Prof. R. M. Carter

Medepromotor: Dr. N. J. Davidson

In hierdie tesis word 'n teoretiese veeldeeltjie–ondersoek geloods na die grondtoestand en die laagste opgewekte toestand van 'n bepaalde klas nie–adiabatiese model–Hamilton operatore wat die interaksie beskryf tussen 'n tweevlak fermionsisteem en een of meer modes van 'n gekwantiseerde bosoniese veld. Hierdie modelle is tans van belang in kwantumoptika, vastetoestandfisika en kwantumchemie, en ons fokus hier spesifiek op die Rabi Hamilton operator (of Jaynes–Cummings model sonder die roterende–golf–benadering) in kwantumoptika, en die lineêre $E \otimes e$ Jahn–Teller en kwasi–Jahn–Teller sisteme in kwantumchemie.

As gevolg van hul eenvoud vertoon hierdie Hamilton operatore interes-

sante simmetrieë, wat hul in staat stel om as 'n toetsterrein te dien vir veeldeeltjietegnieke. Ons analiseer hierdie modelle hier deur middel van die gekoppelde–bondel–tegniek (CCM). Die CCM het 'n indrukwekkende rekord, en is al suksesvol aangewend in kernfisika, kwantumchemie, rooster–yk– en kontinuumveldteorië, en spin– en elektron–matriksmodelle. Ter vergelyking wys ons ook resultate vir ons model–Hamilton operatore wat deur middel van 'n verskeidenheid ander metodes verkry is. In die besonder bied ons 'n akkurate variasie berekening vir die Rabi Hamilton operator aan wat die belang van die insluiting van die korrekte simmetrieë in die variasie aanname beklemtoon, asook 'n elegante operatormetode wat in die analise van die lineêre $E \otimes e$ Jahn–Teller en kwasi–Jahn–Teller sisteme benut kan word.

Die CCM analise van die klas Hamilton operatore wat hier beskou word toon 'n kritiese afhanklikheid van die keuse van modeltoestand en ooreenstemmende skeppingsoperatore wat die metode karakteriseer. Vir bepaalde fisies verantwoordbare keuses, toon ons formeel aan dat daar 'n essentiële ontoereikendheid bestaan, tot enige eindige orde, in die CCM–aanname vir die grondtoestand–golffunksie van die sisteem. As gevolg hiervan bied die CCM resultate sterk getuienis vir 'n fase–oorgang wat in werklikheid nie bestaan nie. Ons toon ook aan dat die CCM, vir sekere ander keuses van die modeltoestand en skeppingsoperatore, faal as gevolg van die nie–Hermitiese aard van die metode.

Hierdie mislukkings van die CCM is nou verwant aan die skerp gedragsverandering in die grondtoestand van die sisteme wat ons hier beskou. Mits 'n modeltoestand gebruik word wat hierdie gedragsverandering naboots, kan uitstekende CCM resultate vir hierdie sisteme verkry word; ons vertoon in

besonder 'n eenvoudige dog uiters akkurate CCM berekening vir die lineêre $E \otimes e$ Jahn–Teller en kwasi–Jahn–Teller sisteme. Die modeltoestand– en skeppingsoperatorafhanklikheid van die CCM resultate vir die Hamilton operatore wat hier beskou word is van groot belang, gegewe dat die CCM nie *a priori* die keuse van of die modeltoestand of skeppingsoperatore voorskryf buiten die oorkoepelende simmetrieë van die Hamilton operator nie. Die resultate demonstreer dat die uitstaande fisieke eienskappe van die eksakte oplossing in die modeltoestand vervat moet word indien selfs kwalitatief korrekte gedrag deur middel van 'n CCM berekening verlang word.

Acknowledgements

I would like to thank the following persons and institutions for their assistance in the preparation and completion of this thesis:

My supervisors, Prof. Rachel Carter and Dr Neil Davidson, for continued guidance, support and encouragement. I could not have asked for two better supervisors.

Prof. Ray Bishop at UMIST, UK, for useful guidance and discussion.

Hermann Uys, at the time an undergraduate student at the University of Pretoria, for his assistance with the numerical work on the strong–coupling perturbative approach to the Rabi Hamiltonian.

The Foundation for Research Development, the University of Pretoria, and Vista University, for financial assistance.

The secretaries of the Physics Department at the University of Pretoria, Mrs. A. Schickerling and Mrs. C. J. Vos, for their friendly assistance on numerous occasions.

Prof. D. J. Brink, University of Pretoria, for proofreading the manuscript.

Dr Glyn Jones, for proofreading the manuscript, and for providing much support and encouragement.

Finally, my wife Lynnette and son Michael, for continued support and encouragement, and for patiently doing without a husband and father, respectively, whenever I was "working on my PhD".

Contents

List of Figures

List of Tables

Chapter 1

Introduction

Non–adiabatic models of a two–level fermionic system interacting with either one or two independent modes of a quantized bosonic field are of topical interest for several reasons. Firstly, these models serve as generic prototypes for a wide variety of physical systems. In quantum optics, models of this form are employed to describe the resonant or near–resonant interaction of a two–level atom with either a single or two perpendicularly polarized modes of a quantized electromagnetic field [Sh93, Mi91]. In the case of a single electromagnetic mode, the model is known as the Rabi Hamiltonian, or equivalently as the Jaynes–Cummings model without the rotating wave approximation (RWA). In quantum chemistry, models of this form describe the vibronic coupling between two electronic levels and two degenerate nuclear vibrational modes in a molecule or crystal. This is known as the linear $E \otimes e$ Jahn–Teller model in the case where the electronic levels are degenerate, and as the linear $E \otimes e$ pseudo Jahn–Teller model in the case where the electronic

levels are non–degenerate [Berb]. The term *non–adiabatic* arises in the context of quantum chemistry, and refers to the intimate coupling between the electronic and nuclear motions which occurs when it is no longer possible for the electrons to adiabatically follow the generally slower displacements of the more massive nuclei. Yet another realization of these models is provided by the two–site polaron in solid state physics, describing the interaction of an electron confined to two sites in a crystal lattice with the quantized phononic field of the lattice [Mah, Hak].

Judd [Ju77, Ju79] and subsequently Reik [Re87], guided by the results of early numerical diagonalizations [Lo58, Th68], proved the existence of analytic solutions for the linear $E \otimes e$ Jahn–Teller and Rabi Hamiltonians at isolated values of the coupling. Complete analytic solutions, valid for all couplings, are however only known for a few special cases of the class of non–adiabatic Hamiltonians considered here. Given their physical relevance, these models have therefore been the subject of much theoretical investigation. Recent many–body analyses of the Rabi Hamiltonian include the use of time–independent perturbation theory (TIPT) [Gr84b, Ph89, Qi98], a variational approach [Qi98], and several methods aimed at finding numerically exact results for the Rabi spectrum [Lo96, Fe96, Qi98]. Several variational calculations have also recently been performed for the linear $E \otimes e$ Jahn–Teller system [Lo91, Hu98].

The theoretical models considered here always represent, to a greater or lesser degree, an idealized simplification of the real physical system under consideration. It is in the very simplicity of these models, however, that

their further utility lies. Besides the isolated analytic solutions, quasi–exact numerical results for these models are also available, or relatively easy to obtain. Furthermore, simple Hamiltonians such as these often contain interesting symmetries, and as such are ideal testing grounds for approximate many–body methods.

Finally, apart from their practical value, these models represent some of the simplest non–trivial examples of quantum many–body physics. The straightforward appearance of these models hides a wealth of interesting quantum behaviour, which is readily contrasted with that of their classical or semi–classical counterparts [Bl96]. It is instructive to note that, despite intensive investigation, a complete analytic description of even the ground state of the Rabi Hamiltonian has not yet been found.

In this thesis, we therefore analyze several of these Hamiltonians from the perspective of quantum many–body theory. As a starting point, it is worth summarizing the characteristics which a good many–body method should embody:

1. It should be a microscopic or *ab initio* method, *i.e.* it should be a first–principles approach which readily reveals the physical significance of both its approximation scheme and its results. This requirement is generally not met by, *e.g.*, a large scale numerical diagonalization, or a quantum Monte Carlo calculation.
2. A related but different requirement is that the method should always be exact in principle, *i.e.*, it should reproduce the exact result in the limit

where the method is applied to infinite order, or equivalently, is applied without any form of approximation. This excludes perturbation theory, which fails in this respect when applied to non–perturbative systems.

3. It should be universal, *i.e.* the method should be applicable, with very little or ideally no modification of its standard form, to any given many–body system. This requirement excludes, *e.g.*, the method of canonical transformation, which generally requires either a lucky guess, a trial–and–error approach, or an inordinate amount of physical insight.

4. The method should be capable of systematic improvement, and should yield results that converge uniformly as the order to which the method is applied is increased. In general, this excludes the variational method.

5. Finally, the application of the method should be computationally simple or, at the very least, tractable.

The coupled cluster method (CCM) is one of the few quantum many–body techniques which can lay claim to satisfying almost all the criteria listed above. This non–perturbative method, originally developed in nuclear physics by Coester and Kümmel [Co58, Co60], has since been successfully applied in the analysis of the many–body ground–state in quantum chemistry [Ci66, Bar78, Pu82, Mo87, No87, No88, Bar89, Wo94, Wo96a], the electron gas [Bi78, Em84], quantum tunneling in the presence of a phonon bath [Wo96b], lattice gauge [Bi93, Le93, Ba96, Le98] and continuum field [Fu87, Ar90] theories, and spin and electron lattice models [Ro90, Bi91b]. An alternative formulation of the CCM, the so–called extended coupled cluster method (ECCM) introduced by Arponen [Ar83a], has also been successfully

applied [Ar83a, Ar83b, Ro89] to the Lipkin–Meshkov–Glick (LMG) model [Li65] in nuclear physics. This is a particularly important application of the method, given that the nucleus in the LMG model is known to exhibit a phase transition from a spherically symmetric to a deformed shape. Both the normal and extended CCM have also been reformulated in order to study excited states [Em81, Ar83a, Ar87].

In addition to its power and scope, the CCM also yields size–extensive results for all ground–state observables, including the ground–state energy, at every level of approximation (the cluster property). This is due to the CCM prescription for calculating the expectation value of an arbitrary ground–state observable, which implies that such expectation values are calculated as a sum over linked diagrams only.

No many–body method is perfect, and the CCM does display some less desirable features. There is no guarantee of uniform convergence in the CCM, although this is often the case in practice. Also, the method can sometimes be computationally expensive, although this is often the result of an injudicious choice for the model state and cluster correlation operator which characterize the CCM.

Perhaps the most serious known criticism of the method is that the CCM, to any finite order, is manifestly non–Hermitian, relying on an independent parameterization of the ground–state bra and ket. Although the CCM is a genuine variational method, this non–Hermiticity implies that an approximate CCM result for the ground–state energy no longer provides an upper

bound to the true ground–state energy [1]. This loss of the upper–bound property is offset by the following factors: firstly, the similarity transformed Hamiltonian which occurs in the CCM formalism is amenable to the Hausdorff expansion, which in most cases either terminates naturally or is resummable to closed form without approximation; secondly, at every level of approximation, the CCM in its purest form is compatible with the Hellman–Feynman theorem.

The primary aim of this thesis is to investigate the applicability of the CCM to the class of non–adiabatic Hamiltonians introduced above. In particular, we apply the CCM to the ground and first excited states of the Rabi Hamiltonian and the linear $E \otimes e$ Jahn–Teller and pseudo Jahn–Teller systems.

For comparison, we also consider the application of other many–body techniques to the Rabi and linear $E \otimes e$ Jahn–Teller systems. We present an operator–based method which simplifies the analysis of the isolated analytic (Juddian) solutions for the linear $E \otimes e$ Jahn–Teller models, and yields explicit closed–form expressions for the wave functions at the Juddian points. We also perform a weak–coupling TIPT calculation, analytic to any finite order, for the Rabi Hamiltonian, as well as a simple variational calculation which yields results, for both the ground and first excited states of the Rabi Hamiltonian, far superior to those obtained by previous methods.

The CCM has previously been applied to the Rabi and linear $E \otimes e$ Jahn–

[1] See also [Sc92] for a discussion of the implementation of a variational principle in certain non–Hermitian systems.

Teller systems. Wong and Lo have used the CCM to calculate the ground–state energy of both the multimode Rabi [Wo96b] and the linear $E \otimes e$ pure (as opposed to pseudo) Jahn–Teller Hamiltonians [Wo94, Wo96a]. In both cases, these authors perform a unitary transformation which destroys at least two of the symmetries of the Hamiltonian, and then apply the CCM to the transformed Hamiltonian. For the linear $E \otimes e$ Jahn–Teller system, where the fermionic levels are degenerate, they obtain very accurate results over the full coupling spectrum. For the Rabi and pseudo Jahn–Teller Hamiltonians, however, the fermionic level splitting is nonzero, and as a result the eigenstates of these systems are of definite symmetry. Thus the approach of Wong and Lo yields quantitatively inaccurate CCM results for the Rabi Hamiltonian in the intermediate coupling regime, does not readily generalize to the pseudo Jahn–Teller system, and also does not allow for a CCM calculation of the first excited state energy.

Our main purpose is to show that it is possible to obtain quantitatively accurate results for the ground and first excited state energies of the Rabi, linear $E \otimes e$ Jahn–Teller, and linear $E \otimes e$ pseudo Jahn–Teller systems within the CCM by maintaining the correct symmetries throughout the analysis. We show that this is in fact possible, provided that a CCM model state is chosen which is also capable of following the change in character which occurs in the ground state of these systems.

We also demonstrate that, for a naive choice of model state and correlation operator, the CCM fails when applied to the Rabi and linear $E \otimes e$ Jahn–Teller Hamiltonians. We show not only that the non–Hermiticity of the

CCM can lead to a breakdown in the method, but also that the method may fail as a result of an essential incompleteness due to the exponential form of the CCM ansatz for the ground–state wave function. Given the broad freedom of choice for the model state and correlation operator implicit in the method, these defects have severe implications not only for the CCM, but also for other methods which employ the exponential form.

To conclude this introduction, we present here an outline of the remainder of this thesis. In Chapter 2 we introduce the general class of model Hamiltonians under consideration. Chapter 3 gives an overview of the coupled cluster method. Chapters 4-6 are devoted to the Rabi Hamiltonian, and Chapters 7-8 to the Jahn–Teller systems. In Chapter 9 we summarize the main results of the thesis, and present conclusions.

Chapter 2

The Model Hamiltonians

In this chapter we introduce the general Hamiltonian which spans the entire class of non–adiabatic systems considered here. We discuss the two special cases of the general model whose analysis forms the remainder of the thesis. The symmetries associated with these systems are of particular interest, and these are discussed in detail.

2.1 The general model Hamiltonian

The most general form for the fully quantized Hamiltonian describing a two–level fermion interacting with two independent bosonic field modes in the dipole approximation is given by

$$\begin{aligned} H &= \frac{1}{2}\omega_0\,\sigma^z + \omega_1\, b_1^\dagger b_1 + \omega_2\, b_2^\dagger b_2 \\ &\quad + \eta_1\,\left(b_1^\dagger + b_1\right)\sigma^x - \eta_2\,\left(b_2^\dagger + b_2\right)\sigma^y\,, \end{aligned} \tag{2.1}$$

where ω_0 is the fermionic level splitting, ω_1 and ω_2 are the frequencies of the two modes and η_1 and η_2 the corresponding dipole coupling constants linking the bosonic modes to the fermion and thus indirectly to each other. The operators b_1, b_2 and $b_1^\dagger, b_2^\dagger$ are boson annihilation and creation operators, respectively, satisfying the standard commutation relations

$$\begin{aligned} \left[b_1, b_1^\dagger\right] &= \left[b_2, b_2^\dagger\right] = 1 \\ [b_1, b_2] &= \left[b_1^\dagger, b_2^\dagger\right] = \left[b_1, b_2^\dagger\right] = \left[b_2, b_1^\dagger\right] = 0\,, \end{aligned} \tag{2.2}$$

and $\sigma^x, \sigma^y, \sigma^z$ are Pauli matrices which form a convenient basis for the two–dimensional fermionic subspace of the full Hilbert space relevant to the Hamiltonian (2.1). The origin of the fermionic energy scale has been chosen such that the lower (upper) fermionic state corresponds to energy $-\frac{1}{2}\omega_0$ ($\frac{1}{2}\omega_0$), and the constant zero point energy $\frac{1}{2}\omega_1 + \frac{1}{2}\omega_2$ of the field modes has been neglected. For convenience, we employ units such that $\hbar = 1$. A derivation of the general model Hamiltonian (2.1) in the context of quantum optics is given in Appendix A.

There is a parity symmetry associated with the Hamiltonian (2.1). We define an operator

$$N \equiv b_1^\dagger b_1 + b_2^\dagger b_2 + \frac{1}{2}\,(\sigma^z + 1) \tag{2.3}$$

which counts the number of bosonic and fermionic quanta (excitations) and

introduce the parity operators (with eigenvalues ± 1)

$$\begin{aligned}
\Pi_1 &\equiv \exp\left\{i\pi\left[b_1^\dagger b_1 + \frac{1}{2}(\sigma_y + 1)\right]\right\} = -\exp\left\{i\pi b_1^\dagger b_1\right\}\sigma_y \\
\Pi_2 &= \exp\left\{i\pi\left[b_2^\dagger b_2 + \frac{1}{2}(\sigma_x + 1)\right]\right\} = -\exp\left\{i\pi b_2^\dagger b_2\right\}\sigma_x \\
\Pi &= -i\Pi_1\Pi_2 \\
&= \exp\left\{i\pi\left[b_1^\dagger b_1 + b_2^\dagger b_2 + \frac{1}{2}(\sigma_z + 1)\right]\right\} \\
&= -\exp\left\{i\pi b_1^\dagger b_1\right\}\exp\left\{i\pi b_2^\dagger b_2\right\}\sigma_z\,. \qquad (2.4)
\end{aligned}$$

Then

$$\begin{aligned}
[H, \Pi_1] &= i\hbar\omega_0 \exp\left\{i\pi b_1^\dagger b_1\right\}\sigma_x \\
[H, \Pi_2] &= -i\hbar\omega_0 \exp\left\{i\pi b_2^\dagger b_2\right\}\sigma_y \\
[H, \Pi] &= 0\,, \qquad (2.5)
\end{aligned}$$

where we have used the relevant identities from Appendix B. The eigenstates of the Hamiltonian (2.1) may thus be chosen to be states of definite Π parity.

2.2 Special cases of the general Hamiltonian

2.2.1 The Rabi Hamiltonian

The dipole interaction between a two–level atom with level–splitting ω_0 and a single electromagnetic field mode of frequency ω may be modelled by the Rabi Hamiltonian

$$\begin{aligned}
H_{\text{Rabi}} &= \frac{1}{2}\omega_0\,\sigma^z + \omega\, b^\dagger b + \eta\,\left(b^\dagger + b\right)\sigma^x \\
&= \frac{1}{2}\omega_0\,\sigma^z + \omega\, b^\dagger b + 2\,g\,\left(b^\dagger + b\right)\sigma^x\,, \qquad (2.6)
\end{aligned}$$

which is the simplest non–trivial realization of the general model Hamiltonian (2.1), obtained by setting $\omega_1 = \omega, \omega_2 = 0$, and with the coupling conventionally relabelled via $\eta_1 = \eta = 2g, \eta_2 = 0$. This model was originally employed in the context of nuclear magnetic resonance [Ra37, Ra54], and is of topical interest in quantum optics [Sh93, Mi91]. The Hamiltonian (2.6) conserves the parity

$$\Pi_{\text{Rabi}} = \exp\left\{i\pi\left[b^\dagger b + \frac{1}{2}(\sigma_z + 1)\right]\right\}. \tag{2.7}$$

It is important to note that the Rabi Hamiltonian is not a continuous limit of the general model Hamiltonian (2.1), since it operates in a fundamentally different Hilbert space where the additional degrees of freedom corresponding to the second bosonic mode are absent.

2.2.2 The linear $E \otimes e$ Jahn–Teller and pseudo Jahn–Teller Hamiltonians

In the case of degenerate bosonic modes ($\omega_1 = \omega_2 = \omega$) equally coupled ($\eta_1 = \eta_2 = \eta$) to a fermionic system, the general Hamiltonian (2.1) reduces to the linear $E \otimes e$ pseudo Jahn–Teller (PJT) model

$$\begin{aligned} H_{\text{PJT}} &= \frac{1}{2}\omega_0\,\sigma^z + \omega\, b_1^\dagger b_1 + \omega\, b_2^\dagger b_2 \\ &\quad + \eta\,\left(b_1^\dagger + b_1\right)\sigma^x - \eta\,\left(b_2^\dagger + b_2\right)\sigma^y . \end{aligned} \tag{2.8}$$

If, in addition, the fermionic levels are degenerate ($\omega_0 = 0$), then we obtain the (pure) linear $E \otimes e$ Jahn–Teller (JT) Hamiltonian H_{JT}. These models are of relevance not only in quantum optics, but also in quantum chemistry [Berb], where they describe the non–adiabatic vibronic interaction between a

two–fold degenerate or quasi–degenerate electronic level (E) and a doubly–degenerate nuclear vibrational mode (e). The designation "linear" indicates that the vibronic interaction terms, expanded in powers of the nuclear configurational coordinates, have been truncated at first order.

There is another symmetry, besides the parity symmetry (2.4), associated with the PJT Hamiltonian (and therefore also with the JT Hamiltonian) which is not obvious from the form (2.8). If we perform the canonical transformation

$$\begin{aligned} a_1 &\equiv \frac{1}{\sqrt{2}}(b_1 + ib_2) \qquad & a_1^\dagger &\equiv \frac{1}{\sqrt{2}}\left(b_1^\dagger - ib_2^\dagger\right) \\ a_2 &\equiv \frac{1}{\sqrt{2}}(b_1 - ib_2) \qquad & a_2^\dagger &\equiv \frac{1}{\sqrt{2}}\left(b_1^\dagger + ib_2^\dagger\right) , \end{aligned} \tag{2.9}$$

which preserves the commutation relations (2.2), then the Hamiltonian (2.8) and parity operator (2.4) become

$$\begin{aligned} H_{\mathrm{PJT}} &= \frac{1}{2}\omega_0\,\sigma^z \;+\; \omega\, a_1^\dagger a_1 \;+\; \omega\, a_2^\dagger a_2 \\ &\quad + \gamma\,\left(a_1 + a_2^\dagger\right)\sigma^+ \;+\; \gamma\,\left(a_1^\dagger + a_2\right)\sigma^- \qquad (2.10) \\ \Pi_{\mathrm{PJT}} &= \exp\left\{i\pi\left[a_1^\dagger a_1 + a_2^\dagger a_2 + \frac{1}{2}(\sigma_z + 1)\right]\right\} . \qquad (2.11) \end{aligned}$$

where $\gamma \equiv \eta/\sqrt{2}$. In the form (2.10), it is readily seen that, for arbitrary ω_0, H_{PJT} commutes with the operator

$$J \;=\; a_1^\dagger a_1 - a_2^\dagger a_2 + \frac{1}{2}\sigma^z \; . \tag{2.12}$$

The transformation (2.9) and the symmetry $[H_{\mathrm{PJT}}, J] = 0$ have a simple physical meaning. In the quantum optics context, Equations (2.9) correspond to a transformation to field modes of circular rather than linear polarization, with $a_1^\dagger$ ($a_2^\dagger$) denoting an operator which creates a photon of positive

(negative) helicity. The operator J then represents a conserved angular momentum component. Since J also commutes with the parity operator (2.11), the eigenstates of H_{PJT} (and H_{JT}) need thus only be sought amongst those states with definite Π_{PJT} and J.

Chapter 3

The Coupled Cluster Method

We present here an overview of the CCM. For a more detailed exposition of the CCM, including a comprehensive list of references and a discussion of the treatment of excited states and dynamics in the CCM, see, *e.g.* [Bi91a], [Ar83a], or [Ar87]. A simple introduction to the CCM is also given in [Bi87].

The basic ingredients of the CCM are the so–called model state $|\Phi\rangle$, together with a set of mutually commuting (independent) multiconfigurational creation operators $\left\{C_I^\dagger\right\}$ defined with respect to the state $|\Phi\rangle$. The model state plays the role of a reference state or "vacuum", so that the state $C_I^\dagger|\Phi\rangle$ may be thought of as a multiparticle cluster configuration obtained by introducing I "elementary excitations" on $|\Phi\rangle$.

The CCM model state and corresponding creation operators must satisfy two essential requirements. Firstly, the state $|\Phi\rangle$ should not be orthogonal to the exact ground state. Thus one must ensure that the model state in-

corporates the underlying statistics and other symmetries of the many–body Hamiltonian. Furthermore, the creation operators $\left\{C_I^\dagger\right\}$ must be chosen such that the set $\left\{C_I^\dagger|\Phi\rangle\right\}$ spans the relevant many–body Hilbert space, *i.e.* such that $\left\{C_I^\dagger|\Phi\rangle\right\}$ is complete.

Besides these formal requirements, the choice of $|\Phi\rangle$ and $\left\{C_I^\dagger\right\}$ is in principle arbitrary [Bi91a]. It is clear that a judicious choice should lead to more rapid convergence of the CCM results, and this consideration should govern the choice of S and $|\Phi\rangle$. In practice, due to the complexity of the CCM calculations, the choice of the model state and cluster operator is often the simplest possible one satisfying the essential requirements listed above. There is no evidence in the literature that this choice has ever led to physically spurious predictions.

Although not essential, it is furthermore convenient for computational purposes if the creation operators are chosen such that

$$C_I|\Phi\rangle = 0 = \langle\Phi|C_I^\dagger \quad \forall \quad I \neq 0 \tag{3.1}$$

and

$$\langle\Phi|C_J C_I^\dagger|\Phi\rangle = 0 \quad \forall \quad J \neq I\,. \tag{3.2}$$

The first condition ensures that the Hermitian adjoint operators $\{C_I\}$ annihilate the model state, and the second that the states $\left\{C_I^\dagger|\Phi\rangle\right\}$ form a mutually orthogonal set. Unless stated otherwise, we will assume in what follows that this is the case.

To obtain a size–extensive result for the ground–state energy of a many–body system, the effective many–body Hamiltonian must be separable when

the system is separated into subsystems which are then removed sufficiently far from each other in configuration space (the so–called cluster property). In diagrammatic perturbation theory, Hugenholtz [Hu57, Tho] showed that linked (connected) diagrams always give contributions to the ground–state energy with the correct dependence on the extent of the system. Thus, in order to obtain results for the ground–state energy which obey the cluster property at any level of approximation, the energy must always be calculated as a sum over linked diagrams only. In the CCM, this is achieved by making the following ansatz for the ground–state wave function $|\Psi\rangle$:

$$|\Psi\rangle = e^S|\Phi\rangle \ , \qquad S = \sum_{I\neq 0} s_I C_I^\dagger \ . \tag{3.3}$$

The exclusion of the identity operator $C_0^\dagger \equiv 1$ from the cluster correlation operator S leads to the intermediate normalization condition

$$\langle\Phi|\Psi\rangle = \langle\Phi|\Phi\rangle = 1 \ , \tag{3.4}$$

provided that (3.1) is satisfied. The operator S, being additively separable, corresponds to a sum over linked diagrams, and therefore ensures the size–extensivity of the CCM ground–state energy at any level of approximation. The exponential form (3.3) also ensures the correct counting of all possible correlated I–body excitations from the model state.

In the CCM, the ground–state energy is now determined by rewriting the ground–state Schrödinger equation $H|\Psi\rangle = E_0|\Psi\rangle$ in the form

$$e^{-S}He^S|\Phi\rangle = E_0|\Phi\rangle \ . \tag{3.5}$$

The inner product of (3.5) with the model state $|\Phi\rangle$ yields

$$E_0 = \langle\Phi|e^{-S}He^S|\Phi\rangle \ , \tag{3.6}$$

which determines the ground–state energy E_0 as a function of the cluster correlation coefficients $\{s_I\}$. In turn, these coefficients are determined via the coupled equations

$$\langle\Phi|C_I e^{-S} H e^{S}|\Phi\rangle = 0\ , \tag{3.7}$$

obtained by taking the inner product of (3.5) with the set $\left\{C_I^{\dagger}|\Phi\rangle\right\}, I \neq 0$. The similarity transformed Hamiltonian $e^{-S}He^{S}$ can be expanded via the Hausdorff (nested commutator) expansion

$$e^{-S}He^{S} = H + [H,S] + \frac{1}{2!}[[H,S],S] + \ldots\ . \tag{3.8}$$

Provided that, as is the case for the model systems considered here, the many–body Hamiltonian contains a finite number of destruction operators defined with respect to the model state $|\Phi\rangle$, the nested commutator expansion (3.8) either terminates naturally at finite order or is resummable to closed form without approximation.

The CCM formalism as presented above, and in particular the ansatz (3.3) for the ground–state wave function, is in principle exact. However, in general the cluster correlation operator S must be summed to infinite order to obtain the exact solution. Therefore, in the application of the method, approximations are introduced since the operator S must be truncated in order to render the CCM equations (3.14) tractable. The truncation of S at finite order, say N, is referred to as the SUB-N approximation scheme, and has a physically intuitive and appealing meaning, namely that all I–body correlations on the model state $|\Phi\rangle$ up to $I = N$ have been included in the CCM approximation to the exact ground–state wave function. Although it is thus possible to systematically increase the order N of the SUB-N approxi-

mation scheme, there is however no guarantee that the corresponding results converge uniformly towards the exact results.

The determination of the ground–state expectation value $\overline{A}$ of an arbitrary operator A via the CCM requires, in addition to the CCM ground–state ket introduced above, also the ground–state bra. If the bra is simply taken as the Hermitian adjoint of the ket, then

$$\overline{A}_{\text{Hermitian}} = \frac{\langle\Phi|e^{S^\dagger}Ae^{S}|\Phi\rangle}{\langle\Phi|e^{S^\dagger}e^{S}|\Phi\rangle} = \langle\Phi|\left(e^{S^\dagger}Ae^{S}\right)_{\mathcal{L}}|\Phi\rangle \tag{3.9}$$

where the suffix $\mathcal{L}$ denotes a sum over linked diagrams. However, when expanded in powers of S and $S^\dagger$, the unitary (rather than similarity) transformed operator $e^{S^\dagger}Ae^{S}$ does not in general terminate after a finite number of terms, and it is not possible to write down an explicit expression for $\overline{A}_{\text{Hermitian}}$. Also, if the operators S and $S^\dagger$ are approximated by truncation at finite order, then $\overline{A}_{\text{Hermitian}}$ is no longer calculated from the same set of diagrams as for the energy [Tho], and therefore does not satisfy the requirements of the Hellmann–Feynman theorem [He35, Fe39].

For a system whose observables are represented by a set of Hermitian operators, the operators obtained via a similarity transform of the members of this set are in general non–Hermitian. It is always possible to regain a Hermitian description of the system, i.e. one where the observables have real eigenvalues and expectation values, via a redefinition of the scalar product (see also [Sc92]). For the reasons mentioned above, this is not done in the CCM. Rather, the ground–state bra $\langle\tilde{\Psi}|$ in the CCM is parameterized independently from the ket state $|\Psi\rangle$, and is thus not (to any finite order) the

manifest Hermitian conjugate of $|\Psi\rangle$ [1]. This non–Hermiticity can lead to imaginary values for the CCM energy, but, in earlier work, the appearance of an imaginary part in the energy has always correctly indicated a phase transition in the system (see e.g. [Ro90, Bi91b]). Also, as a result of the non–Hermiticity of the method, an approximate CCM result for the ground–state energy does not necessarily provide an upper bound for the true ground–state energy, despite the fact that, as will be shown shortly, the method may be formulated variationally. This loss of the upper–bound property is offset by the fact that the parameterization of the bra can be done in a manner which leads to explicit expressions for arbitrary expectation values, and which is compatible with the Hellmann–Feynman theorem at any level of approximation. Here we present two such formulations of the method [Ar83a]: In the so–called normal CCM (NCCM),

$$\langle\tilde{\Psi}|_{\rm NCCM} = \langle\Phi|\tilde{S}e^{-S}\ , \qquad \tilde{S} = 1 + \sum_{I\neq 0}\tilde{s}_I C_I\ , \tag{3.10}$$

whilst in the extended CCM (ECCM),

$$\langle\tilde{\Psi}|_{\rm ECCM} = \langle\Phi|e^{\Sigma}e^{-S}\ , \qquad \Sigma = \sum_{I\neq 0}\sigma_I C_I\ . \tag{3.11}$$

Here the bra–state coefficients $\{\tilde{s}_I\}$ ($\{\sigma_I\}$) are regarded as independent parameters; the Hermitian adjoint relation which formally specifies these parameters in terms of the ket–state coefficients $\{s_I\}$ is ignored. In both the NCCM and ECCM, condition (3.1) leads to the normalization

$$\langle\tilde{\Psi}|\Psi\rangle = \langle\Phi|\Phi\rangle = 1\ , \tag{3.12}$$

[1] To infinite order, the CCM prescription for the ground–state bra is formally identical to the Hermitian adjoint of the ground–state ket, and this non–Hermiticity disappears. In the application of the method, however, the cluster operator must in general be truncated for computational purposes, and this observation is thus mostly of academic interest.

and the expectation value of an arbitrary observable A is given by $\overline{A} \equiv \langle\tilde{\Psi}|A|\Psi\rangle$. In particular, the expectation value

$$\overline{H} \equiv \langle\tilde{\Psi}|H|\Psi\rangle \tag{3.13}$$

of the Hamiltonian becomes a functional of the NCCM (ECCM) coefficients $\{s_I, \tilde{s}_I\}$ ($\{s_I, \sigma_I\}$), which are then determined by the variational conditions

$$\frac{\partial\overline{H}}{\partial s_I} = 0 = \frac{\partial\overline{H}}{\partial\tilde{s}_I} \quad \left(\frac{\partial\overline{H}}{\partial s_I} = 0 = \frac{\partial\overline{H}}{\partial\sigma_I}\right) . \tag{3.14}$$

In both the NCCM and ECCM, the CCM ground–state energy is obtained by evaluating the energy functional $\overline{H}$ at the stationary point where the variational conditions (3.14) are satisfied. In the NCCM, the coefficients $\{\tilde{s}_I\}$ appear only linearly in the functional

$$\overline{H}_{\rm NCCM} = \langle\Phi|\tilde{S}e^{-S}He^{S}|\Phi\rangle , \tag{3.15}$$

so that the conditions

$$\frac{\partial\overline{H}}{\partial\tilde{s}_I} = \langle\Phi|C_I e^{-S}He^{S}|\Phi\rangle = 0 \tag{3.16}$$

identically reduce to the previous equations (3.7), and it is clear that the expression (3.6) for the CCM ground–state energy again obtains. Thus in the NCCM the coefficients $\{s_I\}$, and therefore also the CCM ground–state energy, are determined independently of $\{\tilde{s}_I\}$, and the bra–state coefficients are only required if other ground–state properties of the system are to be calculated. In the ECCM, however,

$$\overline{H}_{\rm ECCM} = \langle\Phi|e^{\Sigma}e^{-S}He^{S}|\Phi\rangle \tag{3.17}$$

and the CCM equations (3.14) for $\{s_I\}$ and $\{\sigma_I\}$ are coupled. Thus both sets of coefficients have to be solved for simultaneously in order to determine

the ground–state energy. As before, in the SUB-N approximation scheme, the operators $S, \tilde{S}$ (S, Σ) in the NCCM (ECCM) truncate at order N.

To any finite order in both the NCCM and ECCM, an arbitrary ground–state observable is calculated as a sum over linked diagrams only, and therefore exhibits the cluster property. In the NCCM, however, the ground–state bra amplitude $\tilde{S}$ itself contains unlinked terms. Due to its double exponential structure, the ECCM has the added advantage that both the ground–state ket and bra amplitudes are fully linked. As such, the ECCM, although computationally more involved than the NCCM, is capable of describing global phenomena such as phase transitions [Bi91a, Ar83a]. In the LMG model, for example, a spherical nucleus consisting of N nucleons undergoes a transition to a deformed shape above a region of critical coupling. The transition is only a true (sharp) phase transition in the thermodynamic limit $N \rightarrow \infty$ with the density of nucleons held fixed. Arponen [Ar82] has shown that, at least in low order (SUB-2), the NCCM based on a model state of spherical symmetry cannot accurately approximate the exact LMG ground–state energy in the deformed phase. Although no formal proof exists, it has been conjectured [Ar82] that the NCCM SUB-n results, for a model state of spherical symmetry, would not be accurate in the deformed phase for any finite n, and that a deformed model state is thus necessarily required for a successful NCCM calculation above the critical coupling regime. Subsequently, it was shown [Ar83a, Ar83b, Ro89] that it is possible, within the ECCM formulation of the method, to obtain accurate CCM results for the LMG ground–state energy over the full coupling spectrum, encompassing both the symmetric and deformed phases, using a single model state.

Chapter 4

The Rabi Hamiltonian

In this chapter, we discuss the analytic limits of the Rabi Hamiltonian, and benchmark the numerical diagonalization results for the Rabi spectrum against known analytic results. We investigate the physical nature of the Rabi ground state, and present a review of some existing results for the ground and first excited states obtained via many–body methods other than the CCM.

4.1 Discussion of the Rabi Hamiltonian

The Rabi Hamiltonian

$$\begin{aligned} H_{\text{Rabi}} &= \frac{1}{2}\omega_0\,\sigma^z + \omega\, b^\dagger b + \eta\,\left(b^\dagger + b\right)\sigma^x \\ &= \frac{1}{2}\omega_0\,\sigma^z + \omega\, b^\dagger b + g\,\left(b^\dagger + b\right)\left(\sigma^+ + \sigma^-\right)\,, \end{aligned} \tag{4.1}$$

where $\eta = 2g$, and its conserved parity

$$\Pi_{\text{Rabi}} \;=\; \exp\{i\pi N\}\,, \qquad N \;=\; b^\dagger b + \frac{1}{2}\,(\sigma^z + 1)\;, \tag{4.2}$$

were introduced in Chapter 2. Given that most recent interest in the Rabi Hamiltonian is in the field of quantum optics, we present our analysis of the Hamiltonian in this context. In typical optical applications, the coupling g is small, and the so–called counter–rotating terms $g\left(b^\dagger\sigma^+ + b\sigma^-\right)$ in the Hamiltonian (4.1), corresponding respectively to the processes where a photon is created as the atom makes an upward transition and where a photon is annihilated as the atom makes a downward transition, may to good approximation be neglected. This rotating wave approximation (RWA) results in the well–known Jaynes–Cummings Hamiltonian [Ja63]

$$H_{\text{JC}} \;=\; \frac{1}{2}\omega_0\,\sigma^z \;+\; \omega\, b^\dagger b \;+\; g\, b^\dagger\sigma^- \;+\; g\, b\sigma^+\,. \tag{4.3}$$

In the Jaynes–Cummings model $[H_{\text{JC}}, N] = 0$ and the model is exactly soluble, since we may diagonalize H_{JC} in each subspace labelled by a fixed number, say n, of quanta. For $n = 0$, there is only one state, namely the product state $|0\rangle|\downarrow\rangle$, where the first ket refers to the field mode in the occupation number (Fock) representation and the second denotes the atomic state with the atom in its lower level, corresponding to energy $E^{\text{JC}}_{0,-} = -\frac{1}{2}\omega_0$ where the notation is convenient in what follows. For $n \geq 1$, the states $|n\rangle|\downarrow\rangle$ and $|n-1\rangle|\uparrow\rangle$ form a basis for the subspace corresponding to a given n, and one may diagonalize the resulting set of 2×2 matrices to obtain

$$E^{\text{JC}}_{n,\pm} = \omega\left(n - \frac{1}{2}\right) \pm \frac{1}{2}\sqrt{(\omega - \omega_0)^2 + 16ng^2} \qquad (n \geq 1)\,. \tag{4.4}$$

Since $E^{\text{JC}}_{n,+} > 0 > E^{\text{JC}}_{0,-}\ \forall\ n \geq 1$, the ground–state energy of H_{JC} is given, at each value of the coupling g, by the smallest element of the set $\{E^{\text{JC}}_{n,-}, n \geq 0\}$.

The corresponding eigenstates are often referred to as "dressed" states in quantum optics, where they are utilized in the study of, amongst others, the time development of the system given particular initial conditions for the atom and field [Mi91, Sh93], and the quasiperiodic recurrence phenomena of collapse and revival which characterize the Jaynes–Cummings model [Na88, Ge90, Mi91, Sh93].

The more general Rabi Hamiltonian (4.1), which extends the Jaynes–Cummings model beyond the RWA, is of interest for a variety of reasons. Given that quantum optics experiments are nowadays being performed with ever–increasing field intensities [An94], there is considerable agreement (see, *e.g.*, [Cr91, Fe96, Lo98]) that the full Rabi Hamiltonian merits investigation. Furthermore, it is known (see [Mi83] and references therein) that quantum chaotic behaviour does not occur in the RWA. Although there is no consensus as to whether the Rabi Hamiltonian does exhibit chaotic behaviour [Gr84a, Ku85, Ei86, Mi91], it is clear that the counter–rotating terms are essential if the possibility of quantum chaos is to exist. Finally, Hamiltonians similar to (4.1) occur in the theory of vibronic interactions [Berb] and in the analysis of a quantum tunneling system under the influence of a phonon bath [Le87], as well as in the study of the two–site polaron Hamiltonian in solid state physics [Mah].

The strict limitation of the fermionic subsystem of the Rabi model to two levels represents an idealization which, from a physical point of view, may generally only be regarded as realistic for $\omega_0 \simeq \omega$. For large atom–field detuning, one might reasonably expect that effects due to the multilevel

nature of the true atomic system would be at least as important as those due to the non–rotating terms included in (4.1); in most of what follows we will therefore focus on the case of resonance. It is then convenient to scale out the ω–dependence by setting $\omega = \omega_0 = 1$, and we will refer to the resulting Hamiltonian as the scaled resonant Rabi Hamiltonian.

4.1.1 Exact limits of the Hamiltonian

The Rabi Hamiltonian is analytically soluble in two limits, namely that of zero coupling ($g = 0$), and that of degenerate electronic levels ($\omega_0 = 0$). For zero coupling and nondegenerate atomic levels ($\omega_0 > 0$), the exact ground state assumes the form $|0\rangle|\downarrow\rangle$, and the corresponding ground–state energy is given by $E_0^{g=0} = \frac{-\omega_0}{2}$. Note that, in this case, the ground state is unique and of positive parity.

The case of nonzero coupling and degenerate atomic levels is important because, as we will demonstrate below, the Hamiltonian with a finite value for ω_0 approaches this case as $g \to \infty$. For $\omega_0 = 0$, $\left[H_{\text{Rabi}}^{\omega_0=0}, \sigma^x\right] = 0$, so that the eigenstates of $H_{\text{Rabi}}^{\omega_0=0}$ may be taken to be eigenstates of σ^x, and we obtain

$$H_{\text{Rabi}}^{\omega_0=0} = \omega\, b^\dagger b \pm 2\, g\, \left(b^\dagger + b\right) , \tag{4.5}$$

where the upper (lower) sign refers to the choice of the upper (lower) eigenstate of σ^x. The Hamiltonian (4.5) represents a shifted harmonic oscillator, as is easily seen by performing the canonical transformations (see *e.g.* [Hak])

$$\tilde{b}_\pm = b \pm \frac{2g}{\omega} , \qquad \tilde{b}_\pm^\dagger = b^\dagger \pm \frac{2g}{\omega} , \tag{4.6}$$

which preserve the bosonic commutation relations, to yield

$$H_{\rm Rabi}^{\omega_0=0} = \omega\, \tilde{b}_\pm^\dagger \tilde{b}_\pm - \frac{4g^2}{\omega}\,. \tag{4.7}$$

For the ground state $|\Psi\rangle$ of $H_{\rm Rabi}^{\omega_0=0}$,

$$\tilde{b}_\pm|\Psi\rangle = 0 \quad \Rightarrow \quad b|\Psi\rangle = \mp\frac{2g}{\omega}|\Psi\rangle\,. \tag{4.8}$$

Thus the (normalized) degenerate ground states $|\Psi_{01}\rangle$ and $|\Psi_{02}\rangle$ of the Rabi Hamiltonian for $\omega_0 = 0$ are the (normalized) coherent bosonic states

$$|\mp x\rangle = e^{-x^2/2}\exp\left[\mp x b^\dagger\right]|0\rangle = e^{-x^2/2}\sum_{n=0}^{\infty}\frac{(\mp x)^n}{\sqrt{n!}}|n\rangle\,, \tag{4.9}$$

with $x = 2g/\omega$, multiplied by the corresponding eigenfunctions of σ^x

$$\frac{1}{\sqrt{2}}\exp\left[\pm\sigma^+/2\right]|\downarrow\rangle = \frac{1}{\sqrt{2}}\left(|\downarrow\rangle \pm |\uparrow\rangle\right)\,, \tag{4.10}$$

and may thus be written as [Gr84b],

$$\begin{aligned}
|\Psi_{01}\rangle &= \frac{1}{\sqrt{2}}|-x\rangle\exp\left[\sigma^+/2\right]|\downarrow\rangle \\
&= \frac{1}{\sqrt{2}}e^{-2g^2/\omega^2}\exp\left[-\frac{2g}{\omega}b^\dagger\right]|0\rangle\ \left(|\downarrow\rangle + |\uparrow\rangle\right) \\
|\Psi_{02}\rangle &= \frac{1}{\sqrt{2}}|x\rangle\exp\left[-\sigma^+/2\right]|\downarrow\rangle \\
&= \frac{1}{\sqrt{2}}e^{-2g^2/\omega^2}\exp\left[\frac{2g}{\omega}b^\dagger\right]|0\rangle\ \left(|\downarrow\rangle - |\uparrow\rangle\right)\,,
\end{aligned} \tag{4.11}$$

with the ground–state energy in both cases given by $E_0^{\omega_0=0} = -4g^2/\omega$.

Having obtained the solution (4.11), we now demonstrate that the equivalence of the limits $\omega_0 \to 0$ and $g \to \infty$, although not formally proven, is at least consistent with this form of the solution. Heuristically treating the set of states $\{|\Psi_{01}\rangle, |\Psi_{02}\rangle\}$ as a basis for the full Rabi Hamiltonian (4.1) with

$\omega_0 > 0$, we obtain the matrix representation

$$\begin{bmatrix} -\frac{4g^2}{\omega} & -\frac{1}{2}\omega_0 e^{-8g^2/\omega^2} \\ -\frac{1}{2}\omega_0 e^{-8g^2/\omega^2} & -\frac{4g^2}{\omega} \end{bmatrix} \tag{4.12}$$

for H_{Rabi}. For finite g, the Hamiltonian couples the states $|\Psi_{01}\rangle$ and $|\Psi_{02}\rangle$ via the off–diagonal terms, and the diagonalization of (4.12) yields the two eigenenergies

$$E_{\pm} = E_0^{\omega_0=0} \mp \frac{1}{2}\omega_0 e^{-8g^2/\omega^2} , \tag{4.13}$$

with corresponding eigenfunctions

$$\begin{aligned} |\Psi_+\rangle &= \frac{1}{\sqrt{2}}\left(|\Psi_{01}\rangle + |\Psi_{02}\rangle\right) \\ |\Psi_-\rangle &= \frac{1}{\sqrt{2}}\left(|\Psi_{01}\rangle - |\Psi_{02}\rangle\right) . \end{aligned} \tag{4.14}$$

As $g \to \infty$ with ω_0 finite, the off–diagonal elements of the matrix (4.12) vanish exponentially. In this limit, the eigenfunctions (4.14), which are linear combinations of the states (4.11), thus become degenerate with energy $E_{\pm}^{g\to\infty} = E_0^{\omega_0=0}$, and the $\omega_0 = 0$ solution is reproduced. Furthermore, since

$$\Pi_{\text{Rabi}}|\Psi_{01}\rangle = |\Psi_{02}\rangle , \qquad \Pi_{\text{Rabi}}|\Psi_{02}\rangle = |\Psi_{01}\rangle , \tag{4.15}$$

we may write the states (4.14) in the form

$$\begin{aligned} |\Psi_+\rangle &= \frac{1}{\sqrt{2}}\left(1 + \Pi_{\text{Rabi}}\right)|\Psi_{01}\rangle \\ |\Psi_-\rangle &= \frac{1}{\sqrt{2}}\left(1 - \Pi_{\text{Rabi}}\right)|\Psi_{01}\rangle . \end{aligned} \tag{4.16}$$

Given that $\Pi_{\text{Rabi}}^2 = 1$, the states $|\Psi_+\rangle$ and $|\Psi_-\rangle$ are therefore of positive and negative parity, respectively. Also, the bosonic coherent states $|\pm 2g/\omega\rangle$ reduce to the bosonic vacuum $|0\rangle$ at $g = 0$, and the state $|\Psi_+\rangle$ ($|\Psi_-\rangle$), although not the exact ground (first excited) state at finite g, is therefore the analytic ground (first excited) state at $g = 0$.

4.1.2 Juddian solutions and the configuration–interaction (CI) method

Several attempts at an analytically exact treatment of the Rabi Hamiltonian have been made. There is very strong numerical support for the conjecture of Reik *et. al.* [Re86, Re87] involving generalized spheroidal wave functions, but a formal proof of the integrability of (4.1) is still missing (note here the work of Szopa *et. al.* [Sz96]). As demonstrated in the introduction to this chapter, the Jaynes–Cummings model, *i.e.* the Rabi Hamiltonian within the RWA, is analytically soluble. This result may also be obtained via a unitary Holstein–Primakoff mapping of both the fermionic and bosonic aspects of the Jaynes–Cummings Hamiltonian into a system composed of two ideal boson modes, where the resulting bosonized Hamiltonian may be solved exactly [Ci98] [1]. This success of this bosonization approach, however, depends crucially on the fact that H_{JC} commutes with the number operator N introduced in (4.2), while $[H_{\mathrm{Rabi}}, N] \neq 0$.

However, isolated analytic solutions for some of the higher lying states in the spectrum of the Rabi Hamiltonian are known. These solutions were first obtained for a class of Jahn–Teller systems by Judd [Ju79], who established explicit finite order equations for the isolated values of the coupling at which the Jahn–Teller eigenvalues can be determined analytically, and these isolated exact solutions are thus known as Juddian solutions. Subsequently, Reik *et.al.* [Re82] showed that the Juddian solutions for the Rabi Hamiltonian

[1] See also the non-unitary Dyson boson mapping technique employed in [Ca87], albeit to a different Hamiltonian.

may be obtained as a special case of those for the linear $E \otimes e$ pseudo Jahn–Teller model. A fuller discussion of the approach taken by Reik *et.al.* is thus deferred to Chapter 7. Here we simply point out that the values of the coupling g for which Juddian solutions for the Rabi system occur are given [Re82] by the solutions of

$$A_N + B_N = 0 \tag{4.17}$$

where $N \in \{0, 1, 2, \ldots\}$, and A_N and B_N are determined recursively via

$$\begin{bmatrix} B_{n+1} \\ A_{n+1} \end{bmatrix} = \begin{bmatrix} M_{11} & M_{12} \\ M_{21} & M_{22} \end{bmatrix} \begin{bmatrix} B_n \\ A_n \end{bmatrix} \qquad n = 0, 1, 2, \ldots, N-1 \tag{4.18}$$

with

$$\begin{aligned}
B_0 &= \frac{2g^2}{\omega^2}, \qquad A_0 = -\frac{2g^2}{\omega^2} - \frac{1}{4} - \delta + \frac{N}{2} \\
M_{11} &= -\frac{2g^2}{\omega^2}\left(\frac{1}{4} - \delta + \frac{N}{2}\right) \\
M_{12} &= -\frac{2g^2}{\omega^2}\left(\frac{1}{4} - \delta + n - \frac{N}{2}\right) \\
M_{21} &= \left(\frac{2g^2}{\omega^2} + \frac{5}{4} + \delta + n - \frac{N}{2}\right)\left(\frac{1}{4} - \delta + \frac{N}{2}\right) - \frac{2g^2}{\omega^2}(n+1) \\
M_{22} &= \left(\frac{2g^2}{\omega^2} + \frac{5}{4} + \delta + n - \frac{N}{2}\right)\left(\frac{1}{4} - \delta + n - \frac{N}{2}\right) - \frac{2g^2}{\omega^2}(n+1) \\
\delta &\equiv \frac{\omega_0 - \omega}{4\omega}.
\end{aligned} \tag{4.19}$$

For a given value of N, the sum $A_N + B_N$ is a polynomial of degree N in g^2, and (4.17) thus yields N solutions for g^2. The positive square roots of the positive g^2 solutions to (4.17) yield the values of the coupling for which Juddian isolated exact solutions exist, and the energies corresponding to these couplings then lie on the Nth so-called baseline, defined by

$$E_N^{\text{Baseline}} = N\omega - \frac{4g^2}{\omega}. \tag{4.20}$$

For $N = 0$, $A_0 + B_0 = -\frac{1}{4} - \delta$, which is independent of the coupling g, and (4.17) is then only satisfied in the special case $\delta = -\frac{1}{4}$, which corresponds to $\omega_0 = 0$ *i.e.* degenerate atomic levels. It is then clear from (4.20) that the Juddian solution for $N = 0$ and $\omega_0 = 0$ yields the $\omega_0 = 0$ solution (4.11) presented in Section 4.1, which is a degenerate ground–state solution analytic for all couplings. This two–fold degeneracy is a generic feature of the Juddian solutions for the Rabi Hamiltonian for all N, and indicates that these solutions always occur at points where two energy levels simultaneously cross the Nth baseline.

For $N = 0$ and $\omega_0 \neq 0$, isolated exact solutions do not exist for any value of the coupling g. In fact, at least at resonance ($\omega_0 = \omega$ or equivalently $\delta = 0$), no Juddian solutions occur for either the ground or first excited states of the Rabi system for any value of the coupling [Re82]. For $N > 0$, however, isolated analytic solutions corresponding to higher lying states of the Rabi Hamiltonian may be found at particular values of g, and these Juddian solutions then provide a useful benchmark against which approximate results may be checked.

Although in this thesis we focus mainly on the coupled cluster method, it is of interest for purposes of comparison to analyze the Rabi system using other many–body techniques. In particular, we consider here techniques which yield quasi–exact numerical results. The configuration–interaction (CI) method (also known as the Rayleigh-Ritz method or simply diagonalization), is generally regarded as such a method, and entails the diagonalization of a Hamiltonian in a subspace of the full many–body Hilbert space. For any

given range of values of the coupling g, care must be taken to ensure that the dimension N of the subspace is large enough so that the calculation may be deemed to have converged at each value of g in the given interval. This typically requires $N \sim 100$, so that the diagonalization has to be done numerically. We construct a typical subspace as the span of a basis consisting of products of bosonic occupation number states and two–level atomic states. Since the Rabi Hamiltonian (4.1) conserves the parity (4.2), the matrix representation of (4.1) blocks into even and odd parity sectors, simplifying the numerical calculation.

It is important to note that there is no *a priori* guarantee that the CI results, even when done to arbitrarily high (finite) order N, are practically exact (see *e.g.* [Lo98], where it is demonstrated that this is not the case for the multiquantum or k–photon Rabi model). For the Rabi Hamiltonian, however, we may use the Juddian solutions to benchmark the CI results. As shown in Table 4.1, a CI diagonalization of the scaled resonant Rabi Hamiltonian in a basis of $N \geq 61$ states reproduces the known exact results for the ninth and tenth excited states at the representative Juddian point $g = g^* = 0.75824924$ to within the limits of numerical precision ($< 10^{-10}$). In Table 4.1 we also tabulate the (even–parity) ground state and (odd–parity) first excited state energies at $g = g^*$. Although there does not appear to be a formal proof of this, it is reasonable to expect that, in the same order N, the error in the lower–lying energies should be at most of the same order of magnitude as that for the higher–lying states, particularly since the lower–lying energy eigenvalues appear to converge at least as quickly with increasing N as their

higher–lying counterparts [2]. Results of similar accuracy may be obtained at other Juddian points, and we may thus assert that the CI results are for all practical purposes exact over the full coupling spectrum.

Table 4.1: *Comparison of the results of a CI diagonalization of the scaled resonant ($\omega = \omega_0 = 1$) Rabi Hamiltonian in a basis of N states with the Juddian solution occurring at $g = g^* = 0.75824924$ for which the exact energies of the ninth (E_9) and tenth (E_{10}) excited states are given by $E_9 = E_{10} = E^* = 1.70023235$. Clearly the CI method effectively reproduces the exact Juddian result for $N \geq 61$. Also shown are the CI results for the even–parity ground (E_0) and odd–parity first excited (E_1) state energies at the same coupling g^*. The converged CI results for E_0 and E_1 are clearly well separated at this value of g.*

N	$E_9^{(N)}$	$E_{10}^{(N)}$	$E_9^{(N)} - E^*$	$E_{10}^{(N)} - E^*$	$E_0^{(N)}$	$E_1^{(N)}$	$E_1^{(N)} - E_0^{(N)}$
11	5.40691445	7.30537548	3.7067×10^{0}	5.6051×10^{0}	-2.2528	-2.1830	6.9734×10^{-2}
21	2.36187405	2.36800390	6.6164×10^{-1}	6.6777×10^{-1}	-2.3361	-2.3247	1.1383×10^{-2}
31	1.70942030	1.74049648	9.1879×10^{-3}	4.0264×10^{-2}	-2.3363	-2.3255	1.0753×10^{-2}
41	1.70024476	1.70027293	1.2407×10^{-5}	4.0578×10^{-5}	-2.3363	-2.3255	1.0753×10^{-2}
51	1.70023235	1.70023236	7.9560×10^{-10}	8.5000×10^{-9}	-2.3363	-2.3255	1.0753×10^{-2}
61	1.70023235	1.70023235	8.8867×10^{-12}	9.8461×10^{-11}	-2.3363	-2.3255	1.0753×10^{-2}
101	1.70023235	1.70023235	1.8695×10^{-11}	8.6098×10^{-11}	-2.3363	-2.3255	1.0753×10^{-2}

[2] Although theorems such as those on interleaving eigenvalues may in certain cases be used to bracket the exact eigenvalues, we have not been able to find any useful theorems relating the rate of convergence (with increasing N) of the higher–lying eigenvalues to that of the lowest eigenvalues in the literature.

4.2 Physical characteristics of the Rabi ground state

Systems similar to the Rabi Hamiltonian are known to exhibit interesting ground–state behaviour. A case in point is the polaron, consisting of an electron interacting with the phononic lattice field in a solid [Mah]. It is well known that there is a crossover from the so–called large polaron regime, where the electron is essentially free to roam the solid (and the Fröhlich Hamiltonian, which treats the ionic background as a continuum, applies), to the small polaron regime, where the discrete nature of the lattice manifests itself and the electron is to a greater or lesser degree localized to a particular atomic site. The crossover from large to small polaron behaviour as the electron–phonon coupling is increased does not constitute a phase transition, but it does signify a drastic change in the character of the polaron ground state in a reasonably well–defined coupling regime. In fact, an application of time–independent (Rayleigh–Schrödinger) perturbation theory (TIPT) to the Fröhlich Hamiltonian yields an infinite effective mass for the electron at a particular value of the coupling (see [Mah] and references therein), an obviously erroneous result which may however be used to identify the crossover regime. Similar crossover behaviour is also observed in the study of a quantum particle tunneling between two wells in the presence of a phonon bath (see [Lo95] and references therein). In this system, which is closely analogous to the Rabi Hamiltonian and which may also be used as a model of the two–site polaron, there is competition between the localization inherent in the interaction with the phonons, and the delocalization inherent in

the tunneling. Again, although several variational studies find evidence for a sharp (discontinuous) transition, the localization–delocalization crossover which occurs for intermediate coupling between the particle and the phonons does not consitute a true phase transition, but simply a change in character in the ground state of the system.

It is thus not surprising to find that a similar crossover regime exists for the quantum optical system described by the Rabi Hamiltonian. Using the (essentially exact) CI results for the resonant Rabi ground–state wave function, we have also determined the expectation value $\langle \sigma^z \rangle$, which indicates to what extent the atom may be regarded as being in its upper or lower state, as well as the fluctuation $\Delta\sigma^z = \sqrt{1 - \langle \sigma^z \rangle^2}$, as a function of the coupling g. The results, which are shown in Figure 4.1, indicate that there is a marked change in the physical character of the ground–state wave function in the region where $g \sim 0.6$. Below this transitional region, the atom is predominantly in its lower state. Above the transitional region, the atom is essentially in an equal superposition of the upper and lower states. The change in character in the ground state also manifests itself in $\langle n \rangle$, the average number of photons in the field in the Rabi ground state, as well as in the fluctuation Δn in the photon number, as a function of the coupling g. Again using the CI result for the Rabi ground–state wave function at resonance, we find that $\langle n \rangle \approx \Delta n \approx 1$ at $g \sim 0.6$, which defines the same transitional region as before.

The change in character in the Rabi ground state, although marked, is not discontinuous, and there is thus no evidence for a phase transition. Note that

the Rabi system has an infinite number of degrees of freedom (the number of bosons can be infinite), and that, unlike a finite system, it could in principle display a true phase transition. If such a phase transition were present, the ground and first excited states would become degenerate at the critical coupling for the transition. The absence of such a transition is thus also substantiated by the CI results for the ground and first excited state energies E_0 and E_1, which are well separated in the transitional region, even (see

Figure 4.1: *The expectation value $\langle\sigma^z\rangle$ (solid line) and the fluctuation $\Delta\sigma^z$ (thick solid line) in the ground state of the scaled resonant ($\omega = \omega_0 = 1$) Rabi Hamiltonian, as a function of the coupling g, as determined via a CI diagonalization in a basis of 101 even–parity states.*

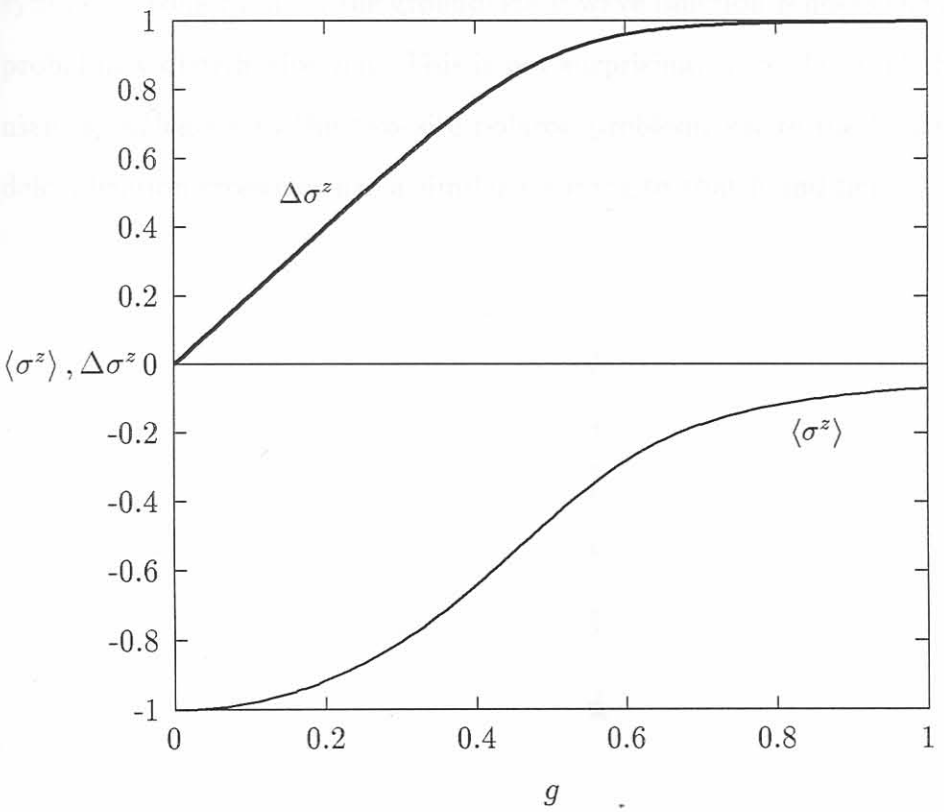

Table 4.1) at the Juddian point $g = g^* = 0.75824924$ located well above this region. Even in the limit $\omega_0 = 0$ where the (analytic) ground state is doubly degenerate for all couplings and there is definitely no phase transition, this continuous yet marked character change still occurs in the even–parity ground state $|\Psi_+\rangle$ (see Figure 4.3).

For the Fröhlich polaron problem, the large–to–small polaron crossover is accompanied by a localization of the electronic wave packet in configuration space. No such localization occurs in the angular wave packet associated with the angle variable conjugate to σ^z [Ca68, Za69, Pei], since the even–parity symmetry constraint on the ground–state wave function renders the angular probability distribution flat. This is not surprising, since the Rabi Hamiltonian is analogous to the two–site polaron problem, where the localization–delocalization crossover has a similar meaning to that found here.

4.3 Approximate many–body approaches to the Rabi Hamiltonian

Historically, the non–rotating terms included in the Rabi Hamiltonian were considered to act merely as sources of small frequency shifts, the so–called Bloch–Siegert shifts, with respect to the Jaynes–Cummings spectrum [Bl40] (see also [Mi91, Sh93] and references therein). As discussed in Section 4.1, however, there has been renewed interest in the full Rabi Hamiltonian (4.1), and recent many–body analyses of the Hamiltonian include, amongst others, a weak–coupling time–independent perturbative expansion in g [Ph89, Qi98], a first–order strong coupling perturbative expansion in ω_0 [Gr84b], a calculation based on a variational coherent state [Qi98], and a path–integral approach applied in the weak coupling regime [Za88]. Also, numerically exact (though not analytic) results for the Rabi system have recently been obtained via the operator method [Fe96], via a power series solution [Qi98], and via a combination of unitary transformations and numerical diagonalization [Lo96].

4.3.1 Time–independent perturbation theory

Consider first the application of time–independent (Rayleigh–Schrödinger) perturbation theory to the Rabi Hamiltonian (see also [Ph89, Qi98]). We write

$$H_{\text{Rabi}} = H^{(0)}_{\text{Rabi}} + gH'_{\text{Rabi}} \tag{4.21}$$

where

$$\begin{aligned} H^{(0)}_{\text{Rabi}} &\equiv \frac{1}{2}\omega_0\sigma^z + \omega b^\dagger b \,, \\ H'_{\text{Rabi}} &\equiv \left(b^\dagger + b\right)\left(\sigma^+ + \sigma^-\right) \,. \end{aligned} \tag{4.22}$$

We restrict the perturbative calculation to the even–parity sector, and only consider $\omega_0 \neq 0$. Since the spectrum of $H^{(0)}_{\text{Rabi}}$, the "noninteracting" ($g = 0$) Rabi Hamiltonian is simply determined as

$$\begin{aligned} H^{(0)}_{\text{Rabi}}|\Psi^{(0)}_m\rangle &= E^{(0)}_m|\Psi^{(0)}_m\rangle \qquad m = 0, 1, 2, \ldots \\ |\Psi^{(0)}_m\rangle &= \begin{cases} |m\rangle|\downarrow\rangle & m \text{ even} \\ |m\rangle|\uparrow\rangle & m \text{ odd} \end{cases} \\ E^{(0)}_m &= m\omega - \frac{(-1)^m}{2}\omega_0 \,, \end{aligned} \tag{4.23}$$

and since furthermore the ground state of $H^{(0)}_{\text{Rabi}}$ is nondegenerate for $\omega_0 \neq 0$, a perturbative ground–state expansion in powers of the coupling g is feasible and in principle straightforward. To Nth order, we expand the true ground–state wave function $|\Psi_0\rangle$ and energy E_0 as

$$\begin{aligned} |\Psi_0\rangle &= |\Psi^{(0)}_0\rangle + \sum_{i=1}^{N} g^i|\Psi^{(i)}_0\rangle = |0\rangle|\downarrow\rangle + \sum_{i=1}^{N} g^i|\Psi^{(i)}_0\rangle \\ E_0 &= E^{(0)}_0 + \sum_{i=1}^{N} g^i E^{(i)}_0 = -\frac{1}{2}\omega_0 + \sum_{i=1}^{N} g^i E^{(i)}_0 \,. \end{aligned} \tag{4.24}$$

We express the ith order correction $|\Psi^{(i)}_0\rangle$ to the ground–state wave function in the basis consisting of the eigenstates of $H^{(0)}_{\text{Rabi}}$ via

$$|\Psi^{(i)}_0\rangle = \sum_{m=1}^{M} c^{(i)}_m|\Psi^{(0)}_m\rangle \,, \qquad i = 1, 2, \ldots, N \,, \tag{4.25}$$

where M is a cutoff introduced for computational purposes. The neglect of the $m = 0$ term in (4.25) simply results in an overall rescaling of the

perturbative ground–state wave function [Mer]. Upon substituting (4.24) and (4.25) into the Schrödinger equation $H|\Psi_0\rangle = E_0|\Psi_0\rangle$, and comparing terms of equal order in g, we obtain the equations

$$\begin{aligned}\left(E_m^{(0)} - E_0^{(0)}\right) c_m^{(i)} &= 2\sum_{j=2}^{i-1} c_1^{(j-1)} c_m^{(i-j)} - 2\sqrt{m+1}\, c_{m+1}^{(i-1)} - 2\sqrt{m}\, c_{m-1}^{(i-1)} \\ & \qquad m = 1, 2, \ldots, M\,, \qquad i = 1, 2, \ldots, N \\ E_0^{(i)} &= 2\, c_1^{(i-1)}\,, \qquad\qquad i = 1, 2, \ldots, N\,, \end{aligned} \tag{4.26}$$

which are to be solved for the required unknowns $\{c_m^{(i)}\}$ and $\{E_0^{(i)}\}$. These equations must be solved for M large enough so that the results are effectively independent of M, *i.e.* so that we may safely neglect $\{c_m^{(i)}; i = 1, 2, \ldots, N\}$ for all $m > M$. This calculation, which we shall refer to as weak–coupling perturbation theory, may be done analytically to arbitrary finite order using algebraic manipulation packages such as *Mathematica* [Mat], and the results at resonance are shown in Figure 4.2. Since the weak–coupling Rayleigh-Schrödinger perturbation series for the ground–state energy, which at resonance ($\omega = \omega_0 = 1$) assumes the form

$$E_0^{\text{Weak}} = -\frac{1}{2} - 2\,g^2 - 2\,g^4 - 2\,g^6 + 6\,g^{10} + \frac{41}{3}\,g^{12} + \frac{113}{18}\,g^{14} + \ldots\,, \tag{4.27}$$

does not appear to follow a discernably regular pattern, we have not been able to analytically determine the radius of convergence of this series. It is apparent from Figure 4.2, however, that the perturbative approach breaks down at $g \approx 0.6$, which defines the same transitional region as described in Section 4.2, and further highlights the analogy between the Rabi system and the polaron problem, where a similar breakdown in TIPT occurs.

Since the spectrum of the Rabi Hamiltonian in the limit $\omega_0 = 0$ is known [Gr84b], it is in principle also possible to analyze the Hamiltonian via strong–

Figure 4.2: *The ground–state energy E_0 of the scaled resonant ($\omega = \omega_0 = 1$) Rabi Hamiltonian as a function of the coupling g as determined via 12th, 20th and 50th order weak–coupling TIPT (solid lines), and via first order strong–coupling TIPT (thin solid line), compared to results obtained via a CI diagonalization in a basis of 101 even–parity states (thick solid line).*

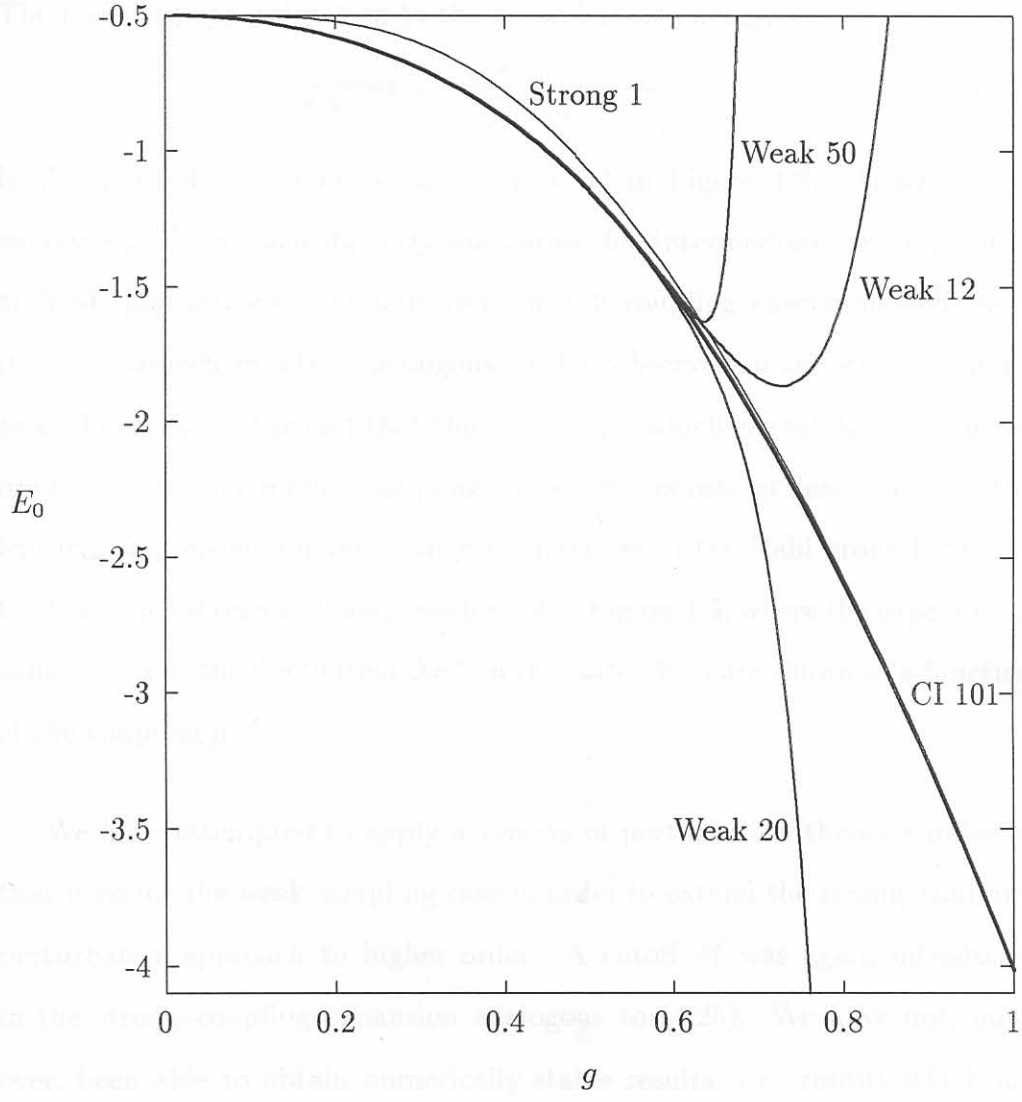

coupling perturbation theory. This involves a ground–state expansion in powers of ω_0 (see comment just before equation (4.11). The first order strong–coupling perturbative correction (which multiplies ω_0) to the $\omega_0 = 0$ ground–state energy $E_0^{(0)} = -4g^2/\omega$ is given by

$$E_0^{(1)} = \langle \Psi_+ | \frac{1}{2}\sigma^z | \Psi_+ \rangle = -\frac{1}{2} e^{-8g^2/\omega^2} , \tag{4.28}$$

where $|\Psi_+\rangle$ is the positive–parity $\omega_0 = 0$ ground state introduced in (4.16). The resulting approximation to the ground–state energy,

$$E_0^{\text{Strong}} = -\frac{4g^2}{\omega} - \frac{1}{2}\omega_0 e^{-8g^2/\omega^2} , \tag{4.29}$$

is also plotted at resonance ($\omega = \omega_0 = 1$) in Figure 4.2. Although the energy E_0^{Strong} is quantitatively inaccurate for intermediate coupling, it is at least qualitatively adequate over the full coupling spectrum, and there is no breakdown in TIPT analogous to that observed in the weak–coupling case. This reflects the fact that the state $|\Psi_+\rangle$, which is analytic in both the limits of zero and infinite coupling, must incorporate at least some of the features responsible for the change in character in the Rabi ground state in the transitional region. This is confirmed in Figure 4.3, where the expectation value $\langle \sigma^z \rangle$ and the fluctuation $\Delta\sigma^z$, in the state $|\Psi_+\rangle$, are shown as a function of the coupling g.

We have attempted to apply a version of perturbation theory similar to that used for the weak–coupling case in order to extend the strong–coupling perturbative approach to higher order. A cutoff M was again introduced in the strong–coupling expansion analogous to (4.25). We have not, however, been able to obtain numerically stable results, *i.e.* results which are effectively independent of the cutoff M, using this approach.

Figure 4.3: *The expectation value* $\langle\sigma^z\rangle$ *(solid line) and the fluctuation* $\Delta\sigma^z$ *(thick solid line) in the even–parity* $\omega_0 = 0$ *ground state* $|\Psi_+\rangle$ *of the scaled resonant* $(\omega = \omega_0 = 1)$ *Rabi Hamiltonian, as a function of the coupling* g*, compared to the same quantities (dotted lines) determined via a CI diagonalization in a basis of 101 even–parity states.*

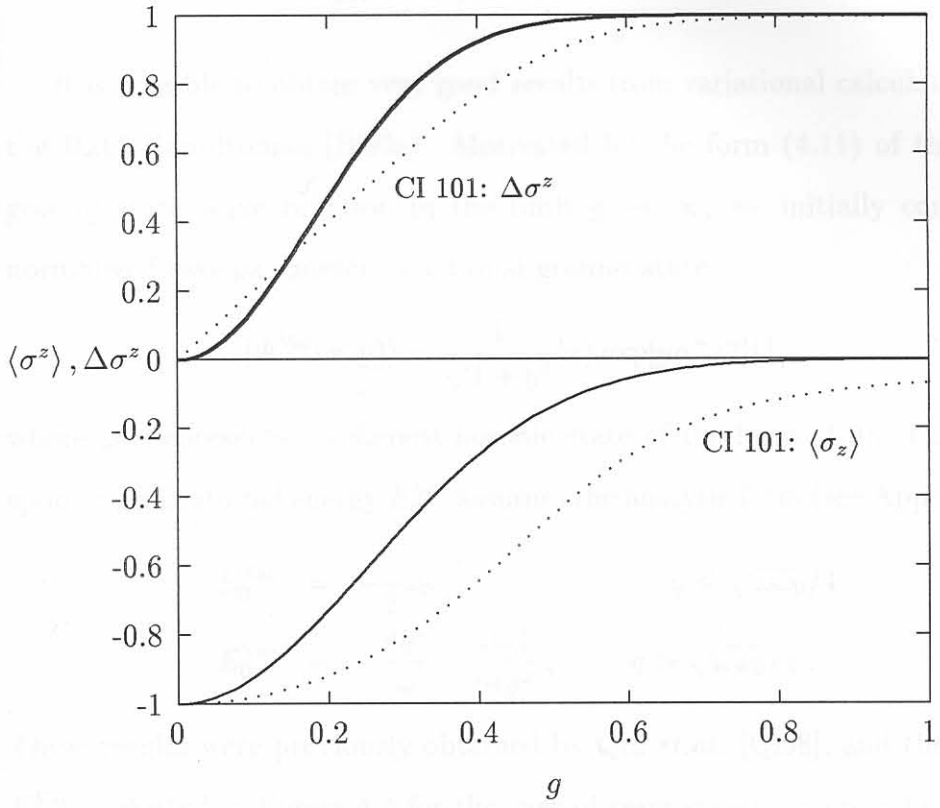

4.3.2 Variational results for the Rabi Hamiltonian

The variational method is a commonly used approach to simple many–body Hamiltonians when a computationally inexpensive estimate of the ground–state energy of the system is required. The basis of the method is a postulated ansatz for the many–body wave function, containing parameters whose values

are determined by minimizing the expectation value $\langle H \rangle$ of the Hamiltonian in the trial state. This minimal expectation value (*i.e.* $\langle H \rangle$ evaluated at the optimal values of the variational parameters) yields an estimate of the ground–state energy. A considerable advantage of the variational method is that the approximate energy thus obtained provides an upper bound for the exact ground–state energy for any choice of the trial wave function.

It is possible to obtain very good results from variational calculations for the Rabi Hamiltonian [Bi99a]. Motivated by the form (4.11) of the exact ground–state wave function in the limit $g \to \infty$, we initially consider a normalized two–parameter variational ground state

$$|\Psi^{\mathrm{Var}}(x,y)\rangle = \frac{1}{\sqrt{1+y^2}}|x\rangle \exp[y\sigma^+/2]|\downarrow\rangle \ , \tag{4.30}$$

where $|x\rangle$ represents a coherent bosonic state of the form (4.9). The corresponding variational energy E_0^{Var} assumes the analytic form (see Appendix C)

$$\begin{aligned} E_0^{\mathrm{Var}} &= -\frac{1}{2}\omega_0 \ , & g \leq \sqrt{\omega\omega_0}/4 \\ E_0^{\mathrm{Var}} &= -\frac{4g^2}{\omega} - \frac{\omega\omega_0^2}{64g^2} \ , & g > \sqrt{\omega\omega_0}/4 \ . \end{aligned} \tag{4.31}$$

These results were previously obtained by Qin *et.al.* [Qi98], and the energy E_0^{Var} is plotted in Figure 4.4 for the case of resonance ($\omega = \omega_0 = 1$).

It is clear that, for a coherent variational state of the form (4.30), the variational ground–state energy may at best be regarded as qualitatively acceptable. Furthermore, although E_0^{Var} is both continuous and differentiable (smooth) at the crossover point $g = \sqrt{\omega\omega_0}/4$ between the two branches of the variational solution, there is a discontinuity in the second derivative $d^2E_0^{\mathrm{Var}}/dg^2$ at this point. By contrast, a numerical differentiation of the CI

(large scale diagonalization) result for the Rabi ground–state energy yields smooth results for both the first and second order derivatives of E_0 with respect to g. We are thus led to seek a variational trial state better capable of following the character change in the Rabi ground state.

Figure 4.4: *The ground–state energy E_0 of the scaled resonant ($\omega = \omega_0 = 1$) Rabi Hamiltonian as a function of the coupling g as determined via a variational calculation based on the mixed parity two–parameter coherent state (4.30) (thin solid line), as well as via an even–parity projection after variation (PAV) based on the same state (dotted solid line, see (4.35)), compared to results obtained via a CI diagonalization in a basis of 101 even–parity states (thick solid line).*

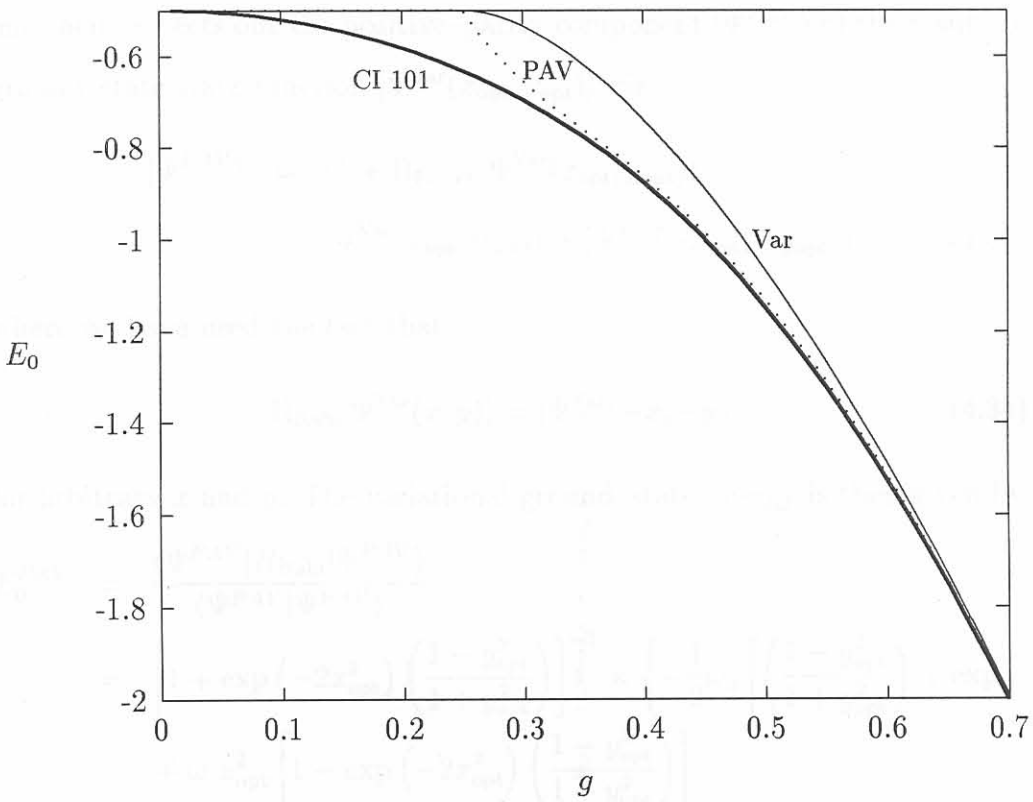

The important omission from the variational ansatz (4.30) is that the parity symmetry $\Pi_{\rm Rabi}$ of the Hamiltonian has not been taken into account. We know from the CI (diagonalization) results that the exact ground state of the Rabi Hamiltonian is of even parity, and it is clear that the state

$$\begin{aligned} |\Psi^{\rm Var}(x,y)\rangle &= \frac{1}{\sqrt{1+y^2}}|x\rangle \exp[y\sigma^+/2]|\downarrow\rangle \\ &= \frac{1}{\sqrt{1+y^2}}\, e^{-x^2/2} \sum_{n=0}^{\infty} \frac{x^n}{\sqrt{n!}}\, |n\rangle \, \{|\downarrow\rangle + y|\uparrow\rangle\} \end{aligned} \tag{4.32}$$

does not have good $\Pi_{\rm Rabi}$ parity. There are two possibilities for incorporating the correct parity symmetry into the variational calculation. In the approach known as projection after variation (PAV), the optimal values $x_{\rm opt}$ and $y_{\rm opt}$ of the variational parameters x and y in (4.30) are determined as before, and one then projects out the positive–parity component $|\Psi^{PAV}\rangle$ of the resulting ground–state wave function $|\Psi^{\rm Var}(x_{\rm opt}, y_{\rm opt})\rangle$ via

$$\begin{aligned} |\Psi^{PAV}\rangle &= (1+\Pi_{\rm Rabi})\,|\Psi^{\rm Var}(x_{\rm opt}, y_{\rm opt})\rangle \\ &= |\Psi^{\rm Var}(x_{\rm opt}, y_{\rm opt})\rangle + |\Psi^{\rm Var}(-x_{\rm opt}, -y_{\rm opt})\rangle\,, \end{aligned} \tag{4.33}$$

where we have used the fact that

$$\Pi_{\rm Rabi}|\Psi^{\rm Var}(x,y)\rangle = |\Psi^{\rm Var}(-x,-y)\rangle \tag{4.34}$$

for arbitrary x and y. The variational ground–state energy is then given by

$$\begin{aligned} E_0^{PAV} &= \frac{\langle\Psi^{PAV}|H_{\rm Rabi}|\Psi^{PAV}\rangle}{\langle\Psi^{PAV}|\Psi^{PAV}\rangle} \\ &= \left[1+\exp\left(-2x_{\rm opt}^2\right)\left(\frac{1-y_{\rm opt}^2}{1+y_{\rm opt}^2}\right)\right]^{-1} \times \left\{-\frac{1}{2}\omega_0\left[\left(\frac{1-y_{\rm opt}^2}{1+y_{\rm opt}^2}\right)+\exp\left(-2x_{\rm opt}^2\right)\right]\right. \\ &\quad + \omega\, x_{\rm opt}^2\left[1-\exp\left(-2x_{\rm opt}^2\right)\left(\frac{1-y_{\rm opt}^2}{1+y_{\rm opt}^2}\right)\right] \\ &\quad \left. + 8g\left(\frac{y_{\rm opt}x_{\rm opt}}{1+y_{\rm opt}^2}\right)\right\}\,. \end{aligned} \tag{4.35}$$

The PAV ground–state energy results are also shown in Figure 4.4, and it is clear that, although there is considerable improvement on the mixed–parity variational results for large coupling, the PAV approach still fails at intermediate coupling where the mixed parity variational results are poor. It is also apparent from Figure 4.4 that the derivative dE_0^{PAV}/dg (rather than $d^2E_0^{PAV}/dg^2$) is already discontinuous at the crossover point $g = \sqrt{\omega\omega_0}/4$, so that the PAV approach actually accentuates the spurious discontinuity in the Rabi ground state.

To include the parity in a self–consistent manner, we consider projection before variation (PBV). We construct (as yet unnormalized) states of good parity from the mixed–parity two–parameter state $|\Psi^{\rm Var}(x,y)\rangle$ (here x and y are still free variational parameters) by projection:

$$\begin{aligned} |\Psi_\pm^{\rm PBV2}(x,y)\rangle &\propto (1 \pm \Pi_{\rm Rabi})\,|\Psi^{\rm Var}(x,y)\rangle \\ &= |\Psi^{\rm Var}(x,y)\rangle \pm |\Psi^{\rm Var}(-x,-y)\rangle \\ &\propto \{|x\rangle \pm |-x\rangle\}\,|\downarrow\rangle \;+\; y\;\{|x\rangle \mp |-x\rangle\}\,|\uparrow\rangle \\ &= |x\rangle_\pm|\downarrow\rangle + y\,|x\rangle_\mp|\uparrow\rangle\,, \end{aligned} \tag{4.36}$$

where

$$\begin{aligned} |x\rangle_+ &\equiv |x\rangle + |-x\rangle = 2\,e^{-x^2/2}\sum_{n=0}^{\infty}\frac{x^{2n}}{\sqrt{(2n)!}}|2n\rangle \\ |x\rangle_- &\equiv |x\rangle - |-x\rangle = 2\,e^{-x^2/2}\sum_{n=0}^{\infty}\frac{x^{2n+1}}{\sqrt{(2n+1)!}}|2n+1\rangle\,, \end{aligned} \tag{4.37}$$

and the upper (lower) sign in (4.36) thus clearly denotes a state with positive (negative) parity. Thus we obtain, besides the positive–parity state which approximates the Rabi ground state, also a negative–parity ansatz for the

first excited state. For numerical reasons, it turns out to be more convenient to normalize the states $|x\rangle_{\pm}|\downarrow\rangle$ and $|x\rangle_{\mp}|\uparrow\rangle$ individually before constructing the combination, and we therefore consider the two–parameter variational states [Bi99a]

$$|\Psi_{\pm}^{\mathrm{PBV2}}(x,v)\rangle = A_v\left(A_{\pm}|x\rangle_{\pm}|\downarrow\rangle + vA_{\mp}|x\rangle_{\mp}|\uparrow\rangle\right) , \tag{4.38}$$

where as before the upper (lower) sign refers to a state of even (odd) Π_{Rabi} parity, and

$$\begin{aligned} A_v &= \left(1+v^2\right)^{-1/2} , \\ A_{\pm} &= \left(2\left[1 \pm e^{-2x^2}\right]\right)^{-1/2} . \end{aligned} \tag{4.39}$$

The minimization of the expectation value

$$\langle H_{\mathrm{Rabi}}\rangle_{\pm}^{\mathrm{PBV2}}(x,v) \equiv \langle\Psi_{\pm}^{\mathrm{PBV2}}(x,v)|H_{\mathrm{Rabi}}|\Psi_{\pm}^{\mathrm{PBV2}}(x,v)\rangle \tag{4.40}$$

with respect to x and v yields two equations for the optimal values x_{opt} and v_{opt} of the variational parameters (see Appendix C). For both the positive– and negative–parity cases, the equation for v_{opt} is analytically soluble, so that the variational (PBV) approach based on the two–parameter state (4.38) only requires the numerical solution of one non–linear equation in the single unknown x_{opt}. We will denote the positive–parity variational ground–state energy thus obtained by E_0^{PBV2}, and the corresponding negative–parity first excited state energy by E_1^{PBV2}.

The inclusion of the correct parity symmetry in the variational ansatz yields a dramatic quantitative improvement in the variational estimate for the ground–state energy of the Rabi system. On the scale of our graphs, the

results for E_0^{PBV2} are indistinguishable from the diagonalization results over the full coupling spectrum, and in Table 4.2 we therefore tabulate E_0^{PBV2}, together with the optimal values x_{opt} and v_{opt}, as a function of g for a range of frequencies. For comparison, we also tabulate the converged CI results

Table 4.2: *Comparison of the ground-state energy of the Rabi Hamiltonian obtained from a PBV calculation based on the even-parity two-parameter ansatz (4.38), E_0^{PBV2}, with the results of a CI diagonalization in a basis of 101 even-parity states, E_0^{CI}. Also shown are the percentage error $\left|E_0^{\mathrm{PBV2}} - E_0^{\mathrm{CI}}\right| / E_0^{\mathrm{CI}} \times 100$, and the values of the variational parameters x_{opt} and v_{opt} at the stationary point of the energy.*

ω_0	ω	g	E_0^{PBV2}	E_0^{CI}	% Error	x_{opt}	v_{opt}
1.0	1.0	0.05	-5.05012×10^{-1}	-5.05013×10^{-1}	2×10^{-4}	0.071	-0.050
		0.1	-5.20201×10^{-1}	-5.20202×10^{-1}	2×10^{-4}	0.142	-0.101
		0.2	-5.83285×10^{-1}	-5.83327×10^{-1}	7×10^{-3}	0.291	-0.208
		0.5	-1.14211	-1.14795	5×10^{-1}	0.859	-0.626
		1.0	-4.01580	-4.01693	3×10^{-2}	1.995	-0.939
		2.0	-1.60039×10^{1}	-1.60040×10^{1}	6×10^{-4}	4.000	-0.984
		5.0	-1.00001×10^{2}	-1.00001×10^{2}	$< 1\times10^{-4}$	10.000	-0.998
1.0	2.0	0.05	-5.03334×10^{-1}	-5.03335×10^{-1}	2×10^{-4}	0.041	-0.033
		0.1	-5.13362×10^{-1}	-5.13363×10^{-1}	2×10^{-4}	0.082	-0.067
		0.2	-5.53807×10^{-1}	-5.53809×10^{-1}	4×10^{-4}	0.164	-0.135
		0.5	-8.51754×10^{-1}	-8.51992×10^{-1}	3×10^{-2}	0.424	-0.416
		1.0	-2.10416	-2.10825	2×10^{-1}	0.938	-0.747
		2.0	-8.00798	-8.00855	7×10^{-3}	1.999	-0.969
		5.0	-5.00012×10^{1}	-5.00013×10^{1}	2×10^{-4}	5.000	-0.995
2.0	1.0	0.05	-1.00334	-1.00334	$< 1\times10^{-4}$	0.058	-0.033
		0.1	-1.01345	-1.01345	$< 1\times10^{-4}$	0.116	-0.067
		0.2	-1.05530	-1.05533	3×10^{-3}	0.237	-0.138
		0.5	-1.42799	-1.43655	6×10^{-1}	0.699	-0.430
		1.0	-4.06288	-4.06746	1×10^{-1}	1.983	-0.882
		2.0	-1.60156×10^{1}	-1.60159×10^{1}	2×10^{-3}	3.998	-0.969
		5.0	-1.00002×10^{2}	-1.00003×10^{2}	1×10^{-3}	10.000	-0.995

for the ground–state energy, as well as the percentage error in E_0^{PBV2} as compared to the CI results. The percentage error is less than 1 % over the full range of couplings and frequencies. Note that the parameters x_{opt} and v_{opt} evolve smoothly from their $g = 0$ values of 0 to their large–g values of $2g/\omega$ and -1, respectively, where it is easily seen that they correspond to a positive–parity solution of the form (4.16).

Table 4.3 contains the analogous results for a two–parameter PBV calculation of the (negative–parity) first excited state energy. The results are good — the large percentage error in regions where the first excited state energy is close to zero is artificial, since the absolute error is small in all cases. The first excited state results are however not in general at the same level of accuracy as those for the ground state, particularly for small coupling in the sub–resonant case ($\omega_0 = 2\omega$). This may be attributed to the absence of two–boson correlations in the variational ansatz (4.38). For ω_0 much larger than ω, it would be necessary to determine which n–boson correlations need to be included in the variational ansatz. For resonance and supra–resonance ($\omega_0 \leq \omega$), however, the calculation presented here is acceptable.

Although variational calculations are useful in determining energies, particularly due to the upper–bound nature of their results, there is no guarantee that the variational wave function itself is accurate. A failure of the wave function is usually revealed in the calculation of expectation values of quantities other than the Hamiltonian. To examine the quality of the (positive–parity) ground–state ansatz (4.38), we have therefore calculated the expectation values $\langle \sigma^z \rangle^{\mathrm{PBV2}}$ and $\langle b^\dagger b \rangle^{\mathrm{PBV2}}$ in this state. Explicit expres-

sions for these quantities are given in Appendix C. In Figure 4.5, the results for $\langle\sigma^z\rangle^{\mathrm{PBV2}}$ at resonance ($\omega = \omega_0 = 1$) are compared to results obtained via numerical diagonalization, as well as results based on the mixed–parity variational ansatz (4.30). The dramatic improvement obtained by the parity

Table 4.3: *Comparison of the first excited state energy of the Rabi Hamiltonian obtained from a PBV calculation based on the odd–parity two–parameter ansatz (4.38),* E_1^{PBV2}*, with the results of a CI diagonalization in a basis of 101 odd–parity states,* E_1^{CI}*. Also shown are the percentage error* $\left|E_1^{\mathrm{PBV2}} - E_1^{\mathrm{CI}}\right| / E_1^{\mathrm{CI}} \times 100$*, and the values of the variational parameters* x_{opt} *and* v_{opt} *at the stationary point of the energy.*

ω_0	ω	g	E_1^{PBV2}	E_1^{CI}	% Error	x_{opt}	v_{opt}
1.0	1.0	0.05	3.96137×10^{-1}	3.95102×10^{-1}	3×10^{-1}	0.279	-0.982
		0.1	2.84083×10^{-1}	2.80666×10^{-1}	1.2	0.401	-0.964
		0.2	3.24806×10^{-2}	2.33675×10^{-2}	40	0.590	-0.932
		0.5	-9.98782×10^{-1}	-1.01018	1.1	1.067	-0.885
		1.0	-4.01545	-4.01658	3×10^{-2}	1.997	-0.940
		2.0	-1.60039×10^{1}	-1.60040×10^{1}	6×10^{-4}	4.000	-0.984
		5.0	-1.00001×10^{2}	-1.00001×10^{2}	$< 1\times10^{-4}$	10.000	-0.998
1.0	2.0	0.05	4.90049×10^{-1}	4.90049×10^{-1}	$< 1\times10^{-4}$	0.070	-10.050
		0.1	4.60760×10^{-1}	4.60758×10^{-1}	4×10^{-4}	0.140	-5.098
		0.2	3.50617×10^{-1}	3.50542×10^{-1}	2×10^{-2}	0.270	-2.864
		0.5	-2.69004×10^{-1}	-2.71650×10^{-1}	1	0.595	-1.355
		1.0	-1.96664	-1.97218	3×10^{-1}	1.042	-1.000
		2.0	-8.00764	-8.00821	7×10^{-3}	1.999	-0.970
		5.0	-5.00013×10^{1}	-5.00013×10^{1}	$< 1\times10^{-4}$	5.000	-0.995
2.0	1.0	0.05	-1.01956×10^{-2}	-1.65009×10^{-2}	38	0.173	-0.102
		0.1	-4.28514×10^{-2}	-6.42075×10^{-2}	33	0.340	-0.212
		0.2	-1.87367×10^{-1}	-2.35841×10^{-1}	21	0.601	-0.419
		0.5	-1.11473	-1.15708	3.8	1.079	-0.706
		1.0	-4.06213	-4.06664	1×10^{-1}	1.986	-0.882
		2.0	-1.60156×10^{1}	-1.60159×10^{1}	2×10^{-4}	3.998	-0.969
		5.0	-1.00002×10^{2}	-1.00003×10^{2}	1×10^{-4}	10.000	-0.995

projection is clearly seen, and the good–parity variational results, like those obtained via the CI method, show no evidence for any discontinuity in the Rabi ground state. The corresponding results for $\langle b^\dagger b\rangle^{\mathrm{PBV2}}$ are shown in Figure 4.6, and here the agreement with the CI diagonalization is even better — the differences between the CI and two–parameter PBV results are not

Figure 4.5: *The ground–state expectation value of σ^z for the scaled resonant ($\omega = \omega_0 = 1$) Rabi Hamiltonian in the mixed–parity two–parameter variational state (4.30) (thick solid line denoted by Var), in the two–parameter PBV state (4.38) (solid line denoted by PBV2), and in the three–parameter PBV state (4.41) (dotted line denoted by PBV3), as a function of the coupling g, compared to results obtained via a CI diagonalization in a basis of 101 even–parity states (thin solid line).*

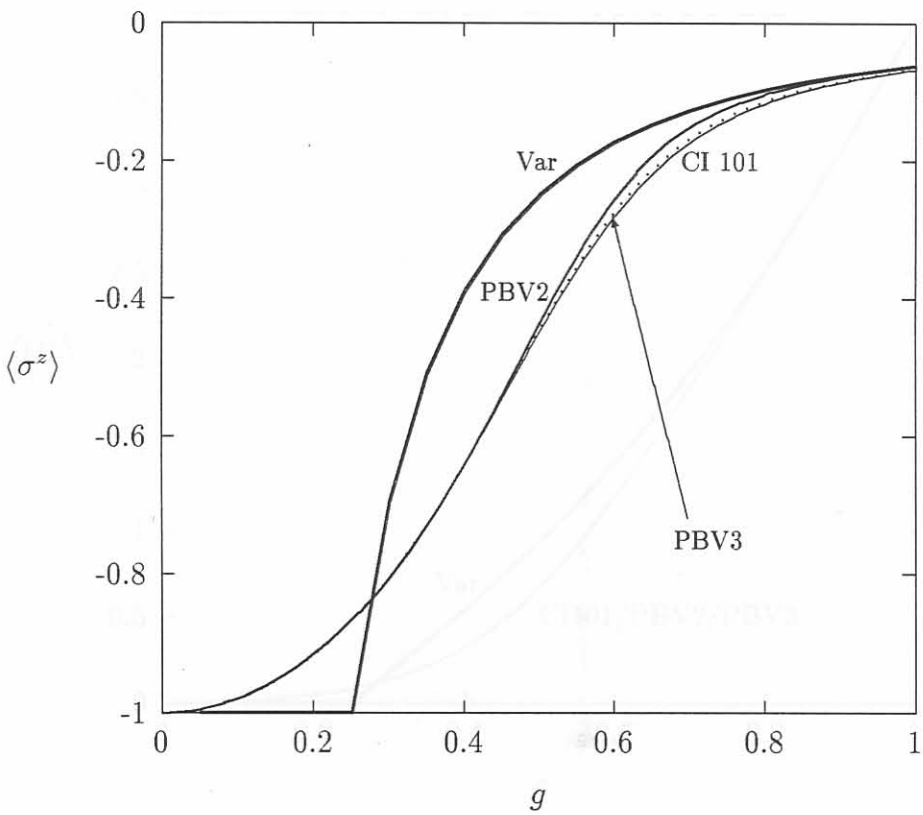

visible in the plot. Examination of the actual values shows that the variational values lie slightly below the diagonalization results for $g < 0.61$, and slightly above for larger couplings.

Figure 4.6: *The ground-state expectation value of $b^\dagger b$ for the scaled resonant ($\omega = \omega_0 = 1$) Rabi Hamiltonian in the mixed-parity two-parameter variational state (4.30) (thick solid line denoted by Var), in the two-parameter PBV state (4.38) (solid line denoted by PBV2), and in the three-parameter PBV state (4.41) (dotted line denoted by PBV3), as a function of the coupling g, compared to results obtained via a CI diagonalization in a basis of 101 even-parity states (thin solid line). On this scale, the PBV results are virtually indistinguishable from the diagonalization results.*

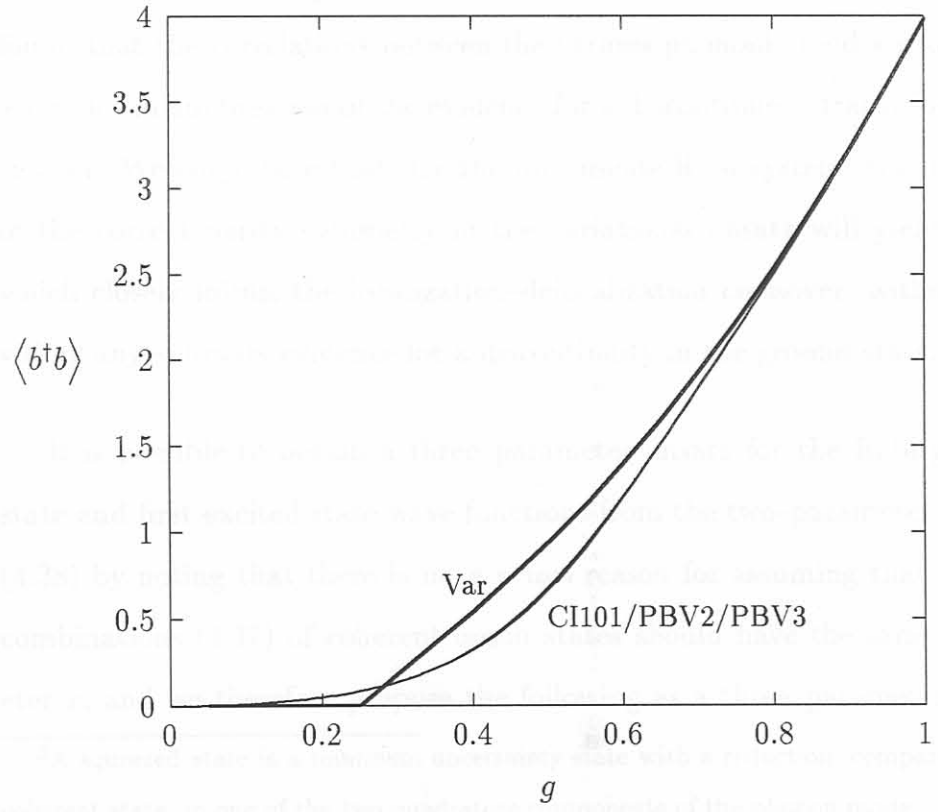

The quality of the results obtained indicates that the even–parity variational wave function (4.38) is very close to the exact ground–state wave function for the Rabi Hamiltonian, and re–emphasizes the importance of incorporating the parity symmetry in the variational calculation. In the context of a quantum tunneling system coupled to several modes of a phonon bath (see [Lo95] and references therein), variational calculations based on both a multimode coherent state and a multimode squeezed state [3] yield results which also provide evidence for a discontinuous localization–delocalization transition which turns out to be nonexistent. These results are thus analogous to the mixed–parity variational results obtained above for the Rabi Hamiltonian. Lo and Wong [Lo95] performed a variational calculation for the quantum tunneling system based on a correlated squeezed state, and found that the correlations between the various phononic modes resulted in a significant suppression of the evidence for a discontinuous transition in the system. We conjecture that, for the multimode Rabi system, the inclusion of the correct parity symmetry in the variational ansatz will yield results which closely mimic the localization–delocalization crossover, without providing any spurious evidence for a discontinuity in the ground state.

It is possible to obtain a three–parameter ansatz for the Rabi ground–state and first excited state wave functions from the two–parameter ansätze (4.38) by noting that there is no *a priori* reason for assuming that the two combinations (4.37) of coherent boson states should have the same parameter x, and we therefore propose the following as a three–parameter ansatz

[3] A squeezed state is a minimum uncertainty state with a reduction, compared to the coherent state, in one of the two quadrature components of the phonon mode.

for the Rabi Hamiltonian [Bi99a]:

$$\begin{aligned} |\Psi_{\pm}^{\mathrm{PBV3}}(x_1, x_2, v)\rangle &= A_v \left(A_{1,\pm} |x_1\rangle_{\pm} |\downarrow\rangle + v A_{2,\mp} |x_2\rangle_{\mp} |\uparrow\rangle \right) \\ &= A_v \left(A_{1,\pm} \left\{ |x_1\rangle \pm |-x_1\rangle \right\} |\downarrow\rangle \right. \\ &\quad \left. + v A_{2,\mp} \left\{ |x_2\rangle \mp |-x_2\rangle \right\} |\uparrow\rangle \right) , \end{aligned} \tag{4.41}$$

where as before the upper (lower) sign refers to a state of positive (negative) Π_{Rabi} parity, and

$$\begin{aligned} A_v &= \left[1 + v^2 \right]^{-1/2} , \\ A_{1,\pm} &= \left[2 \left(1 \pm \exp\left[-2x_1^2 \right] \right) \right]^{-1/2} , \\ A_{2,\pm} &= \left[2 \left(1 \pm \exp\left[-2x_2^2 \right] \right) \right]^{-1/2} . \end{aligned} \tag{4.42}$$

We note here that the positive–parity (negative–parity) ansatz (4.41) is clearly invariant under the replacement $x_1 \to -x_1$ ($x_2 \to -x_2$) as well as under the simultaneous replacements $x_2 \to -x_2$, $v \to -v$ ($x_1 \to -x_1$, $v \to -v$). For convenience, we consider here only the case $x_1, x_2 \geq 0$.

As shown in Appendix C, the minimization of the expectation value of H_{Rabi} in the state (4.41) again yields an analytically soluble equation for the optimal value v_{opt} of the parameter v, and it remains only to solve two coupled non-linear equations for the optimal values $x_{1,\mathrm{opt}}$ and $x_{2,\mathrm{opt}}$. Our variational results for the ground and first excited state energies for the three–parameter ansätze (4.41) are shown in Tables 4.4 and 4.5, and the percentage error relative to the diagonalization results is also plotted in Figures 4.7 and 4.8. It is clear from the values presented that we have obtained very accurate approximations for both the ground–state and first excited state energies of the Rabi Hamiltonian with very little numerical effort. The results for

the ground–state energy agree to within 0.1 % with the CI results over the full coupling and frequency spectrum, while the maximum error in the first excited state energy is of the order of 2 % (the same comments as for the two–parameter case apply here).

Table 4.4: *Comparison of the ground–state energy of the Rabi Hamiltonian obtained from a PBV calculation based on the even–parity three–parameter ansatz (4.41),* E_0^{PBV3}*, with the results of a CI diagonalization in a basis of 101 even–parity states,* E_0^{CI}*. Also shown are the percentage error* $\left|E_0^{\mathrm{PBV3}} - E_0^{\mathrm{CI}}\right| / E_0^{\mathrm{CI}} \times 100$*, and the values of the variational parameters* $x_{1,\mathrm{opt}}$*,* $x_{2,\mathrm{opt}}$*, and* v_{opt} *at the stationary point of the energy.*

ω_0	ω	g	E_0^{PBV3}	E_0^{CI}	% Error	$x_{1,\mathrm{opt}}$	$x_{2,\mathrm{opt}}$	v_{opt}
1.0	1.0	0.05	-5.05013×10^{-1}	-5.05013×10^{-1}	$< 1\times10^{-4}$	0.071	0.087	-0.050
		0.1	-5.20202×10^{-1}	-5.20202×10^{-1}	$< 1\times10^{-4}$	0.142	0.174	-0.101
		0.2	-5.83326×10^{-1}	-5.83327×10^{-1}	2×10^{-4}	0.292	0.351	-0.208
		0.5	-1.14676	-1.14795	1×10^{-1}	0.856	0.942	-0.618
		1.0	-4.01677	-4.01693	4×10^{-3}	1.987	2.003	-0.935
		2.0	-1.60040×10^{1}	-1.60040×10^{1}	$< 1\times10^{-4}$	3.999	4.000	-0.984
		5.0	-1.00001×10^{2}	-1.00001×10^{2}	$< 1\times10^{-4}$	10.000	10.000	-0.997
1.0	2.0	0.05	-5.03334×10^{-1}	-5.03335×10^{-1}	2×10^{-4}	0.041	0.046	-0.033
		0.1	-5.13363×10^{-1}	-5.13363×10^{-1}	$< 1\times10^{-4}$	0.082	0.093	-0.067
		0.2	-5.53809×10^{-1}	-5.53809×10^{-1}	$< 1\times10^{-4}$	0.164	0.186	-0.135
		0.5	-8.51976×10^{-1}	-8.51992×10^{-1}	2×10^{-3}	0.424	0.470	-0.351
		1.0	-2.10739	-2.10825	4×10^{-2}	0.932	0.977	-0.738
		2.0	-8.00847	-8.00855	1×10^{-3}	1.995	2.003	-0.967
		5.0	-5.00013×10^{1}	-5.00013×10^{1}	$< 1\times10^{-4}$	5.000	5.000	-0.995
2.0	1.0	0.05	-1.00334	-1.00334	$< 1\times10^{-4}$	0.058	0.078	-0.033
		0.1	-1.01345	-1.01345	$< 1\times10^{-4}$	0.116	0.155	-0.067
		0.2	-1.05533	-1.05533	$< 1\times10^{-4}$	0.238	0.314	-0.138
		0.5	-1.43491	-1.43655	1×10^{-1}	0.712	0.857	-0.432
		1.0	-4.06678	-4.06746	2×10^{-2}	1.966	1.998	-0.875
		2.0	-1.60159×10^{1}	-1.60159×10^{1}	$< 1\times10^{-4}$	3.996	4.000	-0.969
		5.0	-1.00003×10^{2}	-1.00003×10^{2}	$< 1\times10^{-4}$	10.000	10.000	-0.995

We note that the ground–state energy is accurately given by the two–parameter ansatz and that the three–parameter ansatz does not significantly improve on these results. Furthermore an examination of the variational parameters for the two ansätze shows that $x_{1,\mathrm{opt}} \simeq x_{2,\mathrm{opt}} \simeq x_{\mathrm{opt}}$. This indicates

Table 4.5: *Comparison of the first excited state energy of the Rabi Hamiltonian obtained from a PBV calculation based on the odd–parity three–parameter ansatz (4.41),* E_1^{PBV3}*, with the results of a CI diagonalization in a basis of 101 odd–parity states,* E_1^{CI}*. Also shown are the percentage error* $\left|E_1^{\mathrm{PBV3}} - E_1^{\mathrm{CI}}\right| / E_1^{\mathrm{CI}} \times 100$*, and the values of the variational parameters* $x_{1,\mathrm{opt}}$*,* $x_{2,\mathrm{opt}}$*, and* v_{opt} *at the stationary point of the energy.*

ω_0	ω	g	E_1^{PBV3}	E_1^{CI}	% Error	$x_{1,\mathrm{opt}}$	$x_{2,\mathrm{opt}}$	v_{opt}
1.0	1.0	0.05	3.95108×10^{-1}	3.95102×10^{-1}	2×10^{-3}	0.119	0.316	-0.956
		0.1	2.80737×10^{-1}	2.80666×10^{-1}	2.5×10^{-2}	0.230	0.448	-0.922
		0.2	2.39619×10^{-2}	2.33675×10^{-2}	2.5	0.437	0.639	-0.877
		0.5	-1.00774	-1.01018	2.4×10^{-1}	1.005	1.097	-0.853
		1.0	-4.01643	-4.01658	3×10^{-3}	1.989	2.004	-0.936
		2.0	-1.60040×10^{1}	-1.60040×10^{1}	$< 1\times10^{-4}$	3.999	4.000	-0.984
		5.0	-1.00001×10^{2}	-1.00001×10^{2}	$< 1\times10^{-4}$	10.000	10.000	-0.997
1.0	2.0	0.05	4.90049×10^{-1}	4.90049×10^{-1}	$< 1\times10^{-4}$	0.055	0.071	-10.050
		0.1	4.60758×10^{-1}	4.60758×10^{-1}	$< 1\times10^{-4}$	0.109	0.140	-5.097
		0.2	3.50544×10^{-1}	3.50542×10^{-1}	5×10^{-4}	0.217	0.271	-2.680
		0.5	-2.71436×10^{-1}	-2.71650×10^{-1}	8×10^{-2}	0.526	0.603	-1.333
		1.0	-1.97098	-1.97218	6×10^{-2}	1.009	1.055	-0.983
		2.0	-8.00813	-8.00821	1×10^{-3}	1.995	2.003	-0.968
		5.0	-5.00013×10^{1}	-5.00013×10^{1}	$< 1\times10^{-4}$	5.000	5.000	-0.995
2.0	1.0	0.05	-1.61742×10^{-2}	-1.65009×10^{-2}	1.9	0.104	0.774	-0.110
		0.1	-6.29720×10^{-2}	-6.42075×10^{-2}	1.9	0.207	0.791	-0.212
		0.2	-2.31762×10^{-1}	-2.35841×10^{-1}	1.7	0.405	0.849	-0.379
		0.5	-1.14872	-1.15708	7×10^{-1}	0.966	1.147	-0.658
		1.0	-4.06603	-4.06664	2×10^{-2}	1.969	2.000	-0.875
		2.0	-1.60159×10^{1}	-1.60159×10^{1}	$< 1\times10^{-4}$	3.996	4.000	-0.969
		5.0	-1.00003×10^{2}	-1.00003×10^{2}	$< 1\times10^{-4}$	10.000	10.000	-0.995

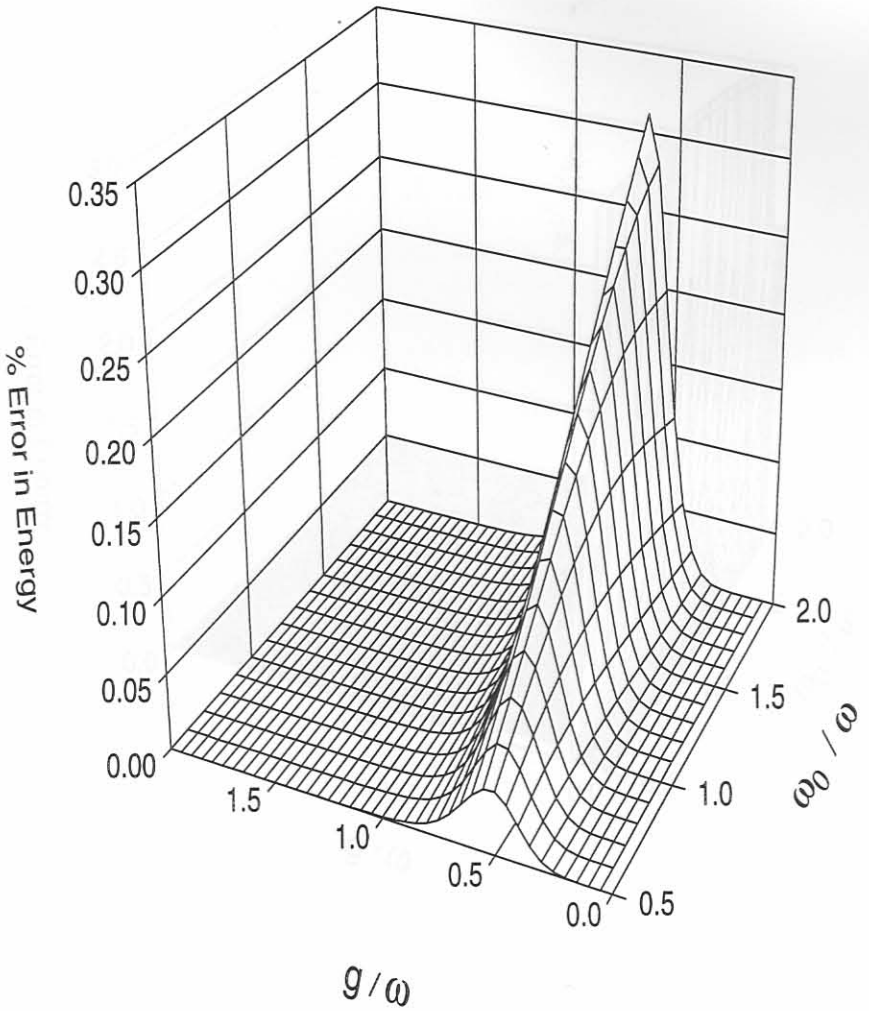

Figure 4.7: *The percentage error in the ground–state energy of the Rabi Hamiltonian obtained from the even–parity three–parameter PBV ansatz (4.41),* E_0^{PBV3}, *compared to the results of a CI diagonalization in a basis of 101 even–parity states, as a function of the coupling* g/ω *and the two–level splitting* ω_0/ω.

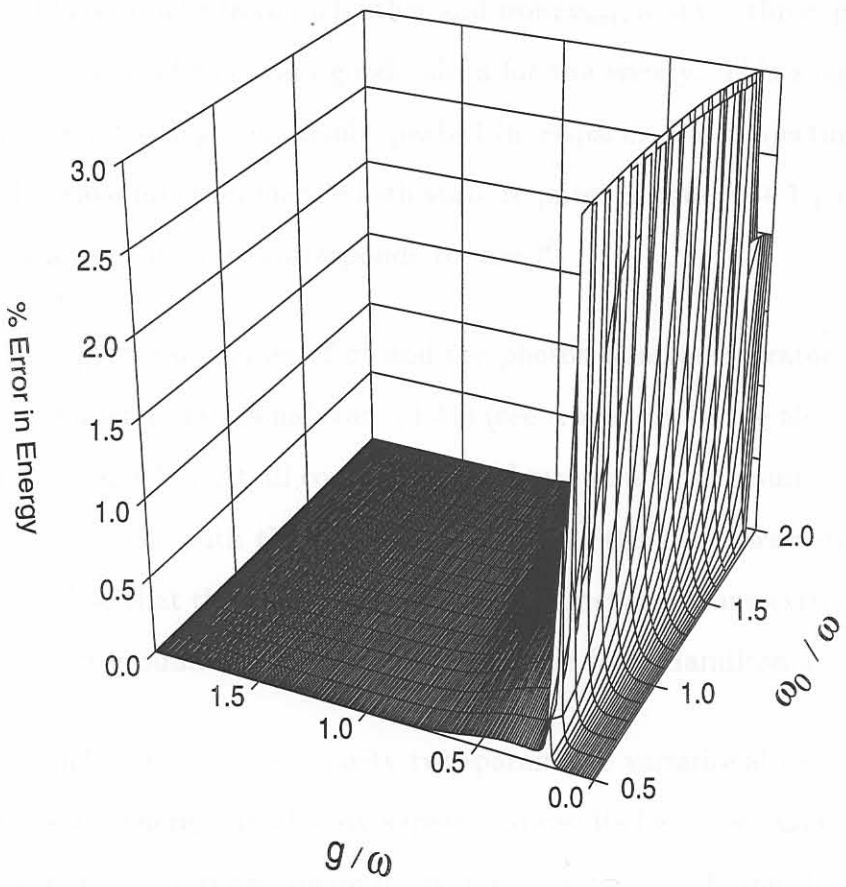

Figure 4.8: *The percentage error in the first excited state energy of the Rabi Hamiltonian obtained from the odd–parity three–parameter PBV ansatz (4.41),* E_1^{PBV3}*, compared to the results of a CI diagonalization in a basis of 101 odd–parity states, as a function of the coupling* g/ω *and the two–level splitting* ω_0/ω*. Note that we have had to truncate the plot in the vertical direction since one obtains an infinite percentage error when the energy becomes zero.*

that the ground state is a singly peaked function in x-space. The same is certainly not true for the first excited state where $x_{1,\mathrm{opt}}$ and $x_{2,\mathrm{opt}}$ are significantly different both from each other and from x_{opt}, and the three–parameter ansatz is essential to obtain good values for the energy. This suggests that the first excited state is doubly peaked in x-space. We conjecture [Bi99a] that the wave function for the n-th state requires in total $n+1$ parameters, where the ground state corresponds to $n=1$.

The expectation values of σ^z and the photon number operator $b^\dagger b$ in the three–parameter variational state (4.41) (see Appendix C) are also plotted in Figures 4.5 and 4.6. At all couplings, the three–parameter results are in even better agreement with the diagonalization than the two–parameter results, and it is clear that the three–parameter wave function is thus extremely close to the exact ground–state wave function of the Rabi Hamiltonian.

In conclusion, our even–parity two–parameter variational results for the ground–state energy are already superior to results (see, *e.g.* [Qi98, Wo96b]) obtained via other approximate many–body techniques. Using the computationally inexpensive three–parameter variational calculation, we obtain even better results for both the energies and wave functions of the ground and first excited states of the Rabi system. This calculation therefore provides a benchmark of simplicity and accuracy against which other methods, such as the CCM, may be measured.

Chapter 5

Simple Applications of the CCM to the Rabi Hamiltonian

In many cases, the non–perturbative nature of the CCM permits calculations based on very simple model states (typically the noninteracting state) to be performed well beyond the perturbative region without convergence problems. However, this is not always the case, as the calculations presented in this chapter indicate. In fact, for the Rabi system, where the ground state undergoes a major character change, it can be shown that the calculation fails due to an essential incompleteness, to arbitrary finite order, in the CCM ansatz for the ground–state wave function for a particularly simple, yet in principle valid, choice of the CCM model state and correlation operator. For a different but equally simple choice, we also show that the non–Hermiticity of the CCM can lead to the breakdown of the method.

5.1 Earlier CCM analyses of the Rabi Hamiltonian

Of particular relevance for this thesis is the recent application of the CCM to a multimode Rabi Hamiltonian by Wong and Lo [Wo96b]. Although their calculation was done in the context of a quantum system tunneling between two levels in the presence of a phonon bath, their model Hamiltonian represents a simple generalization of the Rabi Hamiltonian to the case of multiple bosonic modes, and the Rabi Hamiltonian may thus be regarded as a special case of the model studied by Wong and Lo. Their results for the ground–state energy of the multimode Rabi system are qualitatively acceptable, and furthermore they find that the CCM results give no indication of the spurious discontinuous localization–delocalization transition of the two–level system observed in earlier variational studies (see [Lo95] and references therein).

Several comments regarding the work of Wong and Lo [Wo96b] are however in order. Firstly, they apply the CCM to a unitary transformed version of the Rabi Hamiltonian (4.1), which leaves the spectrum unaffected. However, their choice of unitary transform destroys the parity symmetry (4.2) associated with the Hamiltonian. As a result, their CCM results for the ground–state energy are, by their own admission, quantitatively inaccurate for intermediate coupling, and it is furthermore not possible in their approach to readily obtain accurate CCM results for the first excited state.

A more minor criticism of the CCM analysis of Wong and Lo relates to their use of the so–called successive coupled cluster approximation (SCCA), a

variant of the standard SUB-N CCM approximation. At a particular order of approximation in the SCCA, the similarity transformed Hamiltonian $e^{-S}He^{S}$ is allowed to act on the CCM model state $|\Phi\rangle$, and the CCM coefficients and ground–state energy are determined via term–by–term comparison, with any remaining nonvanishing terms being neglected. At the subsequent level of approximation, terms are added to the cluster correlation operator S in such a manner that their contribution cancels the nonvanishing terms in the previous order of approximation, and the procedure is repeated. The advantage of this approximation scheme is that it naturally tends to select the most important terms which are to be included in the cluster correlation operator, and in some cases (see, *e.g.* [Wo94, Wo96a]), the SCCA leads to rapid, accurate convergence of the CCM. However, not only is the intuitively simple physical meaning of the SUB-N approximation scheme lost, but it is also not clear that the SCCA may be rigorously justified, particularly since there is no gaurantee in the SCCA that the set of configurations $\{C_I^{\dagger}|\Phi\rangle\}$, where the index I runs over all possible configurations generated within the SCCA, satisfies the requirement of completeness.

5.2 Evidence for a spurious symmetry–breaking phase transition

We turn now to our CCM calculations for the Rabi Hamiltonian. For ease of reference, we shall refer to a particular choice of CCM model state and corresponding creation operators as a CCM *scheme*. We have considered a

variety of CCM schemes for the Rabi Hamiltonian (see Table D.1 in Appendix D). An obvious choice for the model state $|\Phi\rangle$ is the positive–parity $g = 0$ ground state $|0\rangle|\downarrow\rangle$ of $H_{\rm Rabi}$, which we shall refer to as the *noninteracting* model state. For our first NCCM calculation of the Rabi ground–state energy, we use the noninteracting model state and the correlation operator [Bi96]

$$\begin{aligned} S &= S_1 + S_2 \\ S_1 &= \sum_{n=1}^{\infty} s_n^{(1)} \left(b^\dagger\right)^n , \qquad S_2 = \sum_{n=1}^{\infty} s_n^{(2)} \left(b^\dagger\right)^{n-1} \sigma^+ , \end{aligned} \tag{5.1}$$

which we shall refer to as Scheme I. For this scheme, the nested commutator expansion (3.8) for the similarity transformed Hamiltonian $e^{-S} H_{\rm Rabi} e^S$ terminates at third order in S, and it is straightforward to show that the CCM ground–state energy assumes the form

$$E_0^{\rm NCCM,I} = -\frac{1}{2}\omega_0 + 4g \left\{ s_1^{(1)} s_1^{(2)} + s_2^{(2)} \right\} . \tag{5.2}$$

In the SUB-N approximation scheme, both S_1 and S_2 truncate at $n = N$, and the $2N$ coefficients $\left\{ s_n^{(1)}, s_n^{(2)} \right\}$, $n = 1, 2, \ldots, N$ are determined via the NCCM equations (3.16). Explicit expressions for the similarity transformed Hamiltonian and NCCM equations for Scheme I are given in Appendix D.

Since the $g = 0$ ground state has even parity, we expect the ground state to have the same parity for $g > 0$. Thus the NCCM calculation based on Scheme I is restricted to states of positive parity. In this case, terms in the cluster correlation operator S with n odd are zero, there are only N CCM coefficients to solve for in the SUB-N approximation, and the CCM ground–state energy then depends only on the single coefficient $s_2^{(2)}$. Starting from $g = 0$, we solve for increasing values of the coupling by using the solution

at the previous coupling as input to the iterative routine for solving the CCM equations. For simplicity, we only quote results for the scaled resonant ($\omega = \omega_0 = 1$) Rabi Hamiltonian.

We find that the even–parity NCCM Scheme I results provide strong evidence for spontaneous breaking of the parity symmetry Π_{Rabi} [Bi96]. For all $N \geq 6$, the positive–parity ground–state solution terminates at a finite value of the coupling which we shall denote by $g_c^{(N)}$. There is a qualitative difference in the nature of the termination depending on whether $N/2$ is even or odd. Here we restrict ourselves to the simpler case where $N/2$ is odd (see [Bi96] for a fuller discussion of the case where $N/2$ is even). The ground–state energy results for $N = 10, 30, 50$ at resonance are shown in Figure 5.1. The termination points $\left\{g_c^{(N)}\right\}$ of the positive–parity NCCM Scheme I results are clearly visible.

The termination in the positive–parity NCCM Scheme I ground–state solution is real rather than numerical. For any N, the NCCM equations (3.16) can in this case be rewritten as a polynomial in $s_2^{(2)}$ (see Appendix D), and the termination in the ground–state solution then corresponds to the vanishing of the relevant real root for $s_2^{(2)}$ at the termination point $g_c^{(N)}$ [Bi97]. Figure 5.2 shows these critical values of the coupling as a function of the cutoff N. An investigation of the behaviour of E_g and its derivatives just below the critical coupling [Bi96] suggests a fit of $g_c^{(N)}$ to the form $a - bN^{\gamma}$, with $\gamma = -2/3$. Using a least–squares fit, we find $a = 0.665$ and $b = 0.722$, and the NCCM based on Scheme I therefore strongly suggests a parity–breaking phase transition at $g_c \equiv \lim_{N\to\infty} g_c^{(N)} = 0.665$.

Figure 5.1: *The ground–state energy E_0 of the scaled resonant ($\omega = \omega_0 = 1$) Rabi Hamiltonian as a function of the coupling g as determined via a SUB-N, N=10,30,50, NCCM analysis based on Scheme I (see Table D.1), compared to results obtained via a CI diagonalization in a basis of 101 even–parity states.*

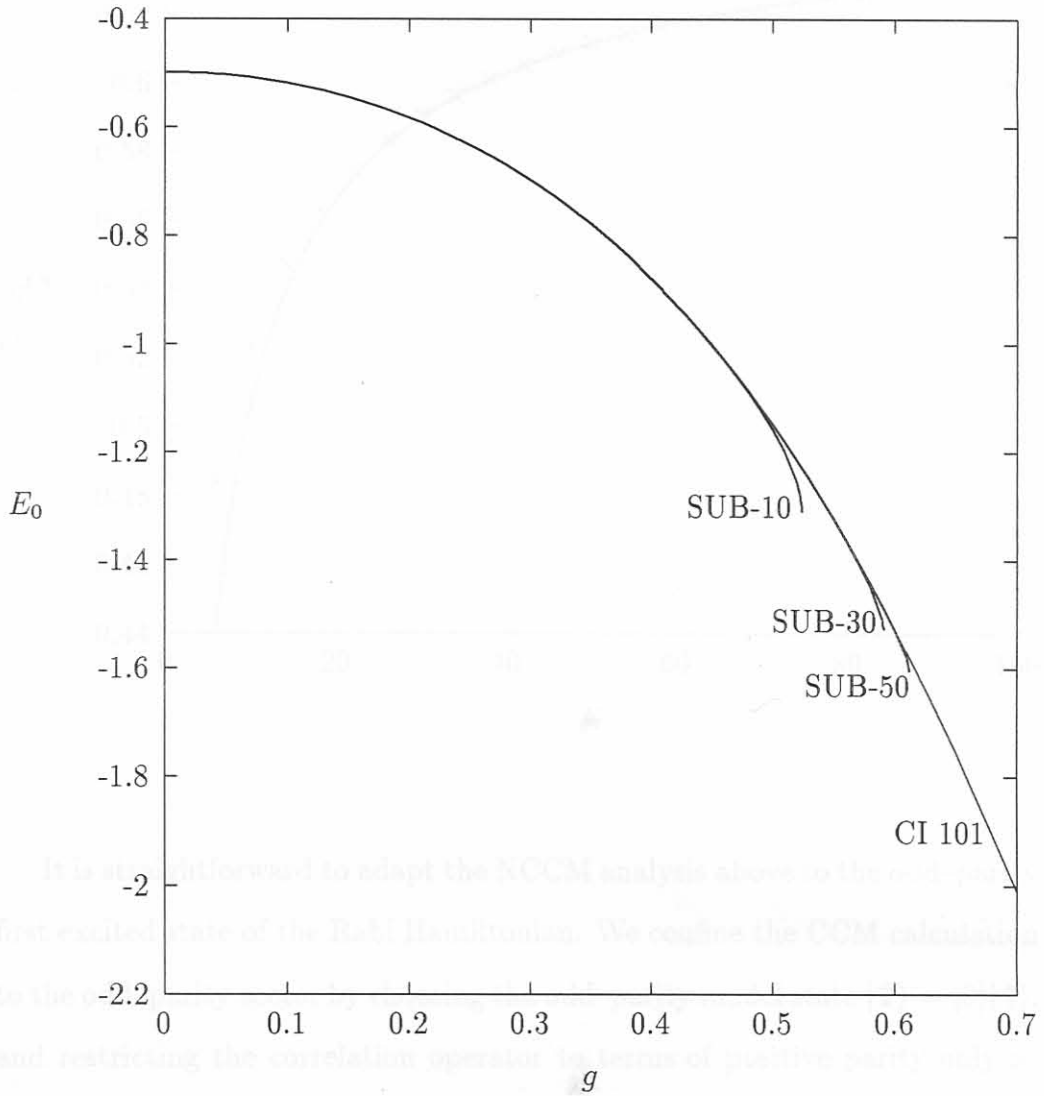

Figure 5.2: *The critical coupling* $g_c^{(N)}$ *as a function of the level of approximation* N *in the NCCM Scheme I analysis of the scaled resonant* ($\omega = \omega_0 = 1$) *Rabi Hamiltonian. The solid line is the function* $0.665 - 0.722N^{-2/3}$ *obtained from a least–squares fit to* $g_c^{(N)}$ *for* $62 \leq N \leq 98$.

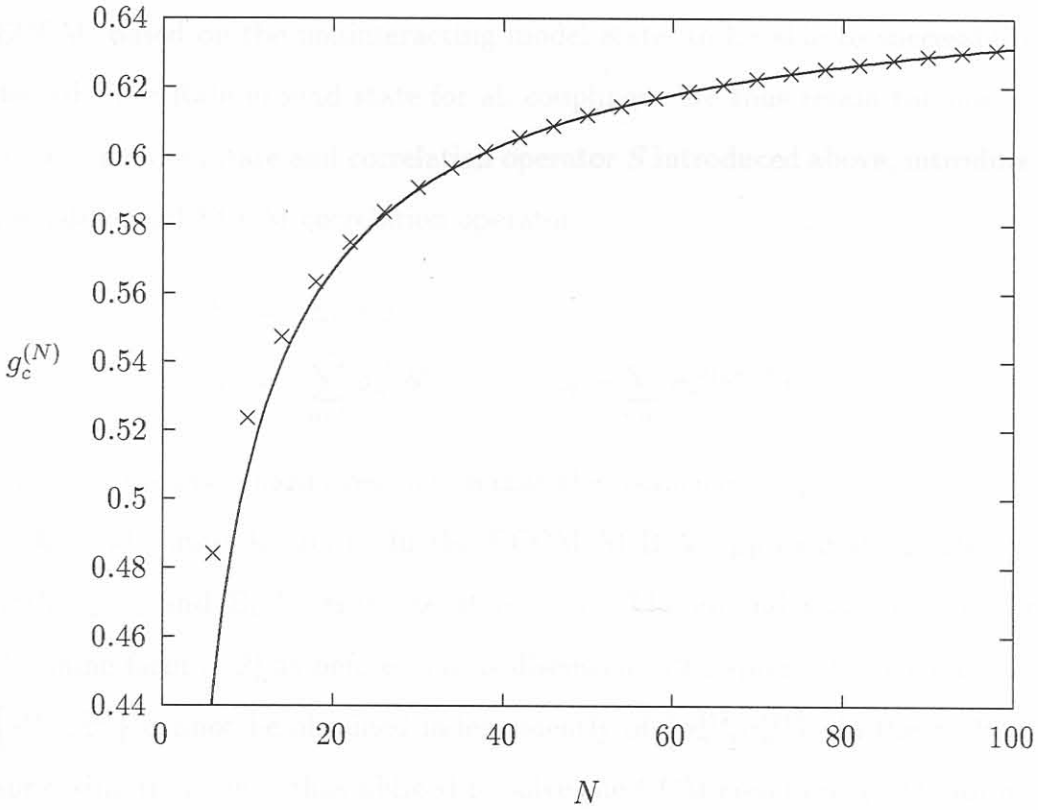

It is straightforward to adapt the NCCM analysis above to the odd–parity first excited state of the Rabi Hamiltonian. We confine the CCM calculation to the odd–parity sector by choosing the odd–parity model state $|\Phi\rangle = |0\rangle|\uparrow\rangle$, and restricting the correlation operator to terms of positive parity only as before. The results are very similar to those obtained for the ground state, with the odd–parity solution terminating at $g_c^{\rm odd} = 0.601$.

Motivated by the results obtained by Arponen and others for the LMG model (see [Ar82, Ar83a, Ar83b, Ro89] and the discussion in Chapter 3), we also apply the ECCM to the Rabi Hamiltonian [Bi98]. The ECCM, based on a single symmetric model state, is capable of correctly describing a symmetry–breaking phase transition. One might therefore expect the ECCM, based on the noninteracting model state, to be able to successfully describe the Rabi ground state for all couplings. We thus retain the noninteracting model state and correlation operator S introduced above, introduce the additional ECCM correlation operator

$$\begin{aligned} \Sigma &= \Sigma_1 + \Sigma_2 \\ \Sigma_1 &= \sum_{n=1}^{\infty} \sigma_n^{(1)} b^n , \qquad \Sigma_2 = \sum_{n=1}^{\infty} \sigma_n^{(2)} b^{n-1} \sigma^- , \end{aligned} \tag{5.3}$$

and drop the even–parity restriction that the coefficients $\left\{ s_n^{(1)}, s_n^{(2)}, \sigma_n^{(1)}, \sigma_n^{(2)} \right\}$ with n odd must be zero. In the ECCM SUB-N approximation scheme, both S_1, S_2 and Σ_1, Σ_2 truncate at $n = N$. The ground–state energy has the same form (5.2) as before, but as discussed in Chapter 3 the coefficients $\left\{ s_n^{(1)}, s_n^{(2)} \right\}$ cannot be obtained independently of $\left\{ \sigma_n^{(1)}, \sigma_n^{(2)} \right\}$. In the SUB-$N$ approximation one is thus obliged to solve the CCM equations (3.14) for all $4N$ unknowns. The ECCM functional $\overline{H}_{\rm Rabi} = \langle \Phi | e^{\Sigma} e^{-S} H_{\rm Rabi} e^{S} | \Phi \rangle$, which is required in order to set up these equations, is shown in Appendix D.

In the SUB-1 approximation, the ECCM Scheme I equations can be solved analytically (see Appendix D). At resonance ($\omega = \omega_0 = 1$), one finds, for $g \leq 1/4$, only the trivial solution where all four SUB-1 ECCM coefficients are identically zero. In this coupling regime the ECCM approximation to the exact ground state is thus simply the even–parity noninteracting model

state $|0\rangle|\downarrow\rangle$, with corresponding energy $E_0 = -1/2$. For $g > 1/4$, the SUB-1 ECCM equations also allow for a mixed–parity solution corresponding to the lower energy $E_0 = -4g^2 - 1/4$. Thus the SUB-1 ECCM ground–state energy is continuous but not differentiable at the crossover point $g = 1/4$ where the symmetry of the ground state is broken. This result in plotted in Figure 5.3,

Figure 5.3: *The ground–state energy E_0 of the scaled resonant ($\omega = \omega_0 = 1$) Rabi Hamiltonian as a function of the coupling g as determined via a SUB-1 (solid line), SUB-2 (thin solid line) and SUB-3 (dotted line) ECCM analysis based on Scheme I (see Table D.1), compared to results obtained via a CI diagonalization in a basis of 101 even–parity states (thick solid line).*

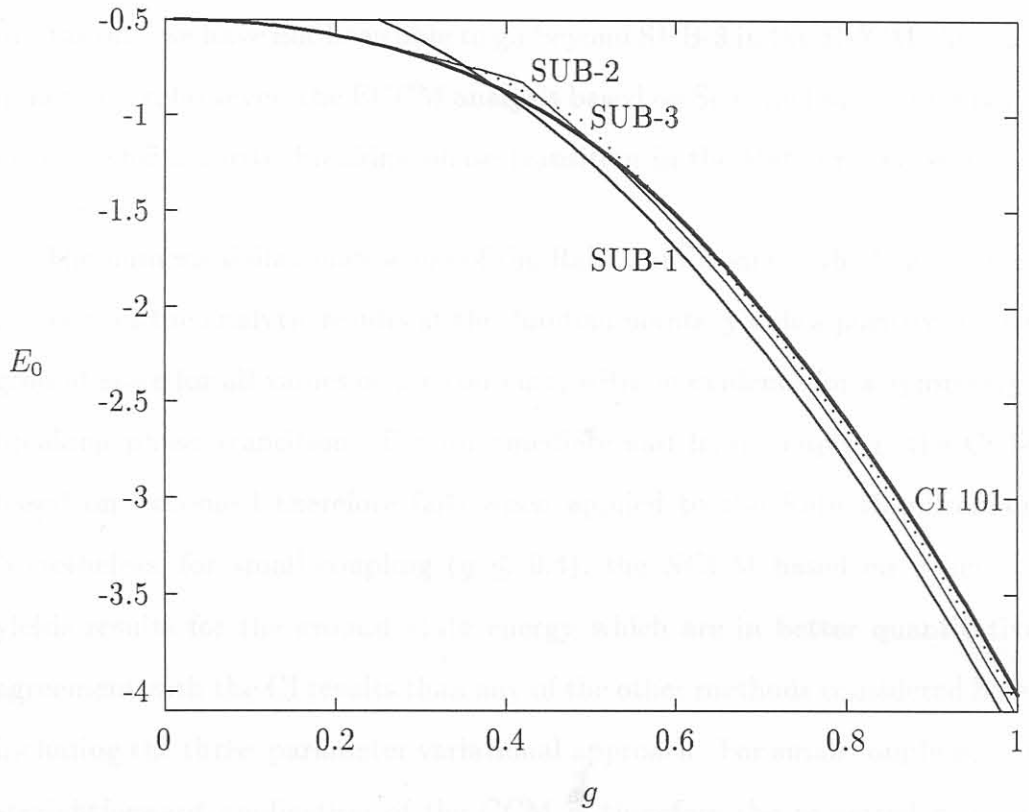

where we also present the results of a numerical SUB-N, $N = 2, 3$, ECCM calculation of the Rabi ground–state energy as a function of the coupling g. Here similar behaviour occurs to that observed in the SUB-1 case. Although the ground–state energy approximates the CI result quite closely for all g, it is evident from the graph there is a narrow coupling region around $g \sim 0.4$ where smooth SUB-2 and SUB-3 ECCM solutions cannot be found. In Table 5.1, we tabulate some of the SUB-3 ECCM coefficients, and it is clear from the behaviour of the coefficients with odd index n that the symmetry of the ECCM ground state is in fact broken at $g \approx 0.37$. This in good agreement with the NCCM SUB-2 result based on the same scheme, for which the even–parity ground–state solution terminates at $g = 0.397$. Due to numerical limitations, we have not been able to go beyond SUB-3 in the ECCM. At least in low order, however, the ECCM analysis based on Scheme I provides further evidence for a parity–breaking phase transition in the Rabi ground state.

The numerical diagonalization of the Rabi Hamiltonian, which accurately reproduces the analytic results at the Juddian points, yields a positive–parity ground state for all values of the coupling, with no evidence for a symmetry–breaking phase transition. For intermediate and large coupling, the CCM based on Scheme I therefore fails when applied to the Rabi Hamiltonian. Nonetheless, for small coupling ($g \leq 0.4$), the NCCM based on Scheme I yields results for the ground–state energy which are in better quantitative agreement with the CI results than any of the other methods considered here, including the three–parameter variational approach. For small coupling, this straightforward application of the CCM is therefore the preferred *a priori* method for determining the Rabi ground–state energy accurately and quickly.

Table 5.1: *The behaviour of the SUB-3 ECCM Scheme I coefficients as a function of the coupling g for the ground state of the scaled resonant ($\omega = \omega_0 = 1$) Rabi Hamiltonian. Coefficients of both even and odd order n are nonzero for $g \geq 0.38$, indicating that the ECCM ground state is of mixed parity in this coupling regime. The odd order coefficients vanish abruptly between $g = 0.38$ and $g = 0.37$, and are effectively zero for $g \leq 0.37$, where the ground state is therefore of positive parity.*

g	n	$s_n^{(1)}$	$s_n^{(2)}$	$\sigma_n^{(1)}$	$\sigma_n^{(2)}$
0.50	1	-5.126×10^{-1}	1.717×10^{-1}	-7.549×10^{-1}	1.843×10^{-1}
	2	1.348×10^{-1}	-1.902×10^{-1}	1.020×10^{-1}	-9.711×10^{-2}
	3	1.164×10^{-2}	-3.941×10^{-2}	2.366×10^{-2}	-3.648×10^{-2}
0.45	1	-3.508×10^{-1}	1.217×10^{-1}	-5.315×10^{-1}	1.457×10^{-1}
	2	1.359×10^{-1}	-1.992×10^{-1}	1.391×10^{-1}	-1.312×10^{-1}
	3	1.157×10^{-2}	-3.620×10^{-2}	2.727×10^{-2}	-3.927×10^{-2}
0.40	1	-2.095×10^{-1}	7.465×10^{-2}	-3.123×10^{-1}	9.821×10^{-2}
	2	1.184×10^{-1}	-1.876×10^{-1}	1.456×10^{-1}	-1.508×10^{-1}
	3	9.046×10^{-3}	-2.363×10^{-2}	1.884×10^{-2}	-2.850×10^{-2}
0.39	1	-1.706×10^{-1}	6.100×10^{-2}	-2.529×10^{-1}	8.194×10^{-2}
	2	1.137×10^{-1}	-1.841×10^{-1}	1.458×10^{-1}	-1.547×10^{-1}
	3	7.747×10^{-3}	-1.939×10^{-2}	1.568×10^{-2}	-2.402×10^{-2}
0.38	1	-1.195×10^{-1}	4.287×10^{-2}	-1.762×10^{-1}	5.885×10^{-2}
	2	1.086×10^{-1}	-1.802×10^{-1}	1.458×10^{-1}	-1.588×10^{-1}
	3	5.701×10^{-3}	-1.366×10^{-2}	1.121×10^{-2}	-1.742×10^{-2}
0.37	1	3.356×10^{-17}	-1.206×10^{-17}	4.888×10^{-17}	-1.683×10^{-17}
	2	1.031×10^{-1}	-1.761×10^{-1}	1.453×10^{-1}	-1.628×10^{-1}
	3	-1.649×10^{-18}	3.807×10^{-18}	-3.222×10^{-18}	5.063×10^{-18}
0.36	1	2.350×10^{-21}	-8.791×10^{-22}	3.414×10^{-21}	-1.207×10^{-21}
	2	9.971×10^{-2}	-1.729×10^{-1}	1.383×10^{-1}	-1.601×10^{-1}
	3	-1.208×10^{-22}	2.550×10^{-22}	-1.423×10^{-22}	2.939×10^{-22}
0.35	1	9.415×10^{-27}	-3.648×10^{-27}	1.344×10^{-26}	-4.852×10^{-27}
	2	9.624×10^{-2}	-1.696×10^{-1}	1.313×10^{-1}	-1.573×10^{-1}
	3	-4.714×10^{-28}	9.446×10^{-28}	-2.732×10^{-28}	9.122×10^{-28}
0.30	1	6.794×10^{-60}	-2.858×10^{-60}	8.247×10^{-60}	-3.350×10^{-60}
	2	7.775×10^{-2}	-1.505×10^{-1}	9.785×10^{-2}	-1.411×10^{-1}
	3	-1.556×10^{-61}	3.143×10^{-61}	4.082×10^{-61}	-1.579×10^{-61}

5.3 Incompleteness of the CCM ground–state ansatz

It is possible to illustrate numerically that the breakdown of the method is formally due to the incompleteness, to any finite order, of the exponential CCM ansatz (3.3) for the ground–state wave function for the model state and creation operators of Scheme I. We investigate whether it is possible, to good approximation for all values of the coupling g, to write

$$|\Psi_{CI}\rangle(g) = e^{S}|\Phi\rangle \; . \tag{5.4}$$

Here $|\Psi_{CI}\rangle(g)$ represents the (essentially exact) positive–parity ground–state ket determined as a function of g via the CI diagonalization, $|\Phi\rangle = |0\rangle|\downarrow\rangle$ is the noninteracting model state, and S is the cluster correlation operator (5.1) of Scheme I in the SUB-N approximation, restricted to terms of even parity as before. We expand both sides of (5.4) in a basis consisting of bosonic oscillator states multiplied by eigenfunctions of σ^z, and determine the coefficients $\left\{s_n^{(1)}(g), s_n^{(2)}(g)\right\}$, $n = 2, 4, 6, \ldots, N$, via term–by–term comparison. Due to the intermediate normalization condition (3.4) imposed by the CCM, the state $|\Psi_{CI}\rangle(g)$ must be scaled so that the coefficient of $|0\rangle|\downarrow\rangle$ is unity. For the sequence $s_2^{(i)}(g), s_4^{(i)}(g), \ldots, s_n^{(i)}(g), \ldots; i = 1, 2$, we numerically determine the ratio

$$R^{(i)}(g) \equiv \lim_{n\to\infty} \left| \frac{s_{n+2}^{(i)}(g)}{s_n^{(i)}(g)} \right| \; , \qquad i = 1, 2 \; . \tag{5.5}$$

At resonance ($\omega = \omega_0 = 1$),.we find

$$\begin{aligned} R^{(1)} < 1,\ R^{(2)} < 1 \qquad & \text{at} \quad g = 0.665 \\ R^{(1)} \approx 1,\ R^{(2)} \approx 1 \qquad & \text{at} \quad g \approx 0.8 \\ R^{(1)} > 1,\ R^{(2)} > 1 \qquad & \text{at} \quad g = 1.0\ . \end{aligned} \tag{5.6}$$

In order for a SUB-N CCM calculation to yield an acceptable approximation to the exact ground state, it is essential that one should safely be able to neglect coefficients in S of order $n > N$. Our results for the ratio R indicate that, for the model state and cluster operator of Scheme I, this is not always possible. For $g \gtrsim 0.8$, the exact resonant Rabi ground state cannot be adequately approximated by the exponential form (5.4) *for any finite value of* N, and it is in this sense that the exponential ground–state ansatz renders the CCM incomplete [1]. Note that the CCM breaks down at a value of the coupling below the critical value determined above. This incompleteness is a serious defect not only of the CCM, but also of other methods reliant on the exp S form, and is compounded by the fact that the model state and creation operators of Scheme I represent perhaps the most obvious choice for a CCM analysis of the Rabi system.

There is some overlap between the breakdown of the CCM observed here and that reported by Arponen [Ar82] who, based on a SUB-2 NCCM analysis of the LMG model, conjectured without proof that a SUB-N NCCM

[1]Note that the incompleteness, to arbitrary finite order, of the CCM based on scheme I does not contradict the fact that the CCM formalism is in principle exact — an expansion of the form (5.4) does exist for arbitrary coupling g, provided that the cluster operator S is not truncated at all. Of course, this is of no practical significance in the application of the method, where a truncation at finite order is unavoidable.

analysis of the LMG ground state based on a spherically symmetric model state would fail for any value of N. In the LMG model, however, a true phase transition occurs in the thermodynamic limit, and the breakdown of the NCCM correctly signals the onset of symmetry–breaking. Also, unlike the situation for the LMG model with a finite number of nucleons, the failure of the CCM for the Rabi Hamiltonian cannot simply be ascribed to the onset of near–degeneracy in the ground state for intermediate coupling. To show this, we have repeated the even–parity NCCM Scheme I calculation for the case of degenerate atomic levels ($\omega_0 = 0$), where the analytic positive– and negative–parity ground states (4.16) are degenerate for all couplings.

For $\omega_0 = 0$, we find that the even–parity NCCM Scheme I ground–state solution again terminates at intermediate coupling. As before, we test the CCM ansatz (3.3) for completeness by writing

$$\begin{aligned} |\Psi_+\rangle &= \sum_{n=0}^{\infty} \frac{x^{2n}}{\sqrt{(2n)!}} |2n\rangle|\downarrow\rangle - \sum_{n=0}^{\infty} \frac{x^{2n+1}}{\sqrt{(2n+1)!}} |2n+1\rangle|\uparrow\rangle \\ &= e^S |\Phi\rangle \,, \end{aligned} \tag{5.7}$$

where $|\Psi_+\rangle$ is the positive–parity ground state (4.16) with $x = 2g/\omega$ (scaled so as to meet the normalization condition (3.4)), and $|\Phi\rangle$ (S) represents the model state (even–parity cluster correlation operator) of Scheme I. Given the explicit expansion (5.7) for the exact ground state $|\Psi_+\rangle$, it can be shown analytically that

$$R_n^{(i)}(g) \equiv \frac{s_{n+2}^{(i)}(g)}{s_n^{(i)}(g)} = \frac{a_{n+1}^{(i)}}{a_n^{(i)}} x^2 = \frac{a_{n+1}^{(i)}}{a_n^{(i)}} \left(\frac{4g^2}{\omega} \right) \,, \qquad i = 1, 2 \,, \tag{5.8}$$

where the parameters $\{a_n^{(i)}\}; i = 1, 2$ are independent of the coupling g. These parameters obey a set of algebraic recurrence relations which we have not

been able to solve in closed form. We therefore scale out the ω–dependence by setting $\omega = 1$, and numerically investigate the ratios

$$A_n^{(1)} \equiv \frac{a_{n+1}^{(1)}}{a_n^{(1)}}$$
$$A_n^{(2)} \equiv \frac{a_{n+1}^{(2)}}{a_n^{(2)}} \tag{5.9}$$

as a function of n. We find that both quantities increase uniformly with increasing n. At $n = 51$, the ratio $A_n^{(2)}$ has converged to the value 0.406, and $A_n^{(1)}$ attains the value 0.396. Although the convergence of $A_n^{(1)}$ with increasing n is not rapid enough to state the true limiting value with certainty, the important conclusion is that

$$A^{(1)} \equiv \lim_{n\to\infty} A_n^{(1)} \geq 0.396$$
$$A^{(2)} \equiv \lim_{n\to\infty} A_n^{(2)} = 0.406\ . \tag{5.10}$$

Therefore

$$\begin{aligned} R^{(1)}(g) &\equiv \lim_{n\to\infty} R_n^{(1)}(g) = 4A^{(1)}g^2 \geq 1.584g^2 \\ R^{(2)}(g) &\equiv \lim_{n\to\infty} R_n^{(2)}(g) = 4A^{(2)}g^2 = 1.624g^2\ , \end{aligned} \tag{5.11}$$

and it is clear that

$$\begin{aligned} R^{(1)}(g) &\geq 1 \text{ for } g \geq \frac{1}{\sqrt{1.584}} = 0.795 \\ R^{(2)}(g) &\geq 1 \text{ for } g \geq \frac{1}{\sqrt{1.624}} = 0.785\ . \end{aligned} \tag{5.12}$$

Thus for $g \geq 0.785$ (and, depending on the true limiting value $A^{(1)}$, possibly even below $g = 0.785$), the exact positive–parity ground state $|\Psi_+\rangle$ cannot, to any finite order, be adequately approximated by the $\exp S$ form required by the CCM. This proof of incompleteness for the case $\omega_0 = 0$ is strengthened by the fact that, unlike the $\omega_0 \neq 0$ case where the exact ground state had to be determined numerically, the state $|\Psi_+\rangle$ is here known analytically.

5.4 An alternative CCM calculation based on the noninteracting model state

Given the above incompleteness for scheme I, we are therefore led to consider alternative CCM schemes for the Rabi Hamiltonian. Using (4.11) and (4.37), it is easily shown that the positive–parity $g \to \infty$ ground state (4.16) may be written in the form

$$|\Psi_+\rangle = e^{-2g^2/\omega^2} \exp\left\{\left(-\frac{2g}{\omega}\right) b^\dagger \sigma^x\right\} |0\rangle|\downarrow\rangle \ . \tag{5.13}$$

Thus for Scheme II (see Table D.1), we retain the noninteracting model state $|\Phi\rangle = |0\rangle|\downarrow\rangle$ of Scheme I, but introduce a new correlation operator

$$S = \sum_{n=1}^{\infty} s_n \left(c^\dagger\right)^n \ , \qquad c^\dagger \equiv b^\dagger \sigma^x \ . \tag{5.14}$$

The nested commutator expansion (3.8), although non–terminating, now assumes a closed (exponential) form, and the CCM ground–state energy is given by

$$E_0^{\mathrm{NCCM,II}} = -\frac{1}{2}\omega_0 + 2gs_1 \ . \tag{5.15}$$

This calculation is also restricted to the positive–parity sector, as is obvious from the form of both the model state and the CCM creation operators. Explicit expressions for the similarity transformed Hamiltonian and NCCM equations for Scheme II are given in Appendix D.

We find that the CCM yields results (not shown here) for the ground–state energy which again fail, in a manner very similar to that observed for Scheme I, at intermediate and large coupling. Although we have not proved this, the breakdown of the NCCM based on Scheme II for intermediate

coupling is almost certainly due to an incompleteness similar to that shown for Scheme I. Furthermore, the failure of this approach at large coupling is particularly significant, since it is obvious from (5.13) that the $g \to \infty$ ground state $|\Psi_+\rangle$ is of SUB-1 form with $s_1 = -2g/\omega$. The two–parameter variational calculation presented in Chapter 4, which was based on a trial state of SUB-1 Scheme II form, correctly determines the limiting behaviour of s_1 as $g \to \infty$. For the CCM, which is based on a similarity rather than a unitary transform (see the discussion in Chapter 3), it can however be shown analytically (see Appendix D) that $s_1 = -2g/(\omega + \omega_0)$ in the SUB-1 approximation, and at resonance the SUB-1 result is thus not even correct to leading order. Thus, for Scheme II, the CCM also fails as a result of the non–Hermiticity of the method.

Chapter 6

Successful Application of the CCM to the Rabi Hamiltonian

In order to determine whether quantitatively accurate results for the Rabi Hamiltonian can be obtained using a CCM calculation which takes into account the symmetries of the Hamiltonian, we investigate the use of various coupling–dependent CCM model states for the Rabi Hamiltonian, as well as the application of the method to a unitary transformed Hamiltonian.

6.1 Coupling–dependent CCM model states for the Rabi Hamiltonian

It is significant that, like TIPT, the CCM based on the noninteracting model state of Schemes I and II breaks down in the transitional region where the Rabi ground state undergoes the marked change in character discussed in Section 4.2. This suggests that the noninteracting model state should be replaced by a coupling–dependent model state capable of following this character change. For Scheme III, we therefore perform an NCCM calculation based on a model state of the form $|\Phi\rangle = |\Psi_+\rangle$ [see (4.16)], which is a coupling–dependent, even–parity superposition of the coherent states (4.11), and which we shall thus refer to as the coherent superposition (CS) model state (see Table D.1). The CS model state is an exact eigenstate of $H_{\rm Rabi}$ not only in the $\omega_0 = 0$ ($g \to \infty$) limit, but also in the $g = 0$ limit, where it reduces to the noninteracting model state. The correlation operator

$$S = \sum_{n=1}^{\infty} s_n \left(c^\dagger\right)^n , \qquad c^\dagger \equiv b^\dagger \sigma^x + \frac{2g}{\omega} \tag{6.1}$$

for Scheme III again incorporates the required even–parity symmetry in the CCM ground state. Note that the CCM creation operators $\left\{\left(c^\dagger\right)^n\right\}$ have been chosen so as to satisfy the requirement that the set $\left\{\left(c^\dagger\right)^n |\Phi\rangle\right\}$ is complete, and also so that their Hermitian conjugates $\{c^n\}$ conveniently annihilate the CS model state. As for Scheme II, the nested commutator expansion (3.8), rather than terminating, assumes a closed form (see Equation (D.21) in Appendix D), and one obtains for the ground–state energy

$$E_0^{\rm NCCM,III} = -\frac{1}{2}\,\omega_0\, e^{-8g^2/\omega^2}\, \exp\left\{\sum_{n=1}^{\infty} s_n \left(\frac{4g}{\omega}\right)^n\right\} - \frac{4g^2}{\omega} . \tag{6.2}$$

We have used *Mathematica* [Mat] to set up the energy functional $\overline{H}$ and the CCM equations (3.14) for the coefficients $\{s_n\}$ and $\{\tilde{s}_n\}$ (see Equations (D.23) and (D.25) in Appendix D).

In Table 6.1 we tabulate the resonant Scheme III ground–state energy results, which are indistinguishable from the CI results on the scale of our

Table 6.1: *The ground–state energy of the scaled resonant ($\omega = \omega_0 = 1$) Rabi Hamiltonian as a function of the coupling g as determined via a SUB-10 NCCM Scheme III calculation, labelled $E_0^{\mathrm{NCCM,III}}$, and via a SUB-10 NCCM analysis based on Scheme IV, labeled $E_0^{\mathrm{NCCM,IV}}$ (see Table D.1). For comparison, we also tabulate results obtained via a CI diagonalization in a basis of 101 even–parity states, labelled E_0^{CI}, as well as the results of the benchmark three–parameter variational calculation, labelled E_0^{PBV3}.*

g	E_0^{CI}	$E_0^{\mathrm{NCCM,IV}}$	$E_0^{\mathrm{NCCM,III}}$	E_0^{PBV3}
0.0	-0.50000	-0.50000	-0.50000	-0.50000
0.1	-0.52020	-0.52020	-0.52020	-0.52020
0.2	-0.58333	-0.58333	-0.58333	-0.58333
0.3	-0.69762	-0.69762	-0.69763	-0.69757
0.4	-0.87855	-0.87847	-0.87882	-0.87822
0.5	-1.14795	-1.14642	-1.14964	-1.14676
0.6	-1.52396	-1.51961	-1.52343	-1.52211
0.7	-2.00825	-2.00414	-1.99657	-2.00685
0.8	-2.59070	-2.58827	-2.57057	-2.58998
0.9	-3.26191	-3.26061	-3.24192	-3.26158
1.0	-4.01693	-4.01620	-4.00028	-4.01677

figures, as a function of g, along with the benchmark three–parameter variational ground–state energy results. To moderate order (SUB-10), the results show good agreement, over the full coupling spectrum, with the results of the CI diagonalization. Some comments are however in order: To higher order ($\sim$ SUB-20 and above), we find that the NCCM Scheme III solution breaks down in isolated coupling regions, possibly for numerical reasons. Furthermore, for Scheme III, the NCCM result for $\langle \sigma_z \rangle$ (which is shown in Figure 6.1 along with the Scheme I results for comparison; explicit expressions for $\langle \sigma_z \rangle$ in both schemes are given in Equations (D.5) and (D.27) in Appendix D) also fails quantitatively in and above the transitional region, even in moderate order (SUB-10) where the CCM ground–state energy is in very good agreement with the CI result. In this regard, it is significant that the Scheme III analysis fails to resolve the (admittedly small) difference between the exact ground–state energy and the so–called baseline energy $-4g^2/\omega$ for $g \sim 1$. Thus the CS model state of Scheme III, though a definite improvement on the noninteracting model state, is still not entirely capable of tracking the character change in the Rabi ground state.

We have therefore also performed an NCCM calculation based on a coupling–dependent model state of the even–parity two–parameter variational form (4.38) (see Scheme IV in Table D.1), which also reduces to the exact ground state in both the limits of small and infinitely large coupling. For Scheme IV, we use the same (even–parity) correlation operator S as for Scheme II. This computationally convenient choice has some drawbacks: The set of states $\{\left(c^\dagger\right)^n |\Phi\rangle\}$; $n = 0, 1, 2, \ldots$ does not span the many–body Hilbert space, and the Hermitian–adjoint destruction operators $\{c^n\}$, $n \geq 1$ do not annihilate

Figure 6.1: *The expectation value of σ_z in the ground state of the scaled resonant ($\omega = \omega_0 = 1$) Rabi Hamiltonian as a function of the coupling g as determined via a SUB-N, N=10,50, NCCM analysis based on Scheme I (thin solid lines), as well as via a SUB-10 NCCM analysis based on Scheme III (dotted line), compared to results obtained via a CI diagonalization (solid line) in a basis of 101 even-parity states.*

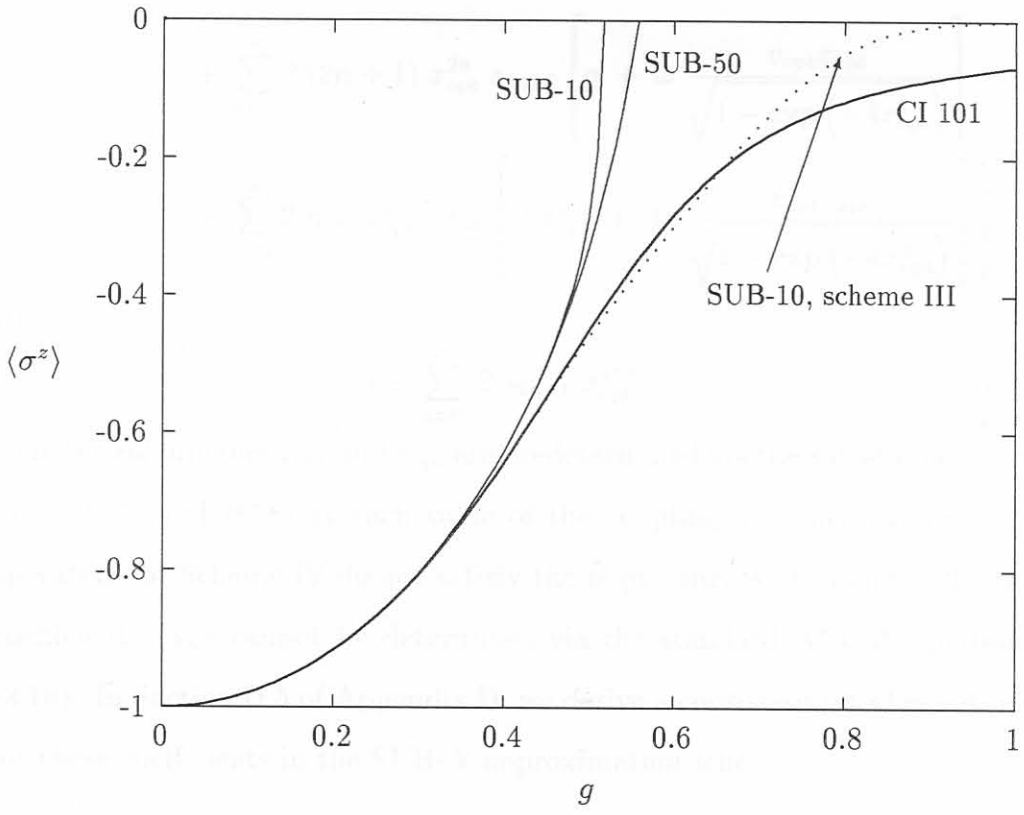

the model state. The purpose of this calculation, however, is simply to show that the CCM may be successfully applied to the Rabi Hamiltonian *provided* that a suitable model state is chosen. As for Schemes II and III, the nested commutator expansion (3.8) assumes a closed form (see Equation (D.28) in

Appendix D), and we obtain for the ground–state energy in Scheme IV

$$
\begin{aligned}
E_0^{\mathrm{NCCM,IV}} \;=\; & \frac{1}{\sqrt{1+v_{\mathrm{opt}}^2}} \Bigg\{ \frac{1}{2}\,\omega_0\,\cosh\alpha\,\left(v_{\mathrm{opt}}^2-1\right) \\
& + \omega_0\,\sinh\alpha\,\frac{v_{\mathrm{opt}}\exp\left(-2x_{\mathrm{opt}}^2\right)}{\sqrt{1-\exp\left(-4x_{\mathrm{opt}}^2\right)}} \\
& + 8\,g\,\frac{v_{\mathrm{opt}}x_{\mathrm{opt}}}{\sqrt{1-\exp\left(-4x_{\mathrm{opt}}^2\right)}} \;+\; \omega\,x_{\mathrm{opt}}^2\,\left(\tanh x_{\mathrm{opt}}^2 + v_{\mathrm{opt}}^2\coth x_{\mathrm{opt}}^2\right) \\
& + \sum_{n=0}^{\infty} 2\,(2n+1)\,x_{\mathrm{opt}}^{2n}\,s_{2n+1}\left[g \;+\; \omega\,\frac{v_{\mathrm{opt}}x_{\mathrm{opt}}}{\sqrt{1-\exp\left(-4x_{\mathrm{opt}}^2\right)}}\right] \\
& + \sum_{n=1}^{\infty} 2\,n\,\omega\,x_{\mathrm{opt}}^{2n-2}\,s_{2n}\left[\omega\,x_{\mathrm{opt}}^2 \;+\; 4g\,\frac{v_{\mathrm{opt}}x_{\mathrm{opt}}}{\sqrt{1-\exp\left(-4x_{\mathrm{opt}}^2\right)}}\right]\Bigg\}, \qquad (6.3)
\end{aligned}
$$

with

$$
\alpha \equiv \sum_{n=0}^{\infty} 2\,s_{2n+1}\,x_{\mathrm{opt}}^{2n+1}\,. \qquad (6.4)
$$

Here the parameters x_{opt} and v_{opt} are predetermined via the variational equations (C.7) and (C.8) at each value of the coupling g. Since the creation operators for Scheme IV do not satisfy the requirements (3.1) and (3.2), the coefficients $\{s_n\}$ cannot be determined via the standard NCCM equations (3.16). In Section D.5 of Appendix D, we derive a consistent set of equations for these coefficients in the SUB-N approximation scheme.

It is clear from ground–state energy results shown in Table 6.1 that the NCCM based on Scheme IV yields excellent agreement with the CI diagonalization for all couplings. Thus it is possible to obtain very good CCM ground–state energy results for the Rabi Hamiltonian, provided that a coupling–dependent model state is chosen which, besides the parity symmetry, also incorporates the important physical features of the exact ground

state, in particular the change in character in the transitional region. It is also straightforward to adapt the NCCM Scheme III and IV approaches above in order to determine the odd–parity first excited state energy E_1 via the CCM (see Table D.2 in Appendix D). In Table 6.2 we tabulate the NCCM Scheme IV results for E_1, which are again in very good agreement with the CI results. Note, however, that when considered over the full coupling spectrum, the three–parameter variational calculation outperforms even the Scheme IV

Table 6.2: *The first excited state energy of the scaled resonant ($\omega = \omega_0 = 1$) Rabi Hamiltonian as a function of the coupling g as determined via a SUB-10 NCCM Scheme IV calculation, labelled $E_1^{\mathrm{NCCM,IV}}$, compared to results obtained via a CI diagonalization in a basis of 101 odd–parity states, labelled E_1^{CI}, and via the benchmark three–parameter variational calculation, labelled E_1^{PBV3}.*

g	E_1^{CI}	$E_1^{\mathrm{NCCM,IV}}$	E_1^{PBV3}
0.0	0.50000	0.50000	0.50000
0.1	0.28067	0.28064	0.28074
0.2	0.02337	0.02328	0.02396
0.3	-0.27391	-0.27386	-0.27237
0.4	-0.61609	-0.61555	-0.61376
0.5	-1.01018	-1.00895	-1.00774
0.6	-1.46444	-1.46268	-1.46256
0.7	-1.98701	-1.98518	-1.98587
0.8	-2.58432	-2.58283	-2.58373
0.9	-3.26028	-3.25924	-3.25999
1.0	-4.01658	-4.01590	-4.01643

NCCM calculation at a fraction of the computational cost.

Due to the fact that the creation operators and model state of Scheme IV do not satisfy the requirements (3.1) and (3.2), it is difficult to set up a consistent set of equations for the NCCM bra state coefficients $\{\tilde{s}_n\}$. We have therefore not calculated the expectation value of observables other than the Hamiltonian in the NCCM Scheme IV ground state. However, given the ground and first excited state energy results presented above, we do not expect that the CCM would yield more accurate results for quantities such as σ^z than those obtained via the even–parity three–parameter variational calculation.

6.2 The method of unitary transformations

The method of unitary transformations offers an alternative approach to the application of the CCM to the Rabi Hamiltonian. In this approach, a unitary rotation $U = \exp R$, $R^\dagger = -R$ is applied to the Hamiltonian, leaving the spectrum unchanged, and the CCM is then applied to the transformed Hamiltonian $H^U = U^\dagger H U$. In their analysis of the multimode Rabi system, Wong and Lo [Wo96b] applied a unitary displacement transformation of the form

$$U_1 = \exp R_1, \quad R_1 = \frac{2g}{\omega}\left(b^\dagger - b\right) , \tag{6.5}$$

to the Hamiltonian. We have performed an NCCM calculation, based on the model state and creation operators of Scheme I, for the transformed Rabi Hamiltonian $H^{U_1}_{\text{Rabi}}$. Since the transformation (6.5) does not conserve the

parity Π_{rabi}, this NCCM calculation is not restricted to the even–parity sector as before, and it is no longer possible within the CCM to distinguish between the ground and first excited states on the basis of their parity symmetry. Due to the disregard for the parity symmetry, the CCM ground–state energy results are quantitatively inaccurate in and above the transitional region (as is the case for the multimode Rabi system considered in [Wo96b]). Futhermore, since the results are considerably less accurate than those obtained via, say, the even–parity two–parameter variational calculation, these results are not presented here.

We have also considered the application of the CCM to the transformed Hamiltonian $H_{\text{Rabi}}^{U_2}$, where U_2 represents a more general unitary rotation of the form

$$U_2 = \exp R_2, \quad R_2 = \beta\left(b^\dagger - b\right) + i\gamma\sigma^y \,. \tag{6.6}$$

However, since the transformation (6.6) does not conserve parity, the same comments apply as for (6.5). The NCCM ground–state energy results (not shown here) are in excellent agreement with the diagonalization results for large coupling ($g \geq 0.7$), and are comparable to the results obtained via the three–parameter variational calculation in this region. The CCM solution, however, terminates upon entering the transitional region from above, and is therefore not shown here.

Thus, despite moderate success, neither of the above CCM calculations based a unitary transformed Rabi Hamiltonian yield good results over the full coupling spectrum. This is at least partly due to the fact that both rotations destroy the parity symmetry Π_{Rabi}. One may also consider a parity–

conserving unitary transformation of the Rabi Hamiltonian of the form

$$U_3 = \exp R_3, \quad R_3 = \frac{2g}{\omega}\left(b - b^\dagger\right)\sigma^x \,. \tag{6.7}$$

The algebra involved in an NCCM analysis of the rotated Hamiltonian $H_{\rm Rabi}^{U_3}$ becomes prohibitively involved beyond the level of the SUB-1 approximation. Note however that, since the CS model state $|\Psi_+\rangle$ of Scheme III may be written in the form

$$|\Psi_+\rangle = e^{-x^2/2}\exp R_3|0\rangle|\downarrow\rangle \,, \tag{6.8}$$

it is clear that a SUB-1 NCCM Scheme I calculation on the rotated Hamiltonian $H_{\rm Rabi}^{U_3}$ is equivalent to a SUB-1 NCCM Scheme III calculation on the unrotated Rabi Hamiltonian (4.1). Although this is no longer true in the SUB-N, $N \geq 2$ approximation, we do not expect the results of this calculation to differ qualitatively from those obtained via our NCCM Scheme III analysis of the unrotated Rabi Hamiltonian.

Chapter 7

The Linear $E \otimes e$ Jahn–Teller and Pseudo Jahn–Teller Hamiltonians

The linear $E \otimes e$ Jahn–Teller (JT) and pseudo Jahn–Teller (PJT) Hamiltonians are of topical interest in the field of quantum chemistry, and, in this chapter, we therefore discuss the relevance of these Hamiltonians in this field. We present a representation–independent operator approach to the numerical diagonalization of H_{JT} and H_{PJT} which also simplifies the analysis of the isolated exact (Juddian) solutions for these models. In particular, we give a simple closed form for the analytic ground–state wave function of the linear $E \otimes e$ resonant pseudo Jahn–Teller (RPJT) Hamiltonian. An analysis of the ground–state behaviour of the linear $E \otimes e$ JT and PJT models is also presented. Finally, we review the results of some earlier approximate

many–body analyses of these systems. The application of the CCM to the linear $E \otimes e$ JT and PJT Hamiltonians forms the subject of Chapter 8, and is therefore not discussed here.

7.1 Discussion of the Hamiltonians

The linear $E \otimes e$ PJT Hamiltonian

$$\begin{aligned} H_{\rm PJT} &= \frac{1}{2}\omega_0\,\sigma^z + \omega\,N_b + \eta\,\left(b_1^\dagger + b_1\right)\sigma^x - \eta\,\left(b_2^\dagger + b_2\right)\sigma^y \\ &= \frac{1}{2}\omega_0\,\sigma^z + \omega\,N_b + \gamma\,\left(a_1 + a_2^\dagger\right)\sigma^+ + \gamma\,\left(a_1^\dagger + a_2\right)\sigma^-, \end{aligned} \tag{7.1}$$

with $\gamma \equiv \eta/\sqrt{2}$ and the bosonic number operator N_b defined by

$$N_b \equiv b_1^\dagger b_1 + b_2^\dagger b_2 = a_1^\dagger a_1 + a_2^\dagger a_2\,, \tag{7.2}$$

was introduced in Chapter 2. The bosonic creation and annihilation operators in the first (second) line of (7.1) refer to modes of linear (circular) polarization, and the zero–point energy ω of these two modes has been neglected. The (pure) linear $E \otimes e$ JT Hamiltonian

$$\begin{aligned} H_{\rm JT} &= \omega\,N_b + \eta\,\left(b_1^\dagger + b_1\right)\sigma^x - \eta\,\left(b_2^\dagger + b_2\right)\sigma^y \\ &= \omega\,N_b + \gamma\,\left(a_1 + a_2^\dagger\right)\sigma^+ + \gamma\,\left(a_1^\dagger + a_2\right)\sigma^-, \end{aligned} \tag{7.3}$$

may formally be regarded as the special case of $H_{\rm PJT}$ where the two fermionic levels are degenerate ($\omega_0 = 0$). Both $H_{\rm JT}$ and $H_{\rm PJT}$ have the symmetries

$$\Pi_{\rm PJT} = \Pi_{\rm JT} = \exp\left\{i\pi\left[N_b + \frac{1}{2}\left(\sigma^z + 1\right)\right]\right\} \tag{7.4}$$

and

$$J = i\left(b_1^\dagger b_2 - b_1 b_2^\dagger\right) + \frac{1}{2}\sigma^z = a_1^\dagger a_1 - a_2^\dagger a_2 + \frac{1}{2}\sigma^z\,, \tag{7.5}$$

where the expression in terms of operators referring to modes of circular polarization highlights the physical meaning of the angular momentum component J in terms of helicity. It is clear that the eigenvalues of J are elements of the set $\left\{\ldots, -\frac{5}{2}, -\frac{3}{2}, -\frac{1}{2}, \frac{1}{2}, \frac{3}{2}, \frac{5}{2}, \ldots\right\}$.

7.1.1 Vibronic interactions and non–adiabaticity in quantum chemistry

The linear $E \otimes e$ JT and PJT Hamiltonians are clearly relevant in quantum optics, where they describe a simple extension of the Rabi Hamiltonian to the case of two degenerate perpendicularly polarized field modes. The Hamiltonians can also be used to model a two–level fermion moving in a circular ring which can undergo elliptical deformation in a plane [Lo58]. Both Hamiltonians, and H_{JT} in particular, have however been extensively studied in quantum chemistry [Bera, Berb], and we present here an introduction to non–adiabatic models in this field.

One of the most important simplifications of the Schrödinger equation for the electrons and nuclei in a molecular system is the separation of their respective motions in the adiabatic approximation [Bo27, Bor]. Based on the mass difference between an electron and a typical nucleus, it is assumed in this approximation that every instantaneous (fixed) configuration Q of the nuclei corresponds to a set of stationary electronic states. The Q–dependent (or so-called vibronic) electron–nuclear interactions which couple different electronic states are ignored, and each electronic energy eigenvalue is used

to construct a corresponding adiabatic potential (also known as a potential–energy surface [Mo87]). The adiabatic potential represents the potential energy of the nuclei in the mean field of the electrons in the corresponding electronic state, and the molecular structure for this state is determined by finding the nuclear configuration Q_0 which minimizes the adiabatic potential.

Landau argued [Berb] that, in the adiabatic approximation, a given symmetric nuclear configuration Q_s would be unstable if any of the corresponding electronic states were degenerate, and that the degeneracy would result in nuclear displacements which destroy the symmetry of Q_s. This statement is not entirely correct. For a system where n sheets of the adiabatic potential intersect (corresponding to n–fold electronic degeneracy) at a particular nuclear configuration Q^*, it is true that at least one of these sheets does not have an extremum at the point Q^* — this is the essence of the Jahn–Teller theorem [Ja37, Berb]. However, the adiabatic potential in the neighbourhood of the point of instability, Q^*, cannot be interpreted as the potential energy of the nuclei in the mean field of the electrons, and therefore cannot be used to draw conclusions about the nuclear behaviour. Rather, the correct conclusion is that the instability at Q^* implies that it is necessary to reexamine the validity of the adiabatic potential in this region.

For the nuclear motion to be localized about a given minimal configuration Q_0, the quantum ω of small nuclear vibrations about Q_0 should not allow for tunneling through the potential barrier (centered at the point Q^*) separating Q_0 from other minima. A criterion for the applicability of the

adiabatic approximation is therefore given by [Bera]

$$\omega \ll |\epsilon_n - \epsilon_k| \ , \tag{7.6}$$

where ϵ_i denotes the eigenenergy of the i–th electronic state, calculated at the point Q_0. If this condition is satisfied, the physical implication is that the adiabatic approximation is self–consistent, *i.e.* that the molecular system may be modelled as a combination of stable electronic states and localized vibrational nuclear states. If condition (7.6) is not satisfied, it is necessary to go beyond the adiabatic approximation. This requires the consideration of the vibronic electron–nuclear interactions, which couple the electronic states of the adiabatic approximation as a function of the nuclear configuration Q, and the resultant effect on the nuclear dynamics is known as the dynamical JT effect. The linear (quadratic) dynamical JT effect occurs when the vibronic interaction terms, expanded in powers of Q, are truncated at first (second) order in Q.

The linear $E \otimes e$ JT Hamiltonian $H_{\rm JT}$ represents a simple non–adiabatic molecular model of the vibronic interaction between a two–fold degenerate electronic level (E) and two degenerate nuclear vibrational modes (e). The bosonic quanta corresponding to the vibrational modes are thus phonons. In the case of electronic near–degeneracy, non–adiabatic (pseudo Jahn–Teller) effects also occur if the electronic level splitting ω_0 is comparable to the nuclear vibrational excitation energy ω. We therefore also consider the linear $E \otimes e$ PJT Hamiltonian $H_{\rm PJT}$, which generalizes the (pure) JT model to the case of nondegenerate electronic levels. In both cases it is assumed that the two levels under consideration are well separated from other electronic levels.

7.1.2 Analytic solutions in the limit of zero coupling

In the analysis of a Hamiltonian describing an interacting many–body system, the eigenbasis of the noninteracting Hamiltonian is often useful both for TIPT and the CI (diagonalization) method. The linear $E \otimes e$ JT and PJT Hamiltonians are analytic in the limit of zero coupling γ. Consider the noninteracting JT Hamiltonian $H_{\rm JT}^{\gamma=0} \equiv \omega N_b$. The exact ground states of $H_{\rm JT}^{\gamma=0}$ are the states $|0\rangle|0\rangle|\downarrow\rangle$ and $|0\rangle|0\rangle|\uparrow\rangle$, where in each case the first (second) ket refers to the bosonic occupation number vacuum for the first (second) bosonic mode, and the third ket denotes the lower ($|\downarrow\rangle$) or upper ($|\uparrow\rangle$) level of the fermionic mode. For $\gamma = 0$ these states are degenerate with ground–state energy $E_{\rm JT}^{\gamma=0} = 0$. The state $|0\rangle|0\rangle|\downarrow\rangle$ ($|0\rangle|0\rangle|\uparrow\rangle$) is of positive (negative) $\Pi_{\rm PJT}$ parity and corresponds to angular momentum component $j = -1/2$ ($j = 1/2$). The complete spectrum of $H_{\rm JT}^{\gamma=0}$ is simply determined; the n–th excited level has energy $E_n = n\omega$ and is $2\,(n+1)$–fold degenerate. The factor 2 arises from the electronic degeneracy, and there are $(n+1)$ ways to distribute the n bosonic quanta over the two modes.

In the limit of zero coupling the noninteracting PJT Hamiltonian

$$H_{\rm PJT}^{\gamma=0} \;=\; \frac{1}{2}\omega_0\,\sigma^z \;+\; \omega N_b \;, \qquad (\omega_0 > 0) \tag{7.7}$$

has the exact ground state $|0\rangle|0\rangle|\downarrow\rangle$, which uniquely corresponds to the ground–state energy $E_{\rm PJT}^{\gamma=0} = -\omega_0/2$. Here the ground state is thus of positive $\Pi_{\rm PJT}$ parity, and has angular momentum component $j = -1/2$. The determination of the complete spectrum of $H_{\rm PJT}^{\gamma=0}$, which is dependent on the relative magnitudes of ω and ω_0, is straightforward.

7.1.3 Numerical diagonalization of the JT and PJT models

Although there is strong numerical support for the conjecture of Reik *et.al.* [Re87], and although the linear $E \otimes e$ JT and PJT Hamiltonians have furthermore been written in canonical form [Sz97], the integrability of these models for arbitrary coupling γ and fermionic level splitting ω_0 has not been explicitly demonstrated. We therefore turn to the CI method, which involves the numerical diagonalization of the Hamiltonian in a finite subspace of the full Hilbert space.

For $\gamma > 0$, the Hamiltonian H_{PJT} (for arbitrary ω_0 and thus including the JT case $\omega_0 = 0$) does not commute with the bosonic number operator N_b, and the noninteracting eigenbasis is no longer the most appropriate basis for the diagonalization of the Hamiltonian. Rather, since the operators H_{PJT}, J and Π_{PJT} form a mutually commuting set, the matrix representation of H_{PJT} in a simultaneous eigenbasis of J and Π_{PJT} blocks into sectors corresponding to fixed eigenvalue j of the operator J and either positive or negative Π_{PJT}–parity. This not only results in a considerable reduction in the numerical effort involved in the diagonalization of the Hamiltonian, but also, as we will show, yields an explanation of the two–fold degeneracy of all energy levels in the spectrum of the linear $E \otimes e$ JT Hamiltonian.

We present here an operator–based approach to the construction of an appropriate simultaneous eigenbasis of the operators J and Π_{PJT}. We introduce the operator $c^\dagger$ and its Hermitian conjugate c via

$$c^\dagger \equiv \frac{1}{\sqrt{2}}\left(b_1^\dagger\sigma^x - b_2^\dagger\sigma^y\right) = \frac{1}{2}\left(a_2^\dagger\sigma^+ + a_1^\dagger\sigma^-\right)$$
$$c = \frac{1}{\sqrt{2}}\left(b_1\sigma^x - b_2\sigma^y\right) = \frac{1}{2}\left(a_2\sigma^- + a_1\sigma^+\right) . \quad (7.8)$$

It is easily shown that

$$[c, J] = \left[c^\dagger, J\right] = 0$$
$$[c, \Pi_{\rm PJT}] = \left[c^\dagger, \Pi_{\rm PJT}\right] = 0 , \quad (7.9)$$

and also that

$$\left(c^\dagger\right)^2 = \frac{1}{2}\left[\left(b_1^\dagger\right)^2 + \left(b_2^\dagger\right)^2\right] = a_1^\dagger a_2^\dagger . \quad (7.10)$$

The Hamiltonian $H_{\rm PJT}$ may, for arbitrary ω_0, be rewritten as

$$H_{\rm PJT} = \frac{1}{2}\omega_0\,\sigma^z + \omega\, N_b + 2\gamma\, c^\dagger + 2\gamma\, c , \quad (7.11)$$

where the bosonic number operator N_b assumes the form

$$N_b = 2\, c^\dagger c + J\sigma^z - \frac{1}{2} . \quad (7.12)$$

Here $J\sigma^z = cc^\dagger - c^\dagger c - \frac{1}{2}$, and the parity operator $\Pi_{\rm PJT}$ retains the form (7.4). The operators c, $c^\dagger$ and σ^z obey the relations [1]

$$\left[c, \left(c^\dagger\right)^{2n}\right] = n\left(c^\dagger\right)^{2n-1} , \qquad \left[c, \left(c^\dagger\right)^{2n+1}\right] = \left(c^\dagger\right)^{2n}\left(J\sigma^z + n + \frac{1}{2}\right)$$
$$\left[\sigma^z, c^{2n}\right] = \left[\sigma^z, \left(c^\dagger\right)^{2n}\right] = \left[\sigma^z, c^{2n+1}\right]_+ = \left[\sigma^z, \left(c^\dagger\right)^{2n+1}\right]_+ = 0 \quad (7.13)$$

for $n = 0, 1, 2, \ldots$. It then follows that

$$\left[N_b, \left(c^\dagger\right)^n\right] = n\left(c^\dagger\right)^n , \qquad [c, N_b] = c \quad (7.14)$$

[1] The subscript + denotes an anticommutator.

and, as expected,

$$[J, \sigma^z] = [J, N_b] = 0 \, . \tag{7.15}$$

Consider an arbitrary j–sector, which is an infinite–dimensional subspace of the full Hilbert space. We postulate that the requirement

$$c|\Psi\rangle_j^{\text{ref}} = 0 \tag{7.16}$$

uniquely determines the state $|\Psi\rangle_j^{\text{ref}}$, which is a reference state of angular momentum component j that will be used as a starting vector for the construction of a suitable basis for this sector. Using (7.13), one obtains

$$c\left\{\sigma^z|\Psi\rangle_j^{\text{ref}}\right\} = -\sigma^z c|\Psi\rangle_j^{\text{ref}} = 0 \, , \tag{7.17}$$

and from (7.15) it follows that the state $\left\{\sigma^z|\Psi\rangle_j^{\text{ref}}\right\}$ is also an eigenstate of J with eigenvalue j. The assumed uniqueness of $|\Psi\rangle_j^{\text{ref}}$ implies that the reference state must therefore be an eigenstate $|\Psi\rangle_{j,s}^{\text{ref}}$ of σ^z with eigenvalue $s \in \{-1, 1\}$. It follows from a similar argument using (7.14) and (7.15) that the reference state must also be an eigenstate of the bosonic number operator N_b with eigenvalue $n_b \in \{0, 1, 2, \ldots\}$. Using the form (7.12) and the requirement (7.16), it is clear that

$$n_b \; = \; j\, s \; - \; \frac{1}{2} \geq 0 \, , \tag{7.18}$$

and also that

$$\Pi_{\text{PJT}} \, |\Psi\rangle_{j,s}^{\text{ref}} \; = \; \exp\left[i\pi \left(j + \frac{1}{2}\right) s\right] \, |\Psi\rangle_{j,s}^{\text{ref}} \, . \tag{7.19}$$

There are now two possibilities:

1. The eigenvalue j is positive, so that $j = p + 1/2$ with $p \in \{0, 1, 2, \ldots\}$. In this case, condition (7.18) implies that $s = 1$ and $n_b = p$, and

we deduce from (7.19) that the reference state $|\Psi\rangle^{\rm ref}_{j=p+1/2,s=1}$ for this positive–j sector is of even (odd) $\Pi_{\rm PJT}$–parity for p odd (even).

2. The eigenvalue j is negative, so that $j = -p - 1/2$ with $p \in \{0, 1, 2, \ldots\}$. In this case, condition (7.18) implies that $s = -1$ and $n_b = p$, and we deduce from (7.19) that the reference state $|\Psi\rangle^{\rm ref}_{j=-p-1/2,s=-1}$ for this negative–j sector is of even (odd) $\Pi_{\rm PJT}$–parity for p even (odd).

Clearly $js = p + 1/2$ in both cases. Given the eigenvalue $j = \pm(p + 1/2)$, the condition (7.16) therefore fully determines the reference state $|\Psi\rangle^{\rm ref}_{j,s}$. For example, in the occupation number representation of modes of circular polarization, the reference state for the $j = p + 1/2$–sector is $|p\rangle|0\rangle|\uparrow\rangle$, and that for the $j = -p - 1/2$–sector is $|0\rangle|p\rangle|\downarrow\rangle$. These examples clearly illustrate the role of the reference state as the "simplest" state in the given sector.

The operator approach now allows for the construction of a suitable basis for this j–sector, without the need to specify the explicit form of the basis states in terms of *e.g.* linearly of circularly polarized bosonic modes. For an arbitrary j–sector eigenstate $|\Psi\rangle_j$ of $H_{\rm RPJT}$, we construct the power series expansion

$$|\Psi\rangle_j \;=\; \sum_{n=0}^{\infty} X_n \left(c^\dagger\right)^n |\Psi\rangle^{\rm ref}_{j,s} \,. \tag{7.20}$$

Since $c^\dagger$ commutes with both J and $\Pi_{\rm PJT}$, it is clear that the state $|\Psi\rangle_j$ has the same J and $\Pi_{\rm PJT}$ quantum numbers as the reference state $|\Psi\rangle^{\rm ref}_{j,s}$. Substituting the expansion (7.20) into the Schrödinger equation

$$H_{\rm PJT}|\Psi\rangle_j = E|\Psi\rangle_j \,, \tag{7.21}$$

and using the relations (7.13), (7.14) and the condition (7.16), one obtains

for the coefficients $\{X_i\}$ the recurrence relations

$$\begin{aligned} 0 &= 2\gamma X_{2n-1} + \left[(p+2n)\omega + s\frac{1}{2}\omega_0 - E\right] X_{2n} + 2\gamma(p+n+1)X_{2n+1} \\ 0 &= 2\gamma X_{2n} + \left[(p+2n+1)\omega - s\frac{1}{2}\omega_0 - E\right] X_{2n+1} + 2\gamma(n+1)X_{2n+2} \end{aligned} \quad (7.22)$$

where $s = 1$ for $j = p + 1/2$ and $s = -1$ for $j = -p - 1/2$. These equations constitute a simple reformulation of the Longuet–Higgins recurrence relations [Lo58, Ju79, Re81a], generalized to incorporate the case $\omega_0 > 0$. The solution of these recurrence relations is equivalent to the diagonalization of the tri–diagonal matrix representation of H_{PJT} in the j–sector,

$$\begin{bmatrix} p\,\omega + \frac{s}{2}\omega_0 & 2\gamma\sqrt{p+1} & 0 & 0 & 0 & \dots \\ 2\gamma\sqrt{p+1} & (p+1)\,\omega - \frac{s}{2}\omega_0 & 2\gamma\sqrt{1} & 0 & 0 & \dots \\ 0 & 2\gamma\sqrt{1} & (p+2)\,\omega + \frac{s}{2}\omega_0 & 2\gamma\sqrt{p+2} & 0 & \dots \\ 0 & 0 & 2\gamma\sqrt{p+2} & (p+3)\,\omega - \frac{s}{2}\omega_0 & 2\gamma\sqrt{2} & \dots \\ 0 & 0 & 0 & 2\gamma\sqrt{2} & (p+4)\,\omega + \frac{s}{2}\omega_0 & \dots \\ \vdots & \vdots & \vdots & \vdots & \vdots & \ddots \end{bmatrix} \quad (7.23)$$

In general (*i.e.* $\omega_0 > 0$ arbitrary), the eigenvalues of the matrix (7.23) will be different for the cases $s = \pm 1$, and the eigenstates of H_{PJT} are thus singlet states of definite parity and angular momentum component j. In particular, the ground state of H_{PJT} is a unique positive–parity state, corresponding to $j = -1/2$, for all values of the coupling γ. Since the Longuet–Higgins relations (7.22) are invariant under the simultaneous replacements $\{\omega_0 \to -\omega_0, j \to -j, s \to -s\}$, it is clear that the first excited state of H_{PJT}, which is a unique negative–parity state corresponding to $j = 1/2$ and $s = 1$, may be obtained by replacing ω_0 by $-\omega_0$.

The matrix representation of the linear $E \otimes e$ JT Hamiltonian H_{JT} in the j–sector is obtained by setting $\omega_0 = 0$ in (7.23). The representations

of H_{JT} in the $j = p + 1/2$ and $j = -p - 1/2$–sectors (which are of opposite parity) are therefore identical, which explains the two–fold degeneracy of all energy levels in the spectrum of the linear $E \otimes e$ JT Hamiltonian. In particular, the diagonalization of (7.23) for $\{\omega_0 = 0; p = 0, j = -1/2\}$ and $\{\omega_0 = 0; p = 0, j = 1/2\}$ yields the energy of the positive– and negative–parity ground states of H_{JT}, which are degenerate for all couplings. Thus the inclusion of the (vibronic) interaction terms transforms the electronic degeneracy of the noninteracting ground state of H_{JT} into a parity degeneracy (also referred to as a vibronic degeneracy [Berb]) at finite coupling. In the H_{PJT} model, the finite fermionic level splitting ω_0 lifts the parity degeneracy of the ground state for all values of the coupling, and the Hamiltonian H_{PJT} is in this sense analogous to the Rabi Hamiltonian.

For the Hamiltonian H_{JT}, *i.e.* for $\omega_0 = 0$, the numerical diagonalization of (7.23) was first performed by Longuet–Higgins *et.al.* [Lo58]). Besides the energy spectrum of the linear $E \otimes e$ JT model, the eigenvalues of the matrix (7.23) with $\omega_0 = 0$ also yield the energies of the linear $\Gamma_8 \otimes \tau_2$ JT model. However, for this model, which describes the vibronic interactions between a fourfold–degenerate electronic state and a triply–degenerate nuclear vibrational mode, the quantum number p is replaced by the quantity m, which assumes half–integer rather than integer values. Numerical results for the energy levels of the linear $\Gamma_8 \otimes \tau_2$ JT Hamiltonian were presented by Thorson and Moffit [Th68].

7.1.4 Juddian solutions for the JT and PJT models

As is the case for the Rabi Hamiltonian, analytic solutions for some of the energy eigenvalues of the Hamiltonians $H_{\rm JT}$ and $H_{\rm PJT}$ occur at isolated values of the coupling γ. Using algebraic methods, Judd [Ju79, Ju77] showed that, for both the linear $\Gamma_8 \otimes \tau_2$ and linear $E \otimes e$ JT models, rational eigenvalues occur at isolated values of γ where the Longuet–Higgins recurrence relations can be solved in closed form. Reik *et.al.* [Re81a, Re81b, Re81c, Re82] simplified the analysis of these Juddian solutions by reformulating the eigenvalue problem for both models in Bargmann's space of analytical functions, and extended the search for Juddian solutions to the Rabi and linear $E \otimes e$ PJT Hamiltonians [Re82]. The important contribution of Reik *et.al.* is the observation that, at the Juddian points, a Neumann expansion of the wave function in modified Bessel functions terminates after a finite number of terms. This allows for the systematic and (at least in principle) straightforward determination, in closed form, of the values of the coupling γ and energy E at the Juddian points.

Here we rederive the results of Reik *et.al.* using the operator approach introduced in the previous section. Our motivation is threefold: the equations which determine the Juddian values of the coupling and energy are more simply derived in this approach; the operator $c^\dagger$, which obeys the relation (7.10), plays the role of the the Bargmann number $\sqrt{z}$ in [Re82], and therefore allows for the construction of explicit expressions for the Juddian wave functions in the Dirac rather than the Bargmann representation; finally, the operator approach yields results which are independent of the explicit realization of

the bosonic modes. By analogy with the approach in [Re82], we therefore construct the following (unnormalized) Neumann expansion for $|\Psi\rangle_j$:

$$\begin{aligned} |\Psi\rangle_j &= \sum_{n=0}^{\infty} \frac{x_n}{\kappa^{4n} n!} \left(\kappa c^\dagger\right)^{n-p} I_{n+p}\left(2\kappa c^\dagger\right) |\Psi\rangle_{j,s}^{\text{ref}} \\ &\quad + \sum_{n=0}^{\infty} \frac{y_n}{\kappa^{4n} n!} \left(\kappa c^\dagger\right)^{n-p} I_{n+p+1}\left(2\kappa c^\dagger\right) |\Psi\rangle_{j,s}^{\text{ref}}, \end{aligned} \tag{7.24}$$

where $\kappa \equiv \gamma/\omega$, I_n is a modified Bessel function of the first kind of order n (see *e.g.* [Abr]), and as before $s = 1$ ($s = -1$) for $j = p + 1/2$ ($j = -p - 1/2$). Then

$$\begin{aligned} |\Psi\rangle_j &= \sum_{n=0}^{\infty} \frac{x_n}{\kappa^{4n} n!} \sum_{k=0}^{\infty} \frac{\left(\kappa c^\dagger\right)^{2n+2k}}{k!(p+n+k)!} |\Psi\rangle_{j,s}^{\text{ref}} \\ &\quad + \sum_{n=0}^{\infty} \frac{y_n}{\kappa^{4n} n!} \sum_{k=0}^{\infty} \frac{\left(\kappa c^\dagger\right)^{2n+2k+1}}{k!(p+n+k+1)!} |\Psi\rangle_{j,s}^{\text{ref}}. \end{aligned} \tag{7.25}$$

Substituting (7.25) into the Schrödinger equation (7.21) we obtain for $n = 0, 1, 2, \ldots$,

$$\begin{aligned} 0 &= \left\{\frac{p}{2} + n + s\frac{\omega_0}{4\omega} - \frac{E}{2\omega}\right\} x_n + \kappa^2 y_n + n\kappa^4 \left(x_{n-1} + y_{n-1}\right) \\ 0 &= \frac{1}{\kappa^2} x_{n+1} + \left\{\frac{p}{2} + n + \frac{1}{2} - s\frac{\omega_0}{4\omega} - \frac{E}{2\omega}\right\} y_n \\ &\quad + \left\{p + n + 1 + \kappa^2\right\} x_n + n\kappa^4 \left(x_{n-1} + y_{n-1}\right) , \end{aligned} \tag{7.26}$$

where by definition $x_{-1} = y_{-1} = 0$. Elimating $x_{n-1} + y_{n-1}$ from the recurrence relations (7.26), and introducing the parameters δ and v via

$$\begin{aligned} \delta &\equiv \frac{\omega_0 - \omega}{4\omega} \\ E &\equiv \left(v - \frac{1}{2} - 2\kappa^2\right)\omega , \end{aligned} \tag{7.27}$$

one obtains, for the case $j = -p - 1/2$ where $s = -1$,

$$\begin{bmatrix} x_{n+1} \\ y_{n+1} \end{bmatrix} = \begin{bmatrix} M_{11} & M_{12} \\ M_{21} & M_{22} \end{bmatrix} \begin{bmatrix} x_n \\ y_n \end{bmatrix} \quad n = 0, 1, 2, \ldots,$$

$$
\begin{aligned}
M_{11} &= -\kappa^2\left(\frac{p}{2}+1+\delta+\frac{v}{2}\right) \\
M_{12} &= -\kappa^2\left(\frac{p}{2}+1+\delta+n-\frac{v}{2}\right) \\
M_{21} &= \left(\kappa^2+\frac{p}{2}+1-\delta+n-\frac{v}{2}\right)\left(\frac{p}{2}+1+\delta+\frac{v}{2}\right)-\kappa^2\,(n+1) \\
M_{22} &= \left(\kappa^2+\frac{p}{2}+1-\delta+n-\frac{v}{2}\right)\left(\frac{p}{2}+1+\delta+n-\frac{v}{2}\right)-\kappa^2\,(n+1), \qquad (7.28)
\end{aligned}
$$

with the initial condition

$$
\kappa^2 y_0 = -\left(\kappa^2+\frac{p}{2}-\delta-\frac{v}{2}\right)x_0\,. \qquad (7.29)
$$

The parameter x_0 simply fixes the norm of $|\Psi\rangle_{-p-1/2}$. For an eigenstate of H_{PJT} corresponding to the positive J eigenvalue $j = p + 1/2$, a similar analysis with $s = 1$ yields equations identical in form to (7.28), but with δ replaced by $-\delta - 1/2$, or equivalently with ω_0 replaced by $-\omega_0$. Taking $x_0 = \kappa^2$ and $s = 1$, Equations (7.28) and (7.29) become identical to Equations (3.4–3.8) and (3.11), respectively, of [Re82], so that the correspondence between (7.24) and the Bargmann analysis of [Re82] is complete.

The derivation of (7.28) is valid for arbitrary ω_0, including the JT case $\omega_0 = 0$. Furthermore, it can be shown [Re82] that, in the case $p = -1/2$, the solution of (7.28) yields the energy eigenvalues $E = (v - 2\kappa^2)\,\omega$ of the Rabi Hamiltonian. Thus the set of equations (7.28) are to be solved for both δ and $\delta \to -\delta - 1/2$, and in each case for arbitrary nonnegative integers p as well as for $p = -1/2$.

Juddian solutions for H_{JT}, H_{PJT} and H_{Rabi} occur whenever the Neumann series (7.24) terminates at finite order; such a termination occurs at the N-th term if and only if both the conditions $v = N$ and $\Sigma_N \equiv x_N + y_N = 0$

are met [Re82]. By (7.27), the condition $v = N$ ensures that the energy corresponding to these solutions lies on the Nth baseline, defined for the JT and PJT systems by

$$E_N^{\text{Baseline}} = \left(N - \frac{1}{2} - 2\kappa^2\right)\omega = \left(N - \frac{1}{2}\right)\omega - \frac{2\gamma^2}{\omega} \,. \tag{7.30}$$

The quantity Σ_N is a polynomial of degree N in κ^2. For given values of the parameters p and δ, the conditions $v = N, \Sigma_N = 0$ therefore algebraically determine the values of the coupling for which Juddian solutions on the N-th baseline exist.

For $v = N = 0$, the condition $\Sigma_0 = x_0 + y_0 = 0$ reduces to

$$p^* - 2\delta^* = 0 \,, \tag{7.31}$$

which is independent of the coupling κ, and thus yields an analytic solution, valid for all coupling, for $p = p^*, \delta = \delta^*$. The case $p^* = -1/2, \delta^* = -1/4$, which refers to the Rabi Hamiltonian with degenerate atomic levels, was discussed in Chapter 4. Here we consider also the case of the linear $E \otimes e$ resonant ($\omega_0 = \omega$) pseudo Jahn–Teller Hamiltonian H_{RPJT}, for which $\delta = 0$. For H_{RPJT}, the condition (7.31) is therefore satisfied for $p^* = 0$, which corresponds to the negative J eigenvalue $j^* = -p^* - 1/2 = -1/2$ and $s = -1$. In this case the reference state $|\Psi\rangle_{j,s}^{\text{ref}}$ has the form $|0\rangle|0\rangle|\downarrow\rangle$, where $|0\rangle|0\rangle$ is the bosonic vacuum for any particular realization of the bosonic modes. Thus we find that the ground ($j = -1/2$) state $|\Psi_0^{\text{RPJT}}\rangle$ of the RPJT Hamiltonian

$$\begin{aligned} H_{\text{RPJT}} \;=\; & \frac{1}{2}\omega\,\sigma^z \;+\; \omega\, a_1^\dagger a_1 \;+\; \omega\, a_2^\dagger a_2 \\ & + \gamma\,\left(a_1 + a_2^\dagger\right)\sigma^+ \;+\; \gamma\,\left(a_1^\dagger + a_2\right)\sigma^- \end{aligned} \tag{7.32}$$

assumes the closed form

$$|\Psi_0^{\mathrm{RPJT}}\rangle = A_{\mathrm{RPJT}} \left\{ I_0\left(2\kappa c^\dagger\right) - I_1\left(2\kappa c^\dagger\right) \right\} |0\rangle|0\rangle|\downarrow\rangle \,, \tag{7.33}$$

where A_{RPJT} is a normalization constant, and the corresponding ground–state energy is

$$E_0^{\mathrm{RPJT}} = E_0^{\mathrm{Baseline}} = -\frac{1}{2}\omega - \frac{2\gamma^2}{\omega} \,. \tag{7.34}$$

This solution, which is analytic for all coupling γ, clearly highlights the advantages of the operator approach. Expressed in terms of bosonic modes of circular polarization, $|\Psi_0^{\mathrm{RPJT}}\rangle$ assumes the explicit form

$$|\Psi_0^{\mathrm{RPJT}}\rangle = A_{\mathrm{RPJT}} \sum_{k=0}^{\infty} \left\{ \frac{\kappa^{2k}}{\sqrt{k!k!}} |k\rangle|k\rangle|\downarrow\rangle - \frac{\kappa^{2k+1}}{\sqrt{k!(k+1)!}} |k\rangle|k+1\rangle|\uparrow\rangle \right\} , \tag{7.35}$$

which allows for the determination of A_{RPJT} via

$$\begin{aligned} A_{\mathrm{RPJT}} &= \left\{ \sum_{k=0}^{\infty} \left(\frac{\kappa^{4k}}{k!k!} + \frac{\kappa^{4k+2}}{k!(k+1)!} \right) \right\}^{-1/2} \\ &= \left\{ I_0\left(2\kappa^2\right) + I_1\left(2\kappa^2\right) \right\}^{-1/2} \,. \end{aligned} \tag{7.36}$$

For $v = N > 0$, the conditions $\Sigma_N = x_N + y_N = 0$ may be used to find other Juddian solutions for H_{Rabi}, H_{JT}, and H_{PJT}. It has been conjectured [Re87] that an expansion of the wave function in generalized spheroidal functions terminates at all values of the coupling, rather than only at the Juddian points. Despite very strong numerical evidence, this conjecture has not been proved. However, the Juddian solutions may be still used to gauge the accuracy of approximate many–body techniques, even if only at isolated values of the coupling. In particular, the converged CI (diagonalization) results for the spectra of H_{JT} and H_{PJT} can be shown to be exact for all practical

purposes. Also, it can be shown [Re81a] that, for large coupling γ, all eigenvalues of $H_{\rm JT}$ and $H_{\rm PJT}$ approach the baselines (7.30). In particular, both the ground and first excited state energies of these Hamiltonians approach the value $E_0^{\rm Baseline} = E_0^{\rm RPJT} = -\omega/2 - 2\gamma^2/\omega$ in the limit $\gamma \to \infty$.

7.2 Physical characteristics of the JT and PJT ground states

The ground–state behaviour of the linear $E \otimes e$ JT and PJT Hamiltonians is analogous to that of the Rabi ground state, in that a marked change in character occurs in the ground state in the intermediate coupling regime. Again, this character change manifests itself in the ground–state expectation value of the operator σ^z, which is readily evaluated using the CI method. In the ground state of H_{PJT} with $\omega_0 > 0$, the fermion is more likely to be found in the lower state for small coupling, and (almost) equally likely to be found in either the upper or lower state at large coupling. The crossover between these two regimes, though not discontinuous, takes place in a fairly well–defined region of coupling, which is dependent on the the fermionic level splitting ω_0. For H_{JT}, the same behaviour is observed, provided that the ground state is restricted to, say, even $\Pi_{\rm PJT}$ parity (or equivalently to the negative J eigenvalue $j = -1/2$). Thus, as before, one may use the expectation value $\langle\sigma^z\rangle$ or, more effectively, the fluctuation $\Delta\sigma^z$, to identify the transitional coupling region.

The physical nature of the crossover observed here may be seen by examining the behaviour of the ground state of the (part of a) molecular system described by either the JT or PJT Hamiltonian, for large values of the scaled coupling κ. Consider first the simpler Hamiltonian H_{JT}. Denoting the energy gap between the two sheets of the adiabatic potential corresponding to the ground state by $\Delta(Q)$, it is readily shown that $\Delta_0 \equiv \Delta(Q_0) \approx 8\omega\kappa^2$, where Q_0 represents the minimum–energy nuclear configuration [Berb]. For large κ, it is evident that Δ_0 is much larger than the nuclear vibrational quantum ω. Thus the criterion (7.6) is satisfied, and the lower sheet of the adiabatic potential may be interpreted as the ground–state potential energy of the nuclei in the average field of the electrons. Quantizing the motion of the nuclei in this potential, one obtains the observed form (7.34) of the ground–state energy for large coupling [Berb]. The criterion $\Delta_0 \sim \omega$ provides a simple measure of the onset of this type of ground–state behaviour, so that we expect a change in character of the ground state of H_{JT} at

$$\kappa^{\mathrm{trans}} \sim \frac{1}{\sqrt{8}} . \tag{7.37}$$

This is in good agreement with the transitional coupling region for H_{JT} identified by considering the behaviour of $\Delta\sigma^z$. Although the finite fermionic level splitting ω_0 in the linear $E \otimes e$ PJT model affects the shape of the adiabatic potentials, the ground–state behaviour for large coupling is similar to that described above for H_{JT} [Berb], and a similar transitional region is observed.

7.3 Approximate many–body approaches to the JT and PJT models

The approach outlined in Section 7.2 above may be used [Berb] to obtain quantitatively accurate results for the spectrum of both H_{JT} and H_{PJT} in the limit of large coupling γ. Accurate results for these models can also be obtained in the opposite limit of small γ, using an operator version of time–independent perturbation theory (see [Bera, Berb] and references therein). For both H_{JT} and H_{PJT}, however, physically realistic values of the vibronic interaction constant mostly correspond to the region of intermediate coupling [Berb], where quasi–analytic results cannot be obtained.

In the intermediate coupling regime, accurate results for the spectra of the Hamiltonians H_{JT} and H_{PJT} can be found using quasi–exact numerical methods such as the CI (diagonalization) approach. Generally, however, these methods do not provide much physical insight into the nature of the solution, and a variety of other many–body techniques have therefore been applied to the linear $E \otimes e$ JT and PJT models, with the bulk of the work being done on the former. Most of these calculations have involved either variational techniques (see [Berb, Lo91] and references therein), or some form of unitary transformation (see *e.g.* [Fu61]). In many cases, these methods are used in combination; recent examples include a variational calculation based on a correlated squeezed state [Lo91] for H_{JT}, and a similar calculation for H_{PJT} [Hu98]. None of these calculations, however, yield quantitatively accurate results in the physically interesting region of intermediate coupling. As

is always the case, the failure of the variational method can be attributed to a shortcoming in the variational ansatz for the wave function. As for the method of unitary transformations (which is often just a variational shift of the Hamiltonian rather than the wave function), the transformations employed often destroy either or both of the symmetries J and Π_{PJT}. This eliminates the use of these symmetries as an aid in simplifying the solution of the H_{JT} and H_{PJT} eigenvalue problems.

Given the excellent variational results [Bi99a] obtained for the Rabi Hamiltonian via a trial state of the coherent superposition form (4.38), we have attempted to perform a variational calculation for both H_{JT} and H_{PJT} based on an analogous ansatz for the case of two bosonic modes. The resulting ansatz is not, however, a state of good j quantum number, and this calculation therefore fails at intermediate and large coupling.

Chapter 8

Application of the CCM to Linear $E \otimes e$ Jahn–Teller Systems

In this chapter, we review previous applications of the CCM to the ground state of the linear $E \otimes e$ JT Hamiltonian, and present new CCM results for the ground and first excited state energies of both the linear $E \otimes e$ JT and PJT models. Given the observed character change in the ground state of these models, it is not surprising to find that, as is the case for the Rabi Hamiltonian, a CCM calculation based on a naive choice of the model state fails in the intermediate coupling regime. We present, however, a CCM calculation, based on the analytic ground state of the linear $E \otimes e$ resonant pseudo Jahn–Teller (RPJT) Hamiltonian, which to first order yields excellent results for both the ground and first excited states of the models considered here.

8.1 Previous CCM calculations for the linear $E \otimes e$ Jahn–Teller Hamiltonian

Monkhorst presented a critical analysis of the treatment of molecular systems in the adiabatic approximation, and argued that the CCM is an especially suitable method for the analysis of such systems in a manner which does not rely on the adiabatic approximation [Mo87]. Wong and Lo have applied the CCM to the ground state of the linear $E \otimes e$ JT Hamiltonian, which is a manifestly non–adiabatic model. Initially, these authors applied the unitary transformation

$$U = \exp R, \quad R = \lambda \left(b_1^\dagger - b_1 \right) , \tag{8.1}$$

with $\lambda = \eta/\omega$, to the Hamiltonian in the form

$$H_{\rm JT} = \omega \left(b_1^\dagger b_1 + b_2^\dagger b_2 \right) + \eta \left(b_1^\dagger + b_1 \right) \sigma^x - \eta \left(b_2^\dagger + b_2 \right) \sigma^y , \tag{8.2}$$

and applied the CCM to the transformed Hamiltonian using the SCCA approximation scheme discussed in Section 5.1 [Wo94]. The same authors subsequently presented an improved ground–state CCM calculation for $H_{\rm JT}$, referred to as the optimal coupled cluster approximation [Wo96a]. In this approach, the parameter λ in the unitary transformation (8.1) is treated as a variational parameter, the optimal value λ^* of which is determined by a method which combines aspects of both the CCM and the variational method. Finally, the CCM is applied to the "optimally" ($\lambda = \lambda^*$) transformed Hamiltonian to yield the required ground–state energy results.

The optimal CCM results of Wong and Lo for the ground–state energy of $H_{\rm JT}$ are more accurate, over the full coupling spectrum, than those ob-

tained via previous calculations based on either the variational method or the method of unitary transformations [Wo96a]. Their calculations, however, take no account of either of the symmetries J and Π_{PJT} of the Hamiltonian; in fact, it is evident that the unitary transformation (8.1) destroys both these symmetries. Besides the resulting loss of accuracy in the ground–state energy results, their approach is therefore also not readily generalized either to the first excited state, or to the case of nondegenerate electronic levels ($\omega_0 > 0$).

8.2 Naive applications of the CCM to H_{JT} and H_{PJT}

We have generalized the CCM schemes [1] employed in our application of the method to the Rabi Hamiltonian (see Table D.1) to the linear $E \otimes e$ JT and PJT case of two degenerate bosonic modes. Given the results obtained for the Rabi Hamiltonian via CCM calculations based on the noninteracting model state, and the character change in the ground states of H_{JT} and H_{PJT}, it is unreasonable to expect that a CCM calculation based on the model state $|0\rangle|0\rangle|\downarrow\rangle$ would be successful here. Indeed, we have confirmed that, for the model state $|0\rangle|0\rangle|\downarrow\rangle$ and a cluster operator S of the form

$$S = \sum_{n=1}^{\infty}\sum_{k=0}^{n} s_{n,k}^{(1)} \left(b_1^\dagger\right)^k \left(b_2^\dagger\right)^{n-k} + \sum_{n=1}^{\infty}\sum_{k=0}^{n-1} s_{n,k}^{(2)} \left(b_1^\dagger\right)^k \left(b_2^\dagger\right)^{n-k-1} \sigma^+ , \quad (8.3)$$

which represents a simple generalization of Scheme I for the Rabi Hamiltonian, the CCM results, although very accurate for weak coupling, again fail

[1] As before, a CCM scheme refers to a particular choice of the model state $|\Phi\rangle$ and cluster operator S.

at intermediate and large coupling. The same holds true for the generalization of Scheme II. Although we have not formally proven this, it is highly likely that the failure of the method is again due to an incompleteness, to any finite order, in the CCM ansatz for the ground–state wave function. Also, these calculations do not conserve the J symmetry of the Hamiltonians $H_{\rm JT}$ and $H_{\rm PJT}$.

We have also performed a CCM calculation for $H_{\rm JT}$ and $H_{\rm PJT}$ based on a coupling–dependent model state of the form

$$|\Phi\rangle = \frac{1}{\sqrt{2}}\{|-x\rangle|0\rangle|\uparrow;\sigma^x\rangle - |x\rangle|0\rangle|\downarrow;\sigma^x\rangle\} \ . \tag{8.4}$$

Here $|x\rangle$ is a bosonic coherent state with coherent parameter $x = \eta/\omega$, the bosonic states refer to modes of linear polarization, and the fermionic states refer to eigenstates of σ^x. The state (8.4) represents a generalized form of the model state $|\Psi_+\rangle$ employed in the Scheme III analysis of the Rabi Hamiltonian. Using a similar form for the cluster operator S to that employed there, we again find that the CCM breaks down at intermediate and large coupling. The reason is two–fold: the model state (8.4) does not mimic the change in character in the ground states of $H_{\rm JT}$ and $H_{\rm PJT}$ with sufficient accuracy, and the J symmetry has again been neglected.

Since an accurate variational calculation similar to that presented in Chapter 4 for the Rabi Hamiltonian is not available for the linear $E \otimes e$ JT and PJT Hamiltonians, it is not possible to generalize the very successful CCM Scheme IV calculation for the Rabi Hamiltonian to the models considered here. For a CCM analysis of $H_{\rm JT}$ and $H_{\rm PJT}$, we therefore seek an alternative model state $|\Phi\rangle$ which must

- incorporate the symmetries Π_{PJT} and J,
- allow for the construction of a suitable cluster operator S which conserves these symmetries, and
- be capable of tracking the character change in the ground state.

8.3 Successful CCM calculations for H_{JT} and H_{PJT}

For the Hamiltonians H_{JT} and H_{PJT}, the analytic ground state of the linear $E \otimes e$ RPJT Hamiltonian, [2]

$$|\Psi_0^{\mathrm{RPJT}}\rangle = \frac{1}{\sqrt{I_0\left(2\kappa^2\right) + I_1\left(2\kappa^2\right)}} \left\{ I_0\left(2\kappa c^\dagger\right) - I_1\left(2\kappa c^\dagger\right) \right\} |0\rangle|0\rangle|\downarrow\rangle \qquad (8.5)$$

with $\kappa \equiv \gamma/\omega$, and where the operator $c^\dagger$ was introduced in (7.8), satisfies all the requirements for an effective CCM model state [Bi99b]. The state $|\Psi_0^{\mathrm{RPJT}}\rangle$ clearly has the correct even–parity and $j = -1/2$ symmetries required of the ground state. Furthermore, since it is easily shown that

$$c|\Psi_0^{\mathrm{RPJT}}\rangle = -\kappa|\Psi_0^{\mathrm{RPJT}}\rangle \,, \qquad (8.6)$$

the operator $c + \kappa$ annihilates the model state $|\Phi\rangle = |\Psi_0^{\mathrm{RPJT}}\rangle$. This suggests the following (clearly symmetry–conserving) form for the cluster correlation operator S:

$$S = \sum_{n=1}^{\infty} s_n \left(c^\dagger + \kappa\right)^n \,. \qquad (8.7)$$

We shall refer to this choice of the model state and correlation operator as the RPJT scheme. Consider the SUB-1 approximation, where $S = s_1\left(c^\dagger + \kappa\right)$.

[2] Here I_n refers to a modified Bessel function of the first kind of order n.

With the Hamiltonian $H_{\rm PJT}$ (for arbitrary ω_0 including the JT case $\omega_0 = 0$) written in the convenient form (7.11), the nested commutator expansion (3.8) may be used to obtain the similarity transformed Hamiltonian

$$\begin{aligned} e^{-S} H_{\rm PJT} e^{S} &= \frac{1}{2}\omega_0 \exp\left\{-2s_1 c^\dagger\right\}\sigma^z + 2\omega c^\dagger c - \frac{1}{2}\omega \\ &\quad + \omega s_1 \left(c^\dagger + \kappa\right) + 2\omega\kappa\left(c^\dagger + c\right) \\ &\quad + \frac{1}{2}\omega\,(2J)\,\sigma^z + \frac{1}{2}\omega \sum_{m=0}^{\infty} \frac{2s_1\kappa\left(-2s_1 c^\dagger\right)^m}{(m+1)!}\,(2J)\,\sigma^z . \end{aligned} \tag{8.8}$$

For the ground state, one may make the replacement $2J \to -1$. Furthermore, given the relation $c|\Phi\rangle = (-\kappa)|\Phi\rangle$ and its Hermitian conjugate $\langle\Phi|c^\dagger = \langle\Phi|(-\kappa)$, it follows that the SUB-1 CCM ground–state energy has the form

$$\begin{aligned} E_0^{\rm CCM} &= \langle\Phi|e^{-S} H_{\rm PJT} e^{S}|\Phi\rangle \\ &= -\frac{1}{2}\omega - 2\omega\kappa^2 + \frac{1}{2}\left(\omega_0 - \omega\right)\exp\left\{2s_1\kappa\right\}\langle\sigma^z\rangle \ , \end{aligned} \tag{8.9}$$

where the model state expectation value $\langle\sigma^z\rangle$ is given by

$$\langle\sigma^z\rangle = \langle\Phi|\sigma^z|\Phi\rangle = -\left[\frac{I_0\left(2\kappa^2\right) - I_1\left(2\kappa^2\right)}{I_0\left(2\kappa^2\right) + I_1\left(2\kappa^2\right)}\right] . \tag{8.10}$$

Using the commutation relations (7.13), one obtains the overlap equation

$$\begin{aligned} 0 &= \langle\Phi|\left(c + \kappa\right) e^{-S} H_{\rm PJT} e^{S}|\Phi\rangle \\ &= \exp\left\{2s_1\kappa\right\}\left(\omega_0 - \omega\right)\left(\kappa - \frac{1}{2}s_1\right)\langle\sigma^z\rangle + \frac{1}{2}\omega s_1\left[1 - \langle\sigma^z\rangle\right] \\ &\quad + \frac{\omega_0}{4\kappa}\sinh\left\{2s_1\kappa\right\} + \frac{\omega}{4\kappa}\left[1 - \cosh\left\{2s_1\kappa\right\}\right] \\ &\quad + \frac{\omega}{4\kappa}\left[1 - \exp\left\{2s_1\kappa\right\}\right]\langle\sigma^z\rangle \ , \end{aligned} \tag{8.11}$$

which determines the coefficient s_1, and thereby also the SUB-1 CCM ground–state energy (8.9) in the RPJT scheme. It is clear from the form (8.9) that, as expected, the SUB-1 CCM ground–state energy $E_0^{\rm CCM}$ for the RPJT scheme is exact in the case of resonance $\omega_0 = \omega$.

For ease of comparison with other results, we scale out the ω–dependence of the Hamiltonian by setting $\omega = 1$, and introduce the coupling parameter

$$k^2 \equiv 4\gamma^2 = 4\kappa^2 = 2\eta^2 \qquad (\omega = 1) \ . \tag{8.12}$$

In Table 8.1 we compare our SUB-1 CCM results for the ground–state energy of the (pure) linear $E \otimes e$ Hamiltonian (for which $\omega_0 = 0$) to the numerically exact results obtained via the CI diagonalization, and also to results obtained

Table 8.1: *Comparison of the ground–state energy $E_0^{\rm CCM}$ of the scaled ($\omega = 1$) linear $E \otimes e$ JT ($\omega_0 = 0$) Hamiltonian, obtained as a function of the coupling k^2 from a SUB-1 CCM calculation based on the RPJT scheme, with the results of other many–body calculations. In accordance with the other results quoted here, we have added unity (the zero–point energy of the bosonic modes for $\omega = 1$) to our results. The (effectively exact) CI results are labeled $E_0^{\rm CI}$. The results from [Wo96a] are the so–called optimal CCM ground–state energy results obtained there. The other columns, which are reproduced from [Wo96a], represent results obtained via an earlier CCM analysis [Wo94], and via variational methods and the method of unitary transformations [Al69, Ba78, Ba77, Zh90, Lo91].*

k^2	$E_0^{\rm CI}+1$	$E_0^{\rm CCM}+1$	[Wo96a]	[Wo94]	[Al69, Ba78]	[Ba77]	[Zh90]	[Lo91]
0.00	1.0000	1.0000	1.0000	1.0000	1.0000	1.0000	1.0000	1.0000
0.25	0.7738	0.7739	0.7741	0.7742	0.7766	0.7883	0.7877	0.7767
0.50	0.5780	0.5785	0.5799	0.5806	0.5920	0.6155	0.6119	0.5877
0.75	0.3997	0.4009	0.4045	0.4066	0.4308	0.4609	0.4522	0.4173
1.00	0.2330	0.2350	0.2415	0.2453	0.2838	0.3168	0.3017	0.2586
2.00	-0.3689	-0.3637	-0.3441	-0.3343	-0.2454	-0.2166	-0.2577	-0.3157
3.00	-0.9189	-0.9117	-0.8824	-0.8704	-0.7494	-0.7281	-0.7886	-0.8466
5.00	-1.9610	-1.9532	-1.9173	-1.9051	-1.9750	-1.7371	-1.8225	-1.8716
7.00	-2.9761	-2.9693	-2.9345	-2.9231	-2.7500	-2.7409	-2.8418	-2.8833
10.00	-4.4850	-4.4797	-4.4492	-4.4391	-4.2500	-4.4360	-4.3600	-4.3937
15.00	-6.9907	-6.9870	-6.9625	-6.9538	-6.7500	-6.7458	-6.8780	-6.9042
20.00	-9.4932	-9.4904	-9.4700	-9.4623	-9.2500	-9.2468	-9.3894	-9.4111
30.00	-14.4956	-14.4937	-14.4783	-14.4719	-14.2500	-14.2479	-14.4035	-14.4202

via a variety of many–body calculations. It is clear that, even in first order, our CCM calculation based on the RPJT scheme yields a considerable improvement, over the full coupling spectrum, on the earlier "optimal" CCM results of [Wo96a], which in turn are far superior to results obtained via other many–body techniques. Furthermore, the CCM results of Wong and Lo given in [Wo96a] were obtained in the third level of their successive coupled cluster approximation scheme, and required the numerical solution of 13 nonlinear coupled equations. It is evident that the proper inclusion of the J and $\Pi_{\rm PJT}$ symmetries in our calculation, which requires the numerical solution of only the single trancendental equation (8.11), leads to a much simpler and considerably more accurate CCM calculation of the linear $E \otimes e$ JT ground–state energy.

In Table 8.2 we present the results of a SUB-1 CCM calculation, based on the RPJT scheme, of the ground–state energy of the scaled ($\omega = 1$) linear $E \otimes e$ PJT Hamiltonian in the sub–resonant cases $\omega_0 = 0$ (this is again the pure JT case) and $\omega_0 = 0.5$, as a function of the coupling k^2. Here we also show the percentage error in the CCM results, as compared to the (converged) results of a CI diagonalization of $H_{\rm PJT}$ in a basis consisting of 101 even–parity $j = -1/2$ states. Similar results for the supra–resonant cases $\omega_0 = 1.5$ and $\omega_0 = 2.0$ are tabulated in Table 8.3. It is clear that, already in the SUB-1 approximation, the CCM ground–state energy results for the RPJT scheme are extremely accurate over the full coupling regime and for a wide range of values of the fermionic level splitting ω_0, with a percentage error, relative to the CI results, of no more than 0.38 % (see Figure 8.1) for the range of parameters considered here.

Table 8.2: *The ground-state energy* E_0^{CCM} *of the scaled* ($\omega = 1$) *linear* $E \otimes e$ *PJT Hamiltonian, in the sub-resonant cases* $\omega_0 = 0.0$ *and* $\omega_0 = 0.5$, *obtained as a function of the coupling* k^2 *from a SUB-1 CCM calculation based on the RPJT scheme, compared to results (labeled* E_0^{CI}) *obtained via a CI diagonalization. Also shown is the percentage error* $\left|E_0^{\mathrm{CCM}} - E_0^{\mathrm{CI}}\right| / E_0^{\mathrm{CI}} \times 100$.

ω_0	k^2	E_0^{CI}	E_0^{CCM}	% Error
0.0	0.00	0.0000	0.0000	0.00
	0.25	-0.2262	-0.2261	0.04
	0.50	-0.4220	-0.4215	0.12
	0.75	-0.6003	-0.5991	0.20
	1.00	-0.7670	-0.7650	0.26
	2.00	-1.3689	-1.3637	0.38
	3.00	-1.9189	-1.9117	0.38
	5.00	-2.9610	-2.9532	0.26
	7.00	-3.9761	-3.9693	0.17
	10.00	-5.4850	-5.4797	0.10
	15.00	-7.9907	-7.9870	0.05
	20.00	-10.4932	-10.4904	0.03
	30.00	-15.4956	-15.4937	0.01
0.5	0.00	-0.2500	-0.2500	0.00
	0.25	-0.4125	-0.4125	0.00
	0.50	-0.5679	-0.5679	0.00
	0.75	-0.7180	-0.7178	0.03
	1.00	-0.8639	-0.8635	0.05
	2.00	-1.4191	-1.4179	0.08
	3.00	-1.9481	-1.9463	0.09
	5.00	-2.9736	-2.9716	0.07
	7.00	-3.9832	-3.9815	0.04
	10.00	-5.4892	-5.4878	0.03
	15.00	-7.9932	-7.9922	0.01
	20.00	-10.4950	-10.4943	0.01
	30.00	-15.4967	-15.4963	0.00

Table 8.3: *The ground–state energy* E_0^{CCM} *of the scaled* $(\omega = 1)$ *linear* $E \otimes e$ *PJT Hamiltonian, in the supra–resonant cases* $\omega_0 = 1.5$ *and* $\omega_0 = 2.0$*, obtained as a function of the coupling* k^2 *from a SUB-1 CCM calculation based on the RPJT scheme, compared to results (labeled* E_0^{CI}*) obtained via a CI diagonalization. Also shown is the percentage error* $\left|E_0^{\mathrm{CCM}} - E_0^{\mathrm{CI}}\right| / E_0^{\mathrm{CI}} \times 100$.

ω_0	k^2	E_0^{CI}	E_0^{CCM}	% Error
1.5	0.00	-0.7500	-0.7500	0.00
	0.25	-0.8510	-0.8510	0.00
	0.50	-0.9540	-0.9539	0.01
	0.75	-1.0589	-1.0588	0.01
	1.00	-1.1656	-1.1654	0.02
	2.00	-1.6095	-1.6085	0.06
	3.00	-2.0745	-2.0728	0.08
	5.00	-3.0402	-3.0382	0.07
	7.00	-4.0264	-4.0245	0.05
	10.00	-5.5174	-5.5159	0.03
	15.00	-8.0111	-8.0101	0.01
	20.00	-10.5082	-10.5074	0.01
	30.00	-15.5054	-15.5048	0.00
2.0	0.00	-1.0000	-1.0000	0.00
	0.25	-1.0845	-1.0845	0.00
	0.50	-1.1714	-1.1713	0.01
	0.75	-1.2607	-1.2604	0.02
	1.00	-1.3525	-1.3519	0.04
	2.00	-1.7440	-1.7407	0.19
	3.00	-2.1708	-2.1645	0.29
	5.00	-3.0945	-3.0861	0.27
	7.00	-4.0625	-4.0549	0.19
	10.00	-5.5413	-5.5354	0.11
	15.00	-8.0266	-8.0224	0.05
	20.00	-10.5196	-10.5164	0.03
	30.00	-15.5129	-15.5107	0.01

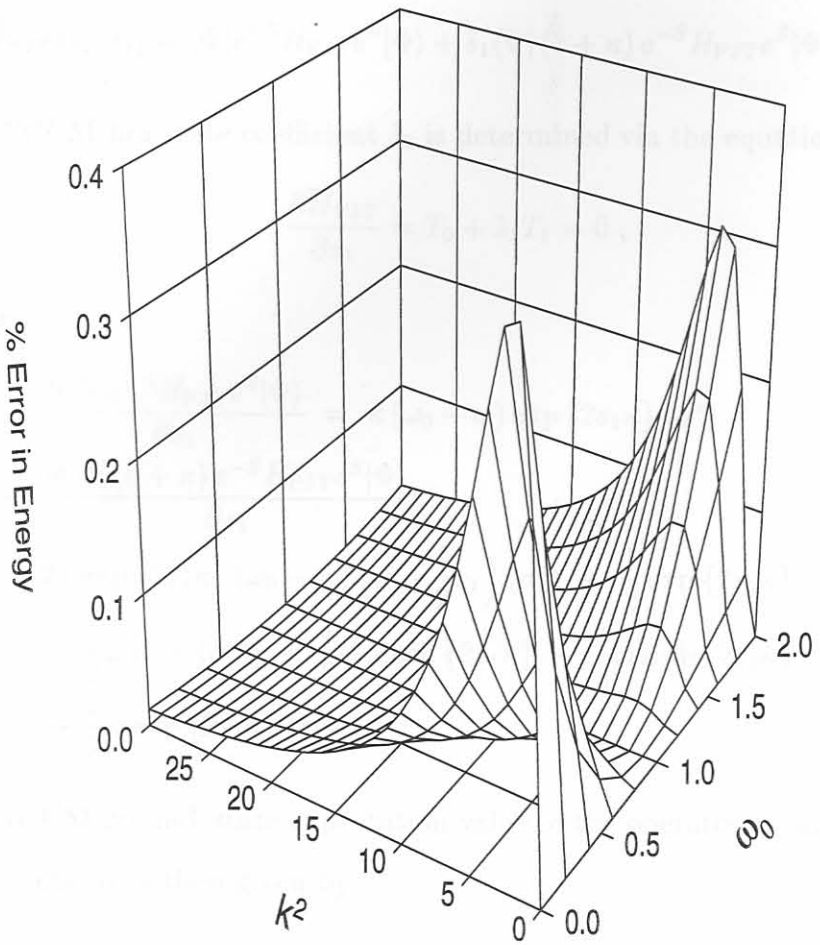

Figure 8.1: *The percentage error, as compared to the results of a CI diagonalization, in the ground–state energy of the scaled* ($\omega = 1$) *linear* $E \otimes e$ *PJT Hamiltonian obtained from a SUB-1 CCM calculation based on the RPJT scheme, as a function of the coupling* k^2 *and the two–level splitting* ω_0.

In order to determine ground–state expectation values other than the energy in the SUB-1 RPJT scheme, we construct the energy functional

$$\overline{H}_{\rm PJT}\left[s_1,\tilde{s}_1\right] = \langle\Phi|e^{-S}H_{\rm PJT}e^{S}|\Phi\rangle + \tilde{s}_1\langle\Phi|\left(c+\kappa\right)e^{-S}H_{\rm PJT}e^{S}|\Phi\rangle\ . \qquad (8.13)$$

The NCCM bra state coefficient $\tilde{s}_1$ is determined via the equation

$$\frac{\partial\overline{H}_{\rm PJT}}{\partial s_1} = T_0 + \tilde{s}_1 T_1 = 0\ , \qquad (8.14)$$

where

$$\begin{aligned}
T_0 &\equiv \frac{\partial\langle\Phi|e^{-S}H_{\rm PJT}e^{S}|\Phi\rangle}{\partial s_1} = \kappa\left(\omega_0-\omega\right)\exp\left\{2s_1\kappa\right\}\langle\sigma^z\rangle \\
T_1 &\equiv \frac{\partial\langle\Phi|\left(c+\kappa\right)e^{-S}H_{\rm PJT}e^{S}|\Phi\rangle}{\partial s_1} \\
&= 2\kappa\exp\left\{2s_1\kappa\right\}\left(\omega_0-\omega\right)\left(\kappa-\frac{1}{2}s_1\right)\langle\sigma^z\rangle + \frac{1}{2}\exp\left\{2s_1\kappa\right\}\left(\omega_0-\omega\right)\langle\sigma^z\rangle \\
&\quad + \frac{1}{2}\omega\left[1-\langle\sigma^z\rangle\right] + \frac{1}{2}\omega_0\cosh\left\{2s_1\kappa\right\} - \frac{1}{2}\omega\sinh\left\{2s_1\kappa\right\} \\
&\quad - \frac{1}{2}\omega\exp\left\{2s_1\kappa\right\}\langle\sigma^z\rangle\ . \qquad (8.15)
\end{aligned}$$

The NCCM ground–state expectation value of the operator σ^z in the SUB-1 RPJT scheme is then given by

$$\langle\sigma^z\rangle^{\rm CCM} = \exp\left\{2s_1\kappa\right\}\langle\sigma^z\rangle\left(1-s_1\tilde{s}_1+2\kappa\tilde{s}_1\right) + \frac{\tilde{s}_1}{2\kappa}\sinh\left\{2s_1\kappa\right\}\ , \qquad (8.16)$$

with s_1 and $\tilde{s}_1$ determined via (8.11) and (8.15), respectively. In Figure 8.2, our results for $\langle\sigma^z\rangle^{\rm CCM}$, for the representative cases $\omega_0 = 0$ and $\omega_0 = 2.0$, are compared to the numerical diagonalization results. Our CCM results, though quantitatively inaccurate for intermediate and large coupling, are at least qualitatively acceptable over the full coupling spectrum.

Figure 8.2: *The ground–state expectation value* $\langle\sigma^z\rangle$ *for the scaled* ($\omega = 1$) *linear* $E \otimes e$ *PJT Hamiltonian, in the representative cases* $\omega_0 = 0.0$ *and* $\omega_0 = 2.0$, *obtained as a function of the coupling* k^2 *from a SUB-1 CCM calculation based on the RPJT scheme (dotted lines labeled* $\langle\sigma^z\rangle^{\rm CCM}$*), compared to results obtained via a CI diagonalization (solid lines labeled* $\langle\sigma^z\rangle^{\rm CI}$*).*

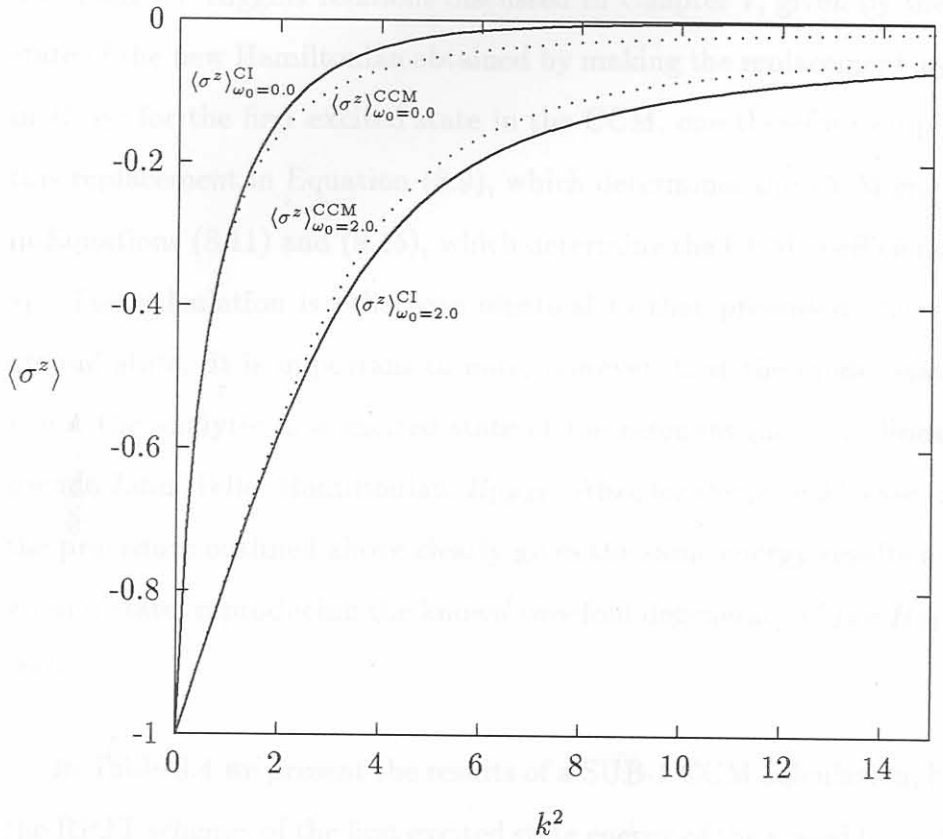

The first excited state energy of $H_{\rm PJT}$ is useful in *e.g.* the analysis of the optical absorption properties of the linear $E \otimes e$ PJT model. Since the symmetries of the Hamiltonian $H_{\rm PJT}$ are built into our calculation, it is straightforward to extend the CCM analysis based on the RPJT scheme to the first excited state of $H_{\rm PJT}$, which is an odd–parity state corresponding to $j = 1/2$. This can be done by repeating the ground–state analysis above,

but with a model state of the form

$$|\Phi\rangle = \frac{1}{\sqrt{I_0\left(2\kappa^2\right) + I_1\left(2\kappa^2\right)}} \left\{ I_0\left(2\kappa c^\dagger\right) - I_1\left(2\kappa c^\dagger\right) \right\} |0\rangle|0\rangle|\uparrow\rangle \,. \qquad (8.17)$$

However, it is easily shown that this is equivalent to the following procedure: the first excited state of $H_{\rm PJT}$ is, due to the invariance properties of the (exact) Longuet–Higgins relations discussed in Chapter 7, given by the ground state of the new Hamiltonian obtained by making the replacement $\omega_0 \rightarrow -\omega_0$ in $H_{\rm PJT}$; for the first excited state in the CCM, one therefore simply makes this replacement in Equation (8.9), which determines the CCM energy, and in Equations (8.11) and (8.15), which determine the CCM coefficients s_1 and $\tilde{s}_1$. The calculation is otherwise identical to that presented above for the ground state. It is important to note, however, that the model state (8.17) is not the analytic first excited state of the resonant ($\omega_0 = \omega$) linear $E \otimes e$ pseudo Jahn–Teller Hamiltonian, $H_{\rm RPJT}$. Also, for the pure JT case ($\omega_0 = 0$), the procedure outlined above clearly gives the same energy results as for the ground state, reproducing the known two–fold degeneracy of the $H_{\rm JT}$ ground state.

In Table 8.4 we present the results of a SUB-1 CCM calculation, based on the RPJT scheme, of the first excited state energy of the scaled ($\omega = 1$) linear $E \otimes e$ PJT Hamiltonian, in the cases $\omega_0 = 0.5$ and $\omega_0 = 1.0$, as a function of the coupling k^2. We also show the percentage error in the CCM results, as compared to the (converged) results of a CI diagonalization of $H_{\rm PJT}$ in a basis consisting of 101 odd–parity $j = 1/2$ states. Though not as good as the ground–state results, the CCM results for the first excited state energy are still very accurate, over the full coupling spectrum, for the range of ω_0

Table 8.4: *The first excited state energy* E_1^{CCM} *of the scaled* $(\omega = 1)$ *linear* $E \otimes e$ *PJT Hamiltonian, in the cases* $\omega_0 = 0.5$ *and* $\omega_0 = 1.0$, *obtained as a function of the coupling* k^2 *from a SUB-1 CCM calculation based on the RPJT scheme, compared to results (labeled* E_1^{CI}*) obtained via a CI diagonalization. Also shown is the percentage error* $\left|E_1^{\mathrm{CCM}} - E_1^{\mathrm{CI}}\right| / E_1^{\mathrm{CI}} \times 100$.

ω_0	k^2	E_1^{CI}	E_1^{CCM}	% Error
0.5	0.00	0.2500	0.2500	0.000000
	0.25	-0.0935	-0.0930	0.531421
	0.50	-0.3325	-0.3307	0.528784
	0.75	-0.5351	-0.5317	0.636452
	1.00	-0.7176	-0.7124	0.726559
	2.00	-1.3505	-1.3387	0.874016
	3.00	-1.9123	-1.8967	0.815322
	5.00	-2.9620	-2.9454	0.559254
	7.00	-3.9785	-3.9641	0.361388
	10.00	-5.4874	-5.4763	0.201573
	15.00	-7.9925	-7.9848	0.096169
	20.00	-10.4946	-10.4888	0.055698
	30.00	-15.4966	-15.4927	0.025425
1.0	0.00	0.5000	0.5000	0.000000
	0.25	-0.0560	-0.0558	0.395322
	0.50	-0.3173	-0.3156	0.552823
	0.75	-0.5307	-0.5267	0.757497
	1.00	-0.7197	-0.7130	0.921794
	2.00	-1.3633	-1.3466	1.227422
	3.00	-1.9277	-1.9047	1.192903
	5.00	-2.9764	-2.9511	0.848603
	7.00	-3.9904	-3.9682	0.554943
	10.00	-5.4963	-5.4792	0.310645
	15.00	-7.9986	-7.9868	0.148102
	20.00	-10.4993	-10.4903	0.085685
	30.00	-15.4997	-15.4936	0.039062

considered here. For $\omega_0 > 1$, the SUB-1 calculation based on the RPJT scheme breaks down, indicating that the model state (8.17) is not a physically realistic starting state for the first excited state beyond $\omega_0 = 1$.

In Figure 8.3 we plot the percentage error in the results of the SUB-1 RPJT scheme calculation of the first excited state energy of H_{PJT}, as compared to results obtained via the CI method, as a function of k^2 and ω_0. For the range $0 \leq \omega_0 \leq 1$, the maximum percentage error of 1.2 % occurs at intermediate coupling for the resonant case $\omega_0 = 1$. Thus we have shown that, even to first order, the CCM can yield very accurate results for the ground and first excited states of the linear $E \otimes e$ JT and PJT Hamiltonians, provided that a model state is chosen which not only mimics the physical behaviour of these states, but also incorporates the correct J and Π_{PJT} symmetries.

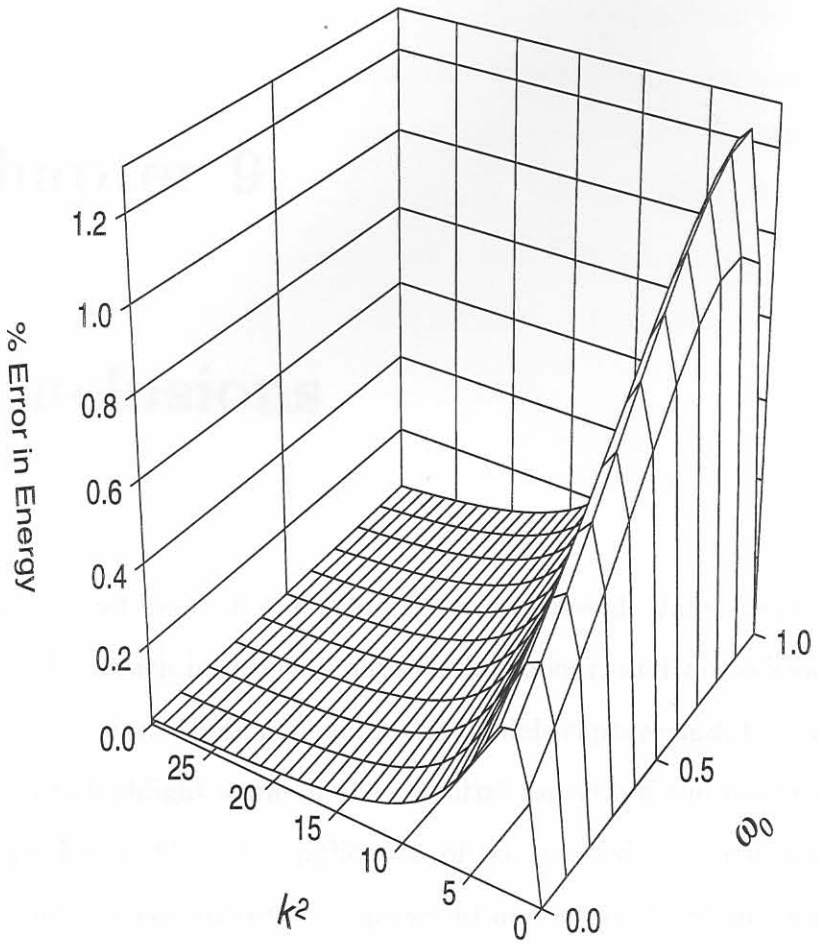

Figure 8.3: *The percentage error, as compared to the results of a CI diagonalization, in the first excited state energy of the scaled* ($\omega = 1$) *linear* $E \otimes e$ *PJT Hamiltonian obtained from a SUB-1 CCM calculation based on the RPJT scheme, as a function of the coupling* k^2 *and the two–level splitting* ω_0.

Chapter 9

Conclusions

The Rabi and linear $E \otimes e$ Jahn–Teller and pseudo Jahn–Teller Hamiltonians exhibit much interesting physical behaviour, and are relevant in many fields in physics. These non–adiabatic models capture and, by virtue of their simplicity, highlight some of the essential aspects of the interacting many–body problem. Thus the application of the coupled cluster method, with its highly impressive history as a powerful and versatile *ab initio* many–body technique, to such apparently straightforward models is of interest. Indeed, in this thesis, we have found that a CCM analysis of the Rabi and linear $E \otimes e$ JT and PJT Hamiltonians is anything but trivial, and that a thorough investigation of these models is required in order to apply the method successfully.

Analytic solutions for the spectra of the Rabi and linear $E \otimes e$ JT and PJT Hamiltonians are available only at the isolated Juddian values of the

parameters which occur in these Hamiltonians. In this thesis, we have presented an elegant operator–based method which simplifies the analysis of the Juddian solutions for the linear $E \otimes e$ JT and PJT models [Bi99b]. For all the Hamiltonians considered here, we have used the isolated analytic solutions as a benchmark for the ground and first excited state results obtained via the configuration–interaction method. We conclude that the numerical diagonalization of these models yields results which are effectively exact, provided that the set of configurations included in the CI method is sufficiently large.

In the analysis of a given many–body Hamiltonian, it is important that the symmetries of the Hamiltonian be taken into account. In general, this not only simplifies the analysis, but also leads to more accurate results. A parity symmetry is associated with each of the Hamiltonians considered here. In the case where the two levels of the fermionic subsystem are degenerate, the eigenstates of the Hamiltonian are doubly degenerate for all values of the coupling strength of the interaction between the fermionic and bosonic degrees of freedom. For finite fermionic level splitting ω_0, however, the parity symmetry lifts this degeneracy; in particular, the ground (first excited) state is then a unique even–parity (odd–parity) state for all values of the coupling.

For the Rabi Hamiltonian with $\omega_0 > 0$, we have presented a simple three–parameter variational calculation which, due to the incorporation of the correct parity symmetry, yields excellent results for both the ground and first excited states of the system; in the physically interesting case of atom–field resonance, the maximal percentage error in the ground–state energy, over

the full coupling spectrum, is 0.1 % [Bi99a]. For the linear $E \otimes e$ JT and PJT Hamiltonians, there is, in addition to the parity, also a conserved angular momentum component J. Due to the neglect of the J symmetry, the variational approach employed for the Rabi Hamiltonian does not readily generalize to the linear $E \otimes e$ JT and PJT case of two bosonic modes.

Using the CI results, the physical nature of the ground state of the Rabi and linear $E \otimes e$ JT and PJT Hamiltonians has been thoroughly examined. Although a phase transition does not occur, we have found that the ground state undergoes a change in character in a fairly well–defined transitional region of intermediate coupling. We have shown that this character change, which is closely analogous to the well–known crossover behaviour in the polaron problem, manifests itself in the occupation probabilities for the two levels of the fermionic system. Furthermore, we have found that this change in character also occurs in the even–parity ground–state in the case $\omega_0 = 0$, where the ground state is in fact doubly degenerate. It follows that the character change in the case $\omega_0 > 0$ is therefore not related to the onset of near–degeneracy in the transitional coupling region.

In previous applications of the CCM to both a multimode Rabi Hamiltonian and the linear $E \otimes e$ JT Hamiltonian, the symmetries of these Hamiltonians have been neglected. Our initial attempts at applying the CCM to the ground and first excited states of the Rabi Hamiltonian, with proper consideration of the parity symmetry, were based on the noninteracting model state of Schemes I and II (see Tables D.1). These calculations yielded very accurate results in the weak–coupling regime. However, the results also pro-

vided strong evidence for a spurious parity–breaking phase transition in the transitional coupling region [Bi96], even in the case $\omega_0 = 0$. Physically, the breakdown of the method in this regime is a result of the marked character change in the exact ground state, which is not in any way reflected in the noninteracting model state. We have formally demonstrated that the method fails as a direct result of the exponential form of the CCM ansatz for the ground–state wave function, which is incomplete, to any finite order, for the model state $|\Phi\rangle$ and cluster operator S of Scheme I. This is despite the fact that $|\Phi\rangle$ and $S = \sum_i s_i C_i^\dagger$ satisfy the requirement, dictated by the CCM formalism (see Chapter 3), that the set of states $\left\{C_i^\dagger|\Phi\rangle\right\}$ should span the many–body Hilbert space. This incompleteness is a serious defect not only of the CCM, but also of any method which relies on an $\exp S|\Phi\rangle$ parameterization of the ground state.

Subsequently, we showed that accurate CCM results for the ground and first excited state energies of the Rabi Hamiltonian can be obtained, provided that a coupling–dependent model state is chosen which mimics the change in character in the Rabi ground state; a common characteristic of such states is that they are exact in both the limits of zero and infinite coupling. In particular, a CCM calculation based on a model state of the two–parameter variational form (see Scheme IV in Table D.1) yields quantitatively accurate results which, for all couplings, compare favourably with results obtained via the benchmark three–parameter variational calculation. This CCM calculation is however not entirely satisfactory, since it involves considerably more computational effort than the variational analysis, and requires the use of a model state which of itself yields the overwhelming contribution to the exact

ground and first excited state energies.

None of the schemes employed in the CCM analysis of the Rabi Hamiltonian effectively generalize to the linear $E \otimes e$ JT and PJT Hamiltonians, since these schemes do not incorporate the J symmetry of the linear $E \otimes e$ models. For these Hamiltonians, however, we have obtained excellent first–order CCM results for the ground and first excited state energies, using as model states the analytic ground state of the linear $E \otimes e$ RPJT Hamiltonian, and the corresponding spin–flipped state, respectively [Bi99b]. These results, which require the solution of only a single transcendental equation, are far superior to those obtained via earlier CCM analyses and other many–body methods, and are quantitatively accurate over the full coupling spectrum for a range of values for the parameter ω_0. Also, in contrast to the Scheme IV calculation for the Rabi Hamiltonian, the CCM energy here dramatically improves on the model–state energy. This is especially true for the (pure) linear $E \otimes e$ JT model in the physically interesting region of intermediate coupling, where the exact energy differs substantially from the model–state energy.

The analyses and results presented in this thesis suggest several avenues for further exploration. It would be of interest to apply the CCM to the polaron problem. This would determine whether the incompleteness of the exponential ansatz for the ground–state wave function is also a feature of other systems which undergo a drastic ground–state character change without a true phase transition. Given the quality of the good–parity variational results for the Rabi Hamiltonian, it would also be interesting to investigate the possibility of constructing a variational ansatz for the linear $E \otimes e$ JT

and PJT Hamiltonians which incorporates all the symmetries of these models. Furthermore, the extension of our variational results for the Rabi Hamiltonian, and of our CCM results for the linear $E \otimes e$ JT and PJT Hamiltonians, to higher–lying states would allow for the consideration of both the time– and temperature–dependence of these models. This would permit comparison with experimental results.

Appendix A

Derivation of the General Model Hamiltonian

Here we present a first–principles derivation (in the context of quantum optics) of the general Hamiltonian (2.1).

A.1 The two–level atom

Consider an two–level atom, with the two relevant atomic states labeled $|a\rangle$ and $|b\rangle$, and let $\hbar\omega_0 = E_b - E_a$ denote the energy gap between the states. Choose the origin of the atomic energy scale midway between the levels, so that $E_a = -\frac{1}{2}\hbar\omega_0$, and $E_b = \frac{1}{2}\hbar\omega_0 = E_a + \hbar\omega_0$. The Pauli matrices (supplemented by the 2×2 unit matrix), form a convenient operator basis in the two–dimensional matrix space corresponding to the atom, and we may

thus, with a suitable choice of the z–axis, write the Hamiltonian for the atom as

$$H_{\text{atom}} = \frac{1}{2}\hbar\omega_0\sigma^z \,. \tag{A.1}$$

A.2 Quantization of the electromagnetic field

Consider now the quantization of the free (zero charge and current density) electromagnetic field [Man]. After eliminating from Maxwell's equations (in rationalized Gaussian units) the electric $[\mathbf{E}(\mathbf{r},t)]$ and magnetic $[\mathbf{B}(\mathbf{r},t)]$ fields in favour of the classical scalar $[\Phi(\mathbf{r},t)]$ and vector $[\mathbf{A}(\mathbf{r},t)]$ potentials via

$$\mathbf{B} = \nabla \times \mathbf{A} \,, \qquad \mathbf{E} = -\frac{1}{c}\frac{\partial \mathbf{A}}{\partial t} \tag{A.2}$$

and then enforcing the Coulomb or transverse gauge $\nabla \cdot \mathbf{A} = 0$, one finds that $\mathbf{A}$ satisfies the wave equation

$$\frac{1}{c^2}\frac{\partial^2 \mathbf{A}}{\partial t^2} - \nabla^2 \mathbf{A} = 0 \,, \tag{A.3}$$

whilst Φ is identically zero. We now treat the field as though it were confined to a cubical box of volume $V = L^3$ and impose periodic boundary conditions. If necessary, one may take the limit $V \to \infty$ at the end of the calculation. We expand the vector potential in a Fourier series

$$\mathbf{A}(\mathbf{r},t) \;=\; -i \sum_{\mathbf{k}} \sum_{s=1}^{2} \sqrt{\frac{\hbar c^2}{2V\omega_k}} \left\{ b_{\mathbf{k},s}(t)\, e^{i\mathbf{k}\cdot\mathbf{r}} \;-\; b^*_{\mathbf{k},s}(t)\, e^{-i\mathbf{k}\cdot\mathbf{r}} \right\} \hat{e}_{\mathbf{k},s} \,, \tag{A.4}$$

with $\omega_k = c|\mathbf{k}|$, where the $\mathbf{k}$–sum is over all wave vectors

$$\mathbf{k} = \frac{2\pi}{L}(n_x, n_y, n_z) \qquad (n_x, n_y, n_z = 0, \pm 1, \pm 2, \ldots) \tag{A.5}$$

satisfying the boundary conditions, and where $\hat{e}_{\mathbf{k},s}, s = 1,2$ represent unit vectors along the two independent directions perpendicular to the wave vector $\mathbf{k}$, thereby also satisfying the requirement of transversality imposed by the Coulomb gauge. Thus (A.4) corresponds to an expansion of the vector potential $\mathbf{A}$ in terms of linearly polarized travelling wave modes. The fact that (A.4) must satisfy the wave equation (A.3) determines the time dependence of the Fourier coefficients as

$$b_{\mathbf{k},s}(t) = b_{\mathbf{k},s} e^{-i\omega_k t} , \tag{A.6}$$

and the constant in (A.4) has been chosen so that the total energy

$$H_{\text{field}} = \frac{1}{2} \int_V \left(\mathbf{E}^2 + \mathbf{B}^2 \right) \, d^3\mathbf{r} \tag{A.7}$$

of the radiation field then assumes the time–independent form

$$H_{\text{field}} = \sum_{\mathbf{k}} \sum_{s=1}^{2} \hbar\omega_k b^*_{\mathbf{k},s} b_{\mathbf{k},s} \, . \tag{A.8}$$

By analogy with a system of decoupled harmonic oscillators, this form for the classical field energy suggests that the field may be quantized by promoting the Fourier coefficients $b_{\mathbf{k},s}(t)$ in the expansion (A.4) to operators $b_{\mathbf{k},s}$ satisfying Bose commutation relations. Confining ourselves to two perpendicularly polarized modes, of frequencies ω_1 and ω_2 and which we shall label modes 1 and 2, and neglecting the constant zero point energy of the two modes, we may then write for the field the Hamiltonian

$$H_{\text{field}} = \hbar\omega_1 \, b_1^\dagger b_1 + \hbar\omega_2 \, b_2^\dagger b_2 \tag{A.9}$$

where the bosonic operators satisfy the standard commutation relations (2.2). Furthermore, $\mathbf{E}_n$, the electric field corresponding to mode n, now becomes

an operator of the form

$$\mathbf{E}_n(\mathbf{r},t) \;=\; -\,\epsilon_n \left\{ b_n\, e^{i\mathbf{k}\cdot\mathbf{r}} \;+\; b_n^\dagger\, e^{-i\mathbf{k}\cdot\mathbf{r}} \right\} \hat{e}_{\mathbf{k},n} \qquad (n=1,2) \qquad \text{(A.10)}$$

where $\epsilon_n = \sqrt{\frac{\hbar\omega_k}{2V}}$ denotes the electric field per quantum (photon) in mode n, $\hat{e}_{\mathbf{k},n} \cdot \hat{e}_{\mathbf{k},m} = \delta_{n,m}$ since the fields are perpendicularly polarized, and with a similar expression for the magnetic field. There are many subtleties in the quantization of the electromagnetic field that have been ignored here (see *e.g.* [Mar], [Coh] or [Hua]).

A.3 The dipole interaction Hamiltonian

In order to determine the interaction Hamiltonian for the coupling of the atom to the field modes, we neglect any interaction with the magnetic field, and make the co–called dipole approximation [Mar, Man]. If we take the origin for $\mathbf{r}$ at the atomic center of mass, and assume that the fields do not vary appreciably over distances of the order of the atomic dimensions so that we may take $\mathbf{k}\cdot\mathbf{r} = 0$, then the dipole interaction between the atom and the two field modes has the form

$$H_{\text{int}} = -\mathbf{p}\cdot(\mathbf{E}_1 + \mathbf{E}_2)\ . \qquad \text{(A.11)}$$

Here the atomic dipole moment operator $\mathbf{p}$ for the N atomic electrons, each of charge e, located at positions $\mathbf{r}_i, i = 1,2,\ldots,N$ has the form

$$\mathbf{p} \;=\; N\,e\left(\frac{1}{N}\sum_{i=1}^{N}\mathbf{r}_i\right) \;\equiv\; e\mathbf{r}\,, \qquad \text{(A.12)}$$

and

$$\mathbf{E}_n(\mathbf{r},t) \;=\; -\,\epsilon_n \left\{ b_n \;+\; b_n^\dagger \right\} \hat{e}_{\mathbf{k},n} \qquad (n=1,2) \qquad \text{(A.13)}$$

due to the dipole approximation. By the atomic parity selection rule, the diagonal elements of the matrix representing the dipole operator $\mathbf{p}$ in the atomic basis $\{|a\rangle, |b\rangle\}$ are zero, and we only consider atomic levels such that the off–diagonal elements

$$\begin{aligned} \mathbf{p}_{ab} &= \langle a|\mathbf{p}|b\rangle = \langle a|ex|b\rangle\hat{x} + \langle a|ey|b\rangle\hat{y} + \langle a|ez|b\rangle\hat{z} \\ \mathbf{p}_{ba} &= \langle b|\mathbf{p}|a\rangle = \mathbf{p}_{ab}^{*} , \end{aligned} \tag{A.14}$$

with $\hat{z}$ representing the atomic quantization axis, are nonzero. It is then straightforward to show that the interaction Hamiltonian (A.11) assumes the form

$$\begin{aligned} H_{\text{int}} &= \hbar\left(b_1^{\dagger} + b_1\right)\left(\text{Re}\left[\beta_1\right]\sigma^x - \text{Im}\left[\beta_1\right]\sigma^y\right) \\ &\quad + \hbar\left(b_2^{\dagger} + b_2\right)\left(\text{Re}\left[\beta_2\right]\sigma^x - \text{Im}\left[\beta_2\right]\sigma^y\right) \end{aligned} \tag{A.15}$$

where

$$\beta_n = \mathcal{P}_n\sqrt{\frac{\omega_n}{2\hbar\mathcal{V}}} \qquad (n = 1, 2) \tag{A.16}$$

and $\mathcal{P}_n$ denotes the component of $\mathbf{p}_{ab}$ along $\hat{e}_n$.

We may now, without loss of generality, take the parameters β_1 and β_2 to be pure real and pure imaginary, respectively, as shown by the following argument: Choose the atomic quantization axis $\hat{z}$ so as to be perpendicular to the plane defined by the orthogonal polarization axes of the two modes. Orient $\hat{x}$ and $\hat{y}$ such that $\hat{e}_n$ makes an angle α_n with $\hat{x}$, with $\alpha_2 = \alpha_1 + \pi/2$, and α_1 as yet arbitrary. By the atomic angular momentum selection rule (or, more formally, via the Wigner-Eckhardt theorem) $\langle a|y|b\rangle = \pm i\langle a|x|b\rangle$. Thus

$$\mathcal{P}_n = \mathbf{p}_{ab}\cdot\hat{e}_n = e\,\langle a|x|b\rangle e^{\pm i\alpha_n} . \tag{A.17}$$

We are free to choose α_1 such that $e^{\pm i\alpha_1}$ cancels the phase of $\langle a|x|b\rangle$, so that $\mathcal{P}_1 = e|\langle a|x|b\rangle|$ is pure real, and $\mathcal{P}_2 = \pm e|\langle a|x|b\rangle|i$ is pure imaginary. Thus the interaction Hamiltonian (A.15) may be written in the final form

$$H_{\text{int}} = \hbar\eta_1 \left(b_1^\dagger + b_1\right)\sigma^x - \hbar\eta_2 \left(b_2^\dagger + b_2\right)\sigma^y \qquad \text{(A.18)}$$

where

$$\eta_n = e|\langle a|x|b\rangle|\sqrt{\frac{\omega_n}{2\hbar\mathcal{V}}} \qquad (n = 1, 2) \qquad \text{(A.19)}$$

denotes the (purely real) dipole coupling constant for mode n. Combining the Hamiltonians (A.1), (A.9) and (A.18), and setting $\hbar = 1$, we obtain the general model Hamiltonian (2.1).

Appendix B

Useful Identities and Commutation Relations

For the model Hamiltonians considered here, the Hausdorff expansion (3.8) often involves commutators either of Pauli matrices or of operators which obey bosonic commutation relations. Here we therefore present several identities for such operators which are useful in the application of the CCM to these models.

B.1 Operators for two–level systems

The Pauli matrices $\sigma^k, k \in \{x, y, z\}$, and the raising and lowering operators σ^+ and σ^- respectively, have the following form in the eigenbasis of σ^z:

$$\sigma^z = \begin{bmatrix} 1 & 0 \\ 0 & -1 \end{bmatrix} \quad , \quad I = \begin{bmatrix} 1 & 0 \\ 0 & 1 \end{bmatrix}$$

$$\sigma^x = \frac{1}{2}\left(\sigma^+ + \sigma^-\right) = \begin{bmatrix} 0 & 1 \\ 1 & 0 \end{bmatrix} \quad , \quad \sigma^y = \frac{i}{2}\left(\sigma^- - \sigma^+\right) = \begin{bmatrix} 0 & -i \\ i & 0 \end{bmatrix}$$

$$\sigma^+ = \sigma^x + i\sigma^y = \begin{bmatrix} 0 & 2 \\ 0 & 0 \end{bmatrix} \quad , \quad \sigma^- = \sigma^x - i\sigma^y = \begin{bmatrix} 0 & 0 \\ 2 & 0 \end{bmatrix} . \quad \text{(B.1)}$$

Note that some authors choose to define $\sigma^\pm = \frac{1}{2}\sigma^x \pm i\sigma^y$, resulting in a rescaling of the dipole coupling constant η in our model Hamiltonians.

In the following identities, $k, l, m \in \{x, y, z\}$, n is an arbitrary integer, and α is an arbitrary real number:

$$\left(\sigma^k\right)^2 = \left(\sigma^k\right)^{2n} = I \, , \quad \left(\sigma^k\right)^{2n+1} = \sigma^k$$

$$\exp\left\{i\alpha\pi\left[\tfrac{1}{2}\left(\sigma^k + 1\right)\right]\right\} = \left[\cos\left(\alpha\tfrac{\pi}{2}\right) + i\sin\left(\alpha\tfrac{\pi}{2}\right)\sigma^k\right]\exp\left(i\alpha\tfrac{\pi}{2}\right)$$

$$\exp\left\{i\pi\left[\tfrac{1}{2}\left(\sigma^k + 1\right)\right]\right\} = -\sigma^k \quad (\alpha = 1) \, . \quad \text{(B.2)}$$

The latter identity is particularly useful in verifying the commutation relations between the various parity operators (2.4) and the general model Hamiltonian (2.1) in Chapter 2.

We make frequent use of the following products and commutation relations (here $k,l,m \in \{x,y,z\}$ with $k \neq l$, and ϵ_{klm} is the totally antisymmetric Levi–Civita symbol):

$$\begin{array}{lll}
\sigma^k\sigma^l = i\epsilon_{klm}\sigma_m \,, & \sigma^l\sigma^k = -i\epsilon_{klm}\sigma_m \,, & \left[\sigma^k,\sigma^l\right] = 2i\epsilon_{klm}\sigma_m \\
\sigma^z\sigma^+ = \sigma^+ \,, & \sigma^+\sigma^z = -\sigma^+ \,, & [\sigma^z,\sigma^+] = 2\sigma^+ \\
\sigma^z\sigma^- = -\sigma^- \,, & \sigma^-\sigma^z = \sigma^- \,, & [\sigma^z,\sigma^-] = -2\sigma^- \\
\sigma^x\sigma^+ = 1-\sigma^z \,, & \sigma^+\sigma^x = 1+\sigma^z \,, & [\sigma^x,\sigma^+] = -2\sigma^z \\
\sigma^x\sigma^- = 1+\sigma^z \,, & \sigma^-\sigma^x = 1-\sigma^z \,, & [\sigma^x,\sigma^-] = 2\sigma^z \\
\sigma^y\sigma^+ = i\,(1-\sigma^z) \,, & \sigma^+\sigma^y = i\,(1+\sigma^z) \,, & [\sigma^y,\sigma^+] = -2i\sigma^z \\
\sigma^y\sigma^- = -i\,(1+\sigma^z) \,, & \sigma^-\sigma^y = -i\,(1-\sigma^z) \,, & [\sigma^y,\sigma^-] = -2i\sigma^z \\
\sigma^+\sigma^- = 2\,(1+\sigma^z) \,, & \sigma^-\sigma^+ = 2\,(1-\sigma^z) \,, & [\sigma^+,\sigma^-] = 4\sigma^z \,.
\end{array} \tag{B.3}$$

B.2 General commutation relations

Let A, B, C, D denote arbitrary operators. We make frequent use of the following standard identities:

$$\begin{aligned}
[A,BC] &= [A,B]\;C + B\;[A,C] \\
[AB,C] &= A\;[B,C] + [A,C]\;B \,.
\end{aligned} \tag{B.4}$$

If $[A,B] = [A,D] = 0$ and also $[C,B] = [C,D] = 0$, then

$$\begin{aligned}
[AB,CD] &= [A,C]\,B\;D + C\;A\,[B,D] \\
&= [A,C]\,D\;B + A\;C\,[B,D] \,.
\end{aligned} \tag{B.5}$$

B.2.1 The Hausdorff expansion

For arbitrary operators A and B, we define

$$[B,A]_0 \equiv B\ , \qquad [B,A]_{m+1} = [[B,A]_m\ ,A] \qquad (m=0,1,2,\ldots)\ . \quad \text{(B.6)}$$

Note that $[B,A]_1 = [B,A]$, the usual commutator. Let $C(k,m)$ denote the binomial coefficient $\frac{k!}{m!(k-m)!}$. Then it can readily be shown by induction that, for any $n \in \{0,1,2,\ldots\}$,

$$\begin{aligned} A^nB &= A^{n-k}\sum_{m=0}^{k}(-1)^m\ C(k,m)\ [B,A]_m\ A^{k-m} \quad \forall\ \ k \in \{0,1,2,\ldots,n\} \\ &= \sum_{m=0}^{n}(-1)^m\ C(n,m)\ [B,A]_m\ A^{n-m} \qquad (k=n)\ . \end{aligned} \quad \text{(B.7)}$$

Assuming that the exponential is well–defined, one may thus write

$$\begin{aligned} e^{-A}Be^{A} &= \sum_{n=0}^{\infty}\frac{(-1)^n}{n!}A^nB\ e^A \\ &= \sum_{n=0}^{\infty}\sum_{m=0}^{n}\frac{(-1)^{n+m}}{m!(n-m)!}[B,A]_m\ A^{n-m}\ e^A \\ &= \sum_{m=0}^{\infty}\sum_{n=m}^{\infty}\frac{(-1)^{n-m}}{m!(n-m)!}[B,A]_m\ A^{n-m}\ e^A \\ &= \left(\sum_{m=0}^{\infty}\frac{[B,A]_m}{m!}\right)\left(\sum_{k=0}^{\infty}\frac{(-1)^k}{k!}A^k\right)e^A \\ &= \sum_{m=0}^{\infty}\frac{1}{m!}[B,A]_m\ , \end{aligned} \quad \text{(B.8)}$$

which is the Hausdorff or nested commutator expansion (3.8) for the similarity transform of B through A (see also [Mer] for an alternative proof). The commutator

$$\begin{aligned} [A^n,B] &= \sum_{m=0}^{n}(-1)^m C(n,m)\,[B,A]_m\,A^{n-m} - BA^n \\ &= \sum_{m=1}^{n}(-1)^m C(n,m)\,[B,A]_m\,A^{n-m} \qquad (n \geq 0) \end{aligned} \quad \text{(B.9)}$$

will also be useful in what follows.

B.2.2 Operators for which the commutator is a number

Consider now two otherwise arbitrary operators A and B for which the commutator is a c–number, say $[A, B] = z$. Then, since $[A, B]_m = 0 \ \forall \ m \geq 2$, it is clear from (B.9) above that

$$[A, B^n] = nB^{n-1}z \quad (n \geq 0) \ . \tag{B.10}$$

Let $f(B)$ now be an arbitrary function of B only, subject to the usual restriction that a convergent power series expansion

$$f(B) = \sum_{n=0}^{\infty} a_n B^n \tag{B.11}$$

exists. It is clear from (B.10) that we may formally write

$$[A, f(B)] = \frac{d\, f(B)}{d\, B}\, z \ , \tag{B.12}$$

where, for the purposes of evaluating the derivative, the operator B is treated as a real variable (see, *e.g.* [Mer] or [Hak]). We have also generalized (B.12) to show that, for any integer $n \geq 0$,

$$[A^n, f(B)] = \sum_{m=1}^{n} C(n,m)\, f^{(m)}(B)\, z^m\, A^{n-m}, \tag{B.13}$$

where $f^{(m)}(B)$ is a convenient shorthand for $\frac{d^m\, f(B)}{d\, B^m}$, and we define $f^{(0)}(B) \equiv f(B)$. The relation (B.13) is easily proved by induction. A final identity which we have often used is the Glauber–Weyl formula [Mer]

$$e^A e^B = e^{A+B+z/2} \ . \tag{B.14}$$

B.3 Bosonic commutation relations

For the bosonic annihilation and creation operators, b and $b^\dagger$ respectively, the standard commutation relation reads $\left[b, b^\dagger\right] = 1$, so that the relations (B.12) and (B.13) apply with $A = b$, $B = b^\dagger$ and $z = 1$ or $A = b^\dagger$, $B = b$ and $z = -1$. Thus for f an arbitrary function of the given argument only,

$$\left[b, f(b^\dagger)\right] = \frac{d\, f(b^\dagger)}{d\, b^\dagger} \quad \text{and} \qquad \left[b^\dagger, f(b)\right] = -\frac{d\, f(b)}{d\, b}\,. \tag{B.15}$$

In particular, for any integer $n \geq 0$

$$\begin{aligned}
\left[b, \left(b^\dagger\right)^n\right] &= n\left(b^\dagger\right)^{n-1} \\
\left[b^\dagger, b^n\right] &= -n b^{n-1} \\
\left[b^\dagger b, \left(b^\dagger\right)^n\right] &= b^\dagger\left[b, \left(b^\dagger\right)^n\right] = n\left(b^\dagger\right)^n \\
\left[b^\dagger b, b^n\right] &= \left[b^\dagger, b^n\right] b = -n b^n\,,
\end{aligned} \tag{B.16}$$

and for all $n, k \geq 0$

$$\left[b^n, \left(b^\dagger\right)^k\right] = \sum_{m=1}^{Min(n,k)} \frac{n!k!}{m!(n-m)!(k-m)!}\left(b^\dagger\right)^{k-m} b^{n-m}\,. \tag{B.17}$$

Other useful identities include

$$\begin{aligned}
e^b e^{b^\dagger} &= e^{b+b^\dagger+1/2} \\
\left[b, b^\dagger b\right]_m &= b \\
\left[\left(b^\dagger b\right)^n, b\right] &= b\left\{\left(b^\dagger b - 1\right)^n - \left(b^\dagger b\right)^n\right\} \\
\left[\exp\left\{i\alpha\pi\, b^\dagger b\right\}, b\right] &= b\, \exp\left\{i\alpha\pi\, b^\dagger b\right\}\left(e^{-i\alpha\pi} - 1\right) \\
\left[\exp\left\{i\pi\, b^\dagger b\right\}, b\right] &= -2\, b\, \exp\left\{i\pi\, b^\dagger b\right\} \qquad (\alpha = 1) \\
\left[b^\dagger, b^\dagger b\right]_m &= (-1)^m b^\dagger\,.
\end{aligned}$$

$$
\begin{aligned}
\left[\left(b^\dagger b\right)^n, b^\dagger\right] &= b^\dagger\left\{\left(b^\dagger b+1\right)^n-\left(b^\dagger b\right)^n\right\} \\
\left[\exp\left\{i\alpha\pi\ b^\dagger b\right\}, b^\dagger\right] &= b^\dagger\ \exp\left\{i\alpha\pi\ b^\dagger b\right\}\ \left(e^{i\alpha\pi}-1\right) \\
\left[\exp\left\{i\pi\ b^\dagger b\right\}, b^\dagger\right] &= -2\ b^\dagger\ \exp\left\{i\pi\ b^\dagger b\right\} \qquad (\alpha=1) \\
\left[b^\dagger b, b\right]_0 &= \left[b^\dagger b, b^\dagger\right]_0 = b^\dagger b \\
\left[b^\dagger b, b\right]_1 &= -b \qquad \left[b^\dagger b, b^\dagger\right]_1 = b^\dagger \\
\left[b^\dagger b, b\right]_m &= \left[b^\dagger b, b^\dagger\right]_m = 0 \quad \forall\ m \geq 2\ , \qquad \text{(B.18)}
\end{aligned}
$$

where it is important to note that the relations (B.15) are in general only valid in the case where f is strictly a function of the indicated argument only, so that a power series expansion for f of the form (B.11) exists.

Appendix C

Explicit Forms for Variational Expressions

Here explicit expressions are shown for the expectation values of the Rabi Hamiltonian, the operator σ^z and the boson number operator $b^\dagger b$ in the various variational states considered in Chapter 4. The equations which determine the corresponding variational parameters are also shown. The analytic behaviour of these parameters in the limit of small coupling is discussed in cases where this is useful for numerical purposes.

C.1 The mixed–parity two–parameter ansatz (4.30)

The expectation value of $H_{\rm Rabi}$ in the state (4.30) is given by

$$\begin{aligned}\langle H_{\rm Rabi}\rangle^{\rm Var}(x,y) &\equiv \langle \Psi^{\rm Var}(x,y)|H_{\rm Rabi}|\Psi^{\rm Var}(x,y)\rangle \\ &= -\frac{1}{2}\omega_0\left(\frac{1-y^2}{1+y^2}\right)+\omega\, x^2+8g\left(\frac{yx}{1+y^2}\right)\,. \end{aligned} \quad \text{(C.1)}$$

The minimization of (C.1) with respect to the variational parameters x and y yields the following results [Qi98] for the optimal values $x_{\rm opt}$ and $y_{\rm opt}$, and the variational ground–state energy $E_0^{\rm Var}=\langle H_{\rm Rabi}\rangle^{\rm Var}(x_{\rm opt},y_{\rm opt})$:

$$y_{\rm opt}=x_{\rm opt}=0\,,\qquad E_0^{\rm Var}=-\frac{1}{2}\omega_0 \quad \text{(C.2)}$$

for $g\le\sqrt{\omega\omega_0}/4$, and

$$\begin{aligned} y_{\rm opt} &= \pm\sqrt{\frac{16g^2-\omega\omega_0}{16g^2+\omega\omega_0}} \\ x_{\rm opt} &= \mp\frac{1}{8g\omega}\sqrt{256g^4-\omega^2\omega_0^2} \\ E_0^{\rm Var} &= -\frac{4g^2}{\omega}-\frac{\omega\omega_0^2}{64g^2} \end{aligned} \quad \text{(C.3)}$$

for $g>\sqrt{\omega\omega_0}/4$. As a check, note that the correct limiting behaviour

$$y_{\rm opt}\to\pm1\,,\qquad x_{\rm opt}\to\mp\frac{2g}{\omega}\,,\qquad E_0^{\rm Var}\to-\frac{4g^2}{\omega} \quad \text{(C.4)}$$

obtains as $g\to\infty$.

The expectation values of σ^z and $b^\dagger b$ are given by

$$\begin{aligned}\langle\sigma^z\rangle^{\rm Var} &= \left(\frac{y_{\rm opt}^2-1}{y_{\rm opt}^2+1}\right) \\ \langle b^\dagger b\rangle^{\rm Var} &= x_{\rm opt}^2\,, \end{aligned} \quad \text{(C.5)}$$

with $x_{\rm opt}$ and $v_{\rm opt}$ determined via (C.2) and (C.3).

C.2 The good–parity two–parameter ansatz (4.38)

The expectation value of $H_{\rm Rabi}$ in the state (4.38) is given by

$$\begin{aligned}\langle H_{\rm Rabi}\rangle_{\pm}^{\rm PBV2}(x,v) &\equiv \langle\Psi_{\pm}^{\rm PBV2}(x,v)|H_{\rm Rabi}|\Psi_{\pm}^{\rm PBV2}(x,v)\rangle \\ &= -\frac{1}{2}\omega_0\left(\frac{1-v^2}{1+v^2}\right) \\ &\quad +\omega\left(\frac{x^2}{1+v^2}\right)\left(\left[\tanh x^2\right]^{\pm 1}+v^2\left[\coth x^2\right]^{\pm 1}\right) \\ &\quad +8g\left(\frac{xv}{1+v^2}\right)\left(1-e^{-4x^2}\right)^{-1/2} \qquad \text{(C.6)}\end{aligned}$$

The derivative of $\langle H_{\rm Rabi}\rangle_{\pm}^{\rm PBV2}(x,v)$ with respect to v yields the first equation,

$$\begin{aligned}0 &= \left[4\,g\,x_{\rm opt}\left(1-\exp\left\{-4x_{\rm opt}^2\right\}\right)^{-1/2}\right]v_{\rm opt}^2 \\ &\quad -\left[\omega_0\mp\omega\,x_{\rm opt}^2\left(\tanh x_{\rm opt}^2-\coth x_{\rm opt}^2\right)\right]v_{\rm opt} \\ &\quad -\left[4\,g\,x_{\rm opt}\left(1-\exp\left\{-4x_{\rm opt}^2\right\}\right)^{-1/2}\right], \qquad \text{(C.7)}\end{aligned}$$

to be satisfied by the optimal values $x_{\rm opt}$ and $v_{\rm opt}$. For the case of positive parity (*i.e.* for the ground state), the derivative of $\langle H_{\rm Rabi}\rangle_{+}^{\rm PBV2}(x,v)$ with respect to x yields the second variational equation

$$\begin{aligned}0 &= \omega\,x_{\rm opt}\left(\tanh x_{\rm opt}^2+v_{\rm opt}^2\coth x_{\rm opt}^2\right) \\ &\quad +\omega\,x_{\rm opt}^3\left(\left[\operatorname{sech} x_{\rm opt}^2\right]^2-v_{\rm opt}^2\left[\operatorname{csch} x_{\rm opt}^2\right]^2\right) \\ &\quad +4\,g\,v_{\rm opt}\left(1-\exp\left\{-4x_{\rm opt}^2\right\}\right)^{-1/2}\times \\ &\quad \left(1-\frac{4x_{\rm opt}^2\exp\left\{-4x_{\rm opt}^2\right\}}{1-\exp\left\{-4x_{\rm opt}^2\right\}}\right). \qquad \text{(C.8)}\end{aligned}$$

The corresponding expression for the negative–parity (first excited) state is obtained by making the substitutions

$$\begin{aligned}\tanh x_{\rm opt}^2 &\longleftrightarrow \coth x_{\rm opt}^2 \\ \left[\operatorname{sech} x_{\rm opt}^2\right]^2 &\longleftrightarrow -\left[\operatorname{csch} x_{\rm opt}^2\right]^2. \qquad \text{(C.9)}\end{aligned}$$

Note that (C.7), being quadratic in $v_{\rm opt}$, is easily solved to yield an analytic expression for the parameter $v_{\rm opt}$ in terms of $x_{\rm opt}$, so that the variational (PBV) approach based on the two–parameter state (4.38) thus only requires the numerical solution of one non–linear equation (C.8) in the single unknown $x_{\rm opt}$.

The expectation values of σ^z and the photon number operator $b^\dagger b$ in the state (4.38) are given by

$$\begin{aligned} \langle \sigma^z \rangle^{\rm PBV2} &= \left(\frac{v_{\rm opt}^2 - 1}{v_{\rm opt}^2 + 1} \right) \\ \langle b^\dagger b \rangle^{\rm PBV2} &= \frac{x_{\rm opt}^2}{v_{\rm opt}^2 + 1} \left(\tanh x_{\rm opt}^2 + v_{\rm opt}^2 \coth x_{\rm opt}^2 \right) , \end{aligned} \tag{C.10}$$

with $x_{\rm opt}$ and $v_{\rm opt}$ determined via the variational equations (C.7) and (C.8).

C.3 The good–parity three–parameter ansatz (4.41)

In the state (4.41), $H_{\rm Rabi}$ has the expectation value

$$\begin{aligned} \langle H_{\rm Rabi} \rangle_{\pm}^{\rm PBV3}(x_1, x_2, v) &\equiv \langle \Psi_{\pm}^{\rm PBV3}(x_1, x_2, v) | H_{\rm Rabi} | \Psi_{\pm}^{\rm PBV3}(x_1, x_2, v) \rangle \\ &= A_v^2 \left[\frac{1}{2} \omega_0 (v^2 - 1) \right. \\ &+ \omega \left(x_1^2 \left[\tanh x_1^2 \right]^{\pm 1} + v^2 x_2^2 \left[\coth x_2^2 \right]^{\pm 1} \right) \\ &+ \left. 8 g v B_{\pm}(x_1, x_2) \right] \end{aligned} \tag{C.11}$$

with

$$B_{\pm}(x_1, x_2) = A_{1,\pm} A_{2,\mp} \left\{ (x_2 + x_1) e^{-(x_1 - x_2)^2/2} \pm (x_2 - x_1) e^{-(x_1 + x_2)^2/2} \right\} . \tag{C.12}$$

The minimization of $\langle H_{\text{Rabi}} \rangle_{\pm}^{\text{PBV3}}(x_1, x_2, v)$ with respect to v yields a quadratic equation for v_{opt} in terms of $x_{1,\text{opt}}$ and $x_{2,\text{opt}}$. The solution with the lowest energy is always given by

$$v_{\text{opt}} = \frac{\omega_0 + \omega C_{\pm}(x_{1,\text{opt}}, x_{2,\text{opt}})}{8gB_{\pm}(x_{1,\text{opt}}, x_{2,\text{opt}})} - \sqrt{1 + \left(\frac{\omega_0 + \omega C_{\pm}(x_{1,\text{opt}}, x_{2,\text{opt}})}{8gB_{\pm}(x_{1,\text{opt}}, x_{2,\text{opt}})}\right)^2}, \quad \text{(C.13)}$$

where

$$C_{\pm}(x_1, x_2) = -x_1^2 \left[\tanh x_1^2\right]^{\pm 1} + x_2^2 \left[\coth x_2^2\right]^{\pm 1}.$$

For the ground state, we are then left with the two coupled non-linear equations to be solved numerically for $x_{1,\text{opt}}$ and $x_{2,\text{opt}}$, namely

$$\begin{aligned}
0 &= \omega\, x_{1,\text{opt}} \left(\tanh x_{\text{opt}}^2 + x_{1,\text{opt}}^2 \left[\operatorname{sech} x_{\text{opt}}^2\right]^2\right) \\
&+ 4\, g\, v_{\text{opt}} x_{1,\text{opt}} \left(1 + \exp\left\{-2x_{1,\text{opt}}^2\right\}\right)^{-3/2} \left(1 - \exp\left\{-2x_{2,\text{opt}}^2\right\}\right)^{-1/2} \times \\
&\quad \exp\left\{-2x_{1,\text{opt}}^2\right\} \times \left(\left[x_{2,\text{opt}} + x_{1,\text{opt}}\right] \exp\left\{-\frac{1}{2}\left[x_{1,\text{opt}} - x_{2,\text{opt}}\right]^2\right\}\right. \\
&\quad \left. + \left[x_{2,\text{opt}} - x_{1,\text{opt}}\right] \exp\left\{-\frac{1}{2}\left[x_{1,\text{opt}} + x_{2,\text{opt}}\right]^2\right\}\right) \\
&+ 2\, g\, v_{\text{opt}} \left(1 + \exp\left\{-2x_{1,\text{opt}}^2\right\}\right)^{-1/2} \left(1 - \exp\left\{-2x_{2,\text{opt}}^2\right\}\right)^{-1/2} \times \\
&\quad \left[x_{2,\text{opt}}^2 - x_{1,\text{opt}}^2 + 1\right] \times \\
&\quad \left(\exp\left\{-\frac{1}{2}\left[x_{1,\text{opt}} - x_{2,\text{opt}}\right]^2\right\} - \exp\left\{-\frac{1}{2}\left[x_{1,\text{opt}} + x_{2,\text{opt}}\right]^2\right\}\right) \qquad \text{(C.14)}
\end{aligned}$$

and

$$\begin{aligned}
0 &= \omega v_{\text{opt}}^2\, x_{2,\text{opt}} \left(\coth x_{\text{opt}}^2 - x_{2,\text{opt}}^2 \left[\operatorname{csch} x_{\text{opt}}^2\right]^2\right) \\
&- 4\, g\, v_{\text{opt}} x_{2,\text{opt}} \left(1 + \exp\left\{-2x_{1,\text{opt}}^2\right\}\right)^{-1/2} \left(1 - \exp\left\{-2x_{2,\text{opt}}^2\right\}\right)^{-3/2} \times \\
&\quad \exp\left\{-2x_{2,\text{opt}}^2\right\} \times \left(\left[x_{2,\text{opt}} + x_{1,\text{opt}}\right] \exp\left\{-\frac{1}{2}\left[x_{1,\text{opt}} - x_{2,\text{opt}}\right]^2\right\}\right. \\
&\quad \left. + \left[x_{2,\text{opt}} - x_{1,\text{opt}}\right] \exp\left\{-\frac{1}{2}\left[x_{1,\text{opt}} + x_{2,\text{opt}}\right]^2\right\}\right) \\
&+ 2\, g\, v_{\text{opt}} \left(1 + \exp\left\{-2x_{1,\text{opt}}^2\right\}\right)^{-1/2} \left(1 - \exp\left\{-2x_{2,\text{opt}}^2\right\}\right)^{-1/2} \times
\end{aligned}$$

$$\left[x_{1,\mathrm{opt}}^2 - x_{2,\mathrm{opt}}^2 + 1\right] \times$$
$$\left(\exp\left\{-\frac{1}{2}\left[x_{1,\mathrm{opt}} - x_{2,\mathrm{opt}}\right]^2\right\} + \exp\left\{-\frac{1}{2}\left[x_{1,\mathrm{opt}} + x_{2,\mathrm{opt}}\right]^2\right\}\right) . \quad \text{(C.15)}$$

The corresponding expressions for the first excited state are obtained by making the substitutions

$$\begin{aligned}
\exp\left\{-2x_{i,\mathrm{opt}}^2\right\} &\longleftrightarrow -\exp\left\{-2x_{i,\mathrm{opt}}^2\right\} \qquad (i = 1, 2) \\
\exp\left\{-\frac{1}{2}\left[x_{1,\mathrm{opt}} + x_{2,\mathrm{opt}}\right]^2\right\} &\longleftrightarrow -\exp\left\{-\frac{1}{2}\left[x_{1,\mathrm{opt}} + x_{2,\mathrm{opt}}\right]^2\right\} \\
\tanh x_{\mathrm{opt}}^2 &\longleftrightarrow \coth x_{\mathrm{opt}}^2 \\
\left[\mathrm{sech}\, x_{\mathrm{opt}}^2\right]^2 &\longleftrightarrow -\left[\mathrm{csch}\, x_{\mathrm{opt}}^2\right]^2 . \qquad \text{(C.16)}
\end{aligned}$$

We note that there are classes of solutions with $x_{1,\mathrm{opt}} = 0$ (ground state) and $x_{2,\mathrm{opt}} = 0$ (excited state), but these do not minimize the energies, and so are not considered.

In the limit of very small couplings, it is possible to obtain asymptotic expressions for the parameters v_{opt}, $x_{1,\mathrm{opt}}$ and $x_{2,\mathrm{opt}}$, for the ground state,

$$\begin{aligned}
v_{\mathrm{opt}} &\rightarrow \frac{-2g}{\omega + \omega_0}, \\
x_{1,\mathrm{opt}} &\rightarrow \frac{2g}{\omega}\left\{1 + \frac{\omega_0}{\omega}\right\}^{-1/2}, \qquad \text{(C.17)} \\
x_{2,\mathrm{opt}} &\rightarrow \frac{2g}{\omega}\left\{1 + \frac{\omega_0}{3\omega}\right\}^{-1/2},
\end{aligned}$$

which yield good starting values for the numerical solution routines.

The situation for the first excited state is more complex, and depends explicitly on whether the system is sub- or supra-resonant. In fact, for the sub-resonant case ($\omega < \omega_0$), the asymptotic forms are the solutions of transcendental equations; however, one can show that in the limit of zero coupling, $x_{1,\mathrm{opt}}$ and v_{opt} are zero, but $x_{2,\mathrm{opt}}$ is a non-zero constant dependent on

the frequencies. For the other two cases, the asymptotic expression are

$$\begin{aligned} v_{\rm opt} &\rightarrow -1 \\ x_{1,\rm opt} &\rightarrow \frac{\sqrt{6g}}{\omega} \\ x_{2,\rm opt} &\rightarrow \sqrt{\frac{2g}{\omega}} \end{aligned} \tag{C.18}$$

for the case $\omega_0 = \omega$, and

$$\begin{aligned} v_{\rm opt} &\rightarrow \frac{\omega_0 - \omega}{2g} \\ x_{1,\rm opt} &\rightarrow \frac{2g}{\omega}\left\{1 - \frac{\omega_0}{3\omega}\right\}^{-1/2}, \\ x_{2,\rm opt} &\rightarrow \frac{2g}{\omega}\left\{1 - \frac{\omega_0}{\omega}\right\}^{-1/2}, \end{aligned} \tag{C.19}$$

for the case $\omega_0 < \omega$.

The expectation values of σ^z and the photon number operator $b^\dagger b$ in the three–parameter variational state (4.41) are given by

$$\begin{aligned} \langle \sigma^z \rangle^{\rm PBV3} &= \left(\frac{v_{\rm opt}^2 - 1}{v_{\rm opt}^2 + 1}\right) \\ \left\langle b^\dagger b \right\rangle^{\rm PBV3} &= \frac{1}{v_{\rm opt}^2 + 1}\left(x_{1,\rm opt}^2 \tanh x_{1,\rm opt}^2 + v_{\rm opt}^2 x_{2,\rm opt}^2 \coth x_{2,\rm opt}^2\right). \end{aligned} \tag{C.20}$$

It is often useful to express the wavefunctions for Hamiltonians such as the Rabi Hamiltonian in terms of their expansion in a basis of products of oscillator and two-level states, as these are often the form in which initial conditions are formulated. We present here the expansions for the three-parameter ansätze for the ground and first excited states:

$$
\begin{aligned}
|\Psi_{+}^{\mathrm{PBV3}}(x_1,x_2,v)\rangle &= A_v\left[A_{1,+}\, e^{-x_1^2/2}\sum_{n=0}^{\infty}\frac{x_1^{2n}}{\sqrt{(2n)!}}|2n\rangle|\downarrow\rangle\right.\\
&\quad\left.+\; vA_{2,-}\, e^{-x_2^2/2}\sum_{n=0}^{\infty}\frac{x_2^{2n+1}}{\sqrt{(2n+1)!}}|2n+1\rangle|\uparrow\rangle\right]\\
|\Psi_{-}^{\mathrm{PBV3}}(x_1,x_2,v)\rangle &= A_v\left[A_{1,-}\, e^{-x_1^2/2}\sum_{n=0}^{\infty}\frac{x_1^{2n+1}}{\sqrt{(2n+1)!}}|2n+1\rangle|\downarrow\rangle\right.\\
&\quad\left.+\; vA_{2,+}\, e^{-x_2^2/2}\sum_{n=0}^{\infty}\frac{x_2^{2n}}{\sqrt{(2n)!}}|2n\rangle|\uparrow\rangle\right]. \qquad \text{(C.21)}
\end{aligned}
$$

The expansions for the two-parameter states can be found by setting $x_1 = x_2 = x$ in these equations.

Appendix D

Explicit Forms for CCM Expressions

We present here explicit expressions for the similarity transformed Hamiltonian (3.5) and the CCM equations (3.14) for the various CCM schemes employed in the ground–state analysis of the Rabi Hamiltonian (see Table D.1). Where quantities other than the ground–state energy are required, we also give expressions for the energy functional $\overline{H}_{\rm Rabi}$ and the expectation value of these quantities in the CCM.

In Table D.2, we also show how the four ground–state CCM schemes may be modified to deal with the odd–parity first excited state of the Rabi Hamiltonian. It is intuitively clear, however, that the first excited state results may be obtained from the ground–state formalism by making the replacement $\omega_0 \rightarrow -\omega_0$, and in practice we have taken this simpler route to

generate, in addition to the ground–state results, first excited state results for the each of the CCM schemes considered here.

Table D.1: *The four schemes, labelled I—IV, employed in the ground–state CCM analysis of the (unrotated) Rabi Hamiltonian, showing the choice of model state* $|\Phi\rangle$ *and cluster correlation operators for each scheme. For all schemes, the cluster correlation operator* S*, which is required for the calculation of the NCCM ground–state energy, is shown. For Schemes I and III, the operator* $\tilde{S}$*, which is required for the calculation of other ground–state properties of the system in the NCCM, is shown, and for Scheme I, the operator* Σ *required for an ECCM ground–state energy calculation is also shown.*

Scheme	Model state $\|\Phi\rangle$	Cluster correlation operators S, $\tilde{S}$, Σ
I	$\|0\rangle\|\downarrow\rangle$	$S = S_1 + S_2$ $S_1 = \sum_{n=1}^{\infty} s_n^{(1)} (b^\dagger)^n$ $S_2 = \sum_{n=1}^{\infty} s_n^{(2)} (b^\dagger)^{n-1} \sigma^+$ $\tilde{S} = 1 + \tilde{S}_1 + \tilde{S}_2$ $\tilde{S}_1 = \sum_{n=1}^{\infty} \tilde{s}_n^{(1)} b^n$ $\tilde{S}_2 = \sum_{n=1}^{\infty} \tilde{s}_n^{(2)} b^{n-1} \sigma^-$ $\Sigma = \Sigma_1 + \Sigma_2$ $\Sigma_1 = \sum_{n=1}^{\infty} \sigma_n^{(1)} b^n$ $\Sigma_2 = \sum_{n=1}^{\infty} \sigma_n^{(2)} b^{n-1} \sigma^-$
II	$\|0\rangle\|\downarrow\rangle$	$S = \sum_{n=1}^{\infty} s_n \left(c^\dagger\right)^n, \quad c^\dagger = b^\dagger \sigma^x$
III	$\|\Psi_+\rangle$ [see (4.16)]	$S = \sum_{n=1}^{\infty} s_n \left(c^\dagger\right)^n, \quad c^\dagger = b^\dagger \sigma^x + 2g/\omega$ $\tilde{S} = 1 + \sum_{n=1}^{\infty} \tilde{s}_n c^n, \quad c = b\sigma^x + 2g/\omega$
IV	$\|\Psi_+^{\mathrm{PBV2}}(x_{\mathrm{opt}}, v_{\mathrm{opt}})\rangle$ [see (4.38)]	$S = \sum_{n=1}^{\infty} s_n \left(c^\dagger\right)^n, \quad c^\dagger = b^\dagger \sigma^x$

Table D.2: *The four schemes, labelled I'—IV', employed in the CCM analysis of the first excited state of the Rabi Hamiltonian, showing the choice of model state $|\Phi\rangle$ and cluster correlation operators for each scheme. For all primed schemes, the cluster correlation operator S is identical to that used for the corresponding unprimed (ground-state) scheme, and the model state is chosen so as to incorporate the odd-parity symmetry of the first excited state.*

Scheme	Model state $\|\Phi\rangle$	Cluster correlation operators S, $\tilde{S}$, Σ
I'	$\|0\rangle\|\uparrow\rangle$	$S = S_1 + S_2$ $S_1 = \sum_{n=1}^{\infty} s_n^{(1)} (b^\dagger)^n$ $S_2 = \sum_{n=1}^{\infty} s_n^{(2)} (b^\dagger)^{n-1} \sigma^+$ $\tilde{S} = 1 + \tilde{S}_1 + \tilde{S}_2$ $\tilde{S}_1 = \sum_{n=1}^{\infty} \tilde{s}_n^{(1)} b^n$ $\tilde{S}_2 = \sum_{n=1}^{\infty} \tilde{s}_n^{(2)} b^{n-1} \sigma^-$ $\Sigma = \Sigma_1 + \Sigma_2$ $\Sigma_1 = \sum_{n=1}^{\infty} \sigma_n^{(1)} b^n$ $\Sigma_2 = \sum_{n=1}^{\infty} \sigma_n^{(2)} b^{n-1} \sigma^-$
II'	$\|0\rangle\|\uparrow\rangle$	$S = \sum_{n=1}^{\infty} s_n \left(c^\dagger\right)^n, \quad c^\dagger = b^\dagger \sigma^x$
III'	$\|\Psi_-\rangle$ [see (4.16)]	$S = \sum_{n=1}^{\infty} s_n \left(c^\dagger\right)^n, \quad c^\dagger = b^\dagger \sigma^x + 2g/\omega$ $\tilde{S} = 1 + \sum_{n=1}^{\infty} \tilde{s}_n c^n, \quad c = b\sigma^x + 2g/\omega$
IV'	$\|\Psi_-^{\mathrm{PBV2}}(x_{\mathrm{opt}}, v_{\mathrm{opt}})\rangle$ [see (4.38)]	$S = \sum_{n=1}^{\infty} s_n \left(c^\dagger\right)^n, \quad c^\dagger = b^\dagger \sigma^x$

D.1 NCCM Scheme I

For Scheme I, we obtain the following form for the similarity transformed Hamiltonian:

$$
\begin{aligned}
e^{-S}H_{\text{Rabi}}e^{S} &= \frac{1}{2}\omega_0\sigma^z + \omega b^\dagger b + g\left(b^\dagger + b\right)\left(\sigma^+ + \sigma^-\right) \\
&\quad + \sum_{n=1}^{\infty} s_n^{(1)}\left\{n\omega\left(b^\dagger\right)^n + ng\left(b^\dagger\right)^{n-1}\left(\sigma^+ + \sigma^-\right)\right\} \\
&\quad + \sum_{n=1}^{\infty} s_n^{(2)}\left\{\left[(n-1)\omega + \omega_0\right]\left(b^\dagger\right)^{n-1}\sigma^+ \right. \\
&\qquad \left. + g(n-1)\left(b^\dagger\right)^{n-2}\sigma^-\sigma^+ - 4g\left(b^\dagger\right)^{n-1}\left(b^\dagger + b\right)\sigma^z\right\} \\
&\quad -4g\sum_{n=1}^{\infty}\sum_{n'=1}^{\infty} s_n^{(1)}s_{n'}^{(2)}\left\{n\left(b^\dagger\right)^{n+n'-2}\sigma^z\right\} \\
&\quad -4g\sum_{n=1}^{\infty}\sum_{n'=1}^{\infty} s_n^{(2)}s_{n'}^{(2)}\left\{(n-1)\left(b^\dagger\right)^{n+n'-3}\sigma^z\sigma^+ \right. \\
&\qquad \left. + \left(b^\dagger\right)^{n+n'-2}\left(b^\dagger + b\right)\sigma^+\right\} \\
&\quad -4g\sum_{n=1}^{\infty}\sum_{n'=1}^{\infty}\sum_{n''=1}^{\infty} s_n^{(1)}s_{n'}^{(2)}s_{n''}^{(2)}\left\{n\left(b^\dagger\right)^{n+n'+n''-3}\sigma^+\right\}\ . \qquad \text{(D.1)}
\end{aligned}
$$

The energy functional

$$
\begin{aligned}
\overline{H} &= \langle\Phi|\tilde{S}e^{-S}H_{\text{Rabi}}e^{S}|\Phi\rangle \\
&= -\frac{1}{2}\omega_0 + 4g\ s_2^{(2)} + 4g\ s_1^{(1)}s_1^{(2)} \\
&\quad + \sum_{k=1}^{\infty} k!\ \tilde{s}_k^{(1)}\left\{\omega k\ s_k^{(1)} + 4g\ s_k^{(2)} + 4g(k+1)\ s_{k+2}^{(2)} + 4g\sum_{n=1}^{k+1} n\ s_n^{(1)}s_{k+2-n}^{(2)}\right\} \\
&\quad +4\sum_{k=1}^{\infty}(k-1)!\ \tilde{s}_k^{(2)}\ \left\{g\delta_{k,2} + gk\ s_k^{(1)} + \left[\omega(k-1) + \omega_0\right]\ s_k^{(2)}\right. \\
&\qquad -4g\sum_{n=1}^{k+1}(n-1)\ s_n^{(2)}s_{k+2-n}^{(2)} - 4g\sum_{n=1}^{k-1}\ s_n^{(2)}s_{k-n}^{(2)} \\
&\qquad \left. -4g\sum_{n=1}^{k}\sum_{n'=1}^{k+1-n} n\ s_n^{(1)}s_{n'}^{(2)}s_{k+2-n-n'}^{(2)}\right\}\ . \qquad \text{(D.2)}
\end{aligned}
$$

may now be used to set up the CCM equations (3.14) for $\left\{s_k^{(1)}, s_k^{(2)};\ k = 1, 2, 3, \ldots\right\}$,

$$\begin{aligned}
0 &= \omega k\ s_k^{(1)} + 4g\ s_k^{(2)} + 4g(k+1)\ s_{k+2}^{(2)} + 4g \sum_{n=1}^{k+1} n\ s_n^{(1)} s_{k+2-n}^{(2)} \\
0 &= g\delta_{k,2} + gk\ s_k^{(1)} + [\omega(k-1) + \omega_0]\ s_k^{(2)} - 4g \sum_{n=1}^{k+1} (n-1)\ s_n^{(2)} s_{k+2-n}^{(2)} \\
&\quad -4g \sum_{n=1}^{k-1} s_n^{(2)} s_{k-n}^{(2)} - 4g \sum_{n=1}^{k} \sum_{n'=1}^{k+1-n} n\ s_n^{(1)} s_{n'}^{(2)} s_{k+2-n-n'}^{(2)}\ , \qquad \text{(D.3)}
\end{aligned}$$

and for $\left\{\tilde{s}_k^{(1)}, \tilde{s}_k^{(2)};\ k = 1, 2, 3, \ldots\right\}$:

$$\begin{aligned}
0 &= 4g\delta_{k,1}\ s_1^{(2)} + \omega k!\ \tilde{s}_k^{(1)} + 4g(k-1)!\ \tilde{s}_k^{(2)} + 4g \sum_{n=Max[k-1,1]}^{\infty} n!\ \tilde{s}_n^{(1)} s_{n+2-k}^{(2)} \\
&\quad -16g \sum_{n=k}^{\infty} \sum_{n'=1}^{n+1-k} (n-1)!\ \tilde{s}_n^{(2)} s_{n'}^{(2)} s_{n+2-k-n'}^{(2)} \\
0 &= g\ \delta_{k,2} + g\delta_{k,1}\ s_1^{(1)} + gk!\ \tilde{s}_k^{(1)} + g(k-1)!(1-\delta_{k,1})(1-\delta_{k,2})\ \tilde{s}_{k-2}^{(1)} \\
&\quad +(k-1)!\,[\omega(k-1) + \omega_0]\ \tilde{s}_k^{(2)} + g \sum_{n=Max[k-1,1]}^{\infty} n!(n+2-k)\ \tilde{s}_n^{(1)} s_{n+2-k}^{(1)} \\
&\quad -4g \sum_{n=Max[k-1,1]}^{\infty} n!\ \tilde{s}_n^{(2)} s_{n+2-k}^{(2)} - 8g \sum_{n=k+1}^{\infty} (n-1)!\ \tilde{s}_n^{(2)} s_{n-k}^{(2)} \\
&\quad -8g \sum_{n=k}^{\infty} \sum_{n'=1}^{n+1-k} (n-1)! n'\ \tilde{s}_n^{(2)} s_{n'}^{(1)} s_{n+2-k-n'}^{(2)}\ . \qquad \text{(D.4)}
\end{aligned}$$

Note that equations (D.3) may be solved for $\left\{s_k^{(1)}, s_k^{(2)}\right\}$, so that these coefficients are known quantities when solving (D.4). The expectation value of σ^z assumes the form

$$\langle \sigma^z \rangle^{\text{NCCM,I}} = -1 + 8 \sum_{k=1}^{\infty} (k-1)!\ \tilde{s}_k^{(2)} s_k^{(2)}\ . \qquad \text{(D.5)}$$

D.1.1 Termination of the even–parity NCCM Scheme I calculation

If the CCM calculation is restricted to the even–parity sector, then

$$s_n^{(1)} = s_n^{(2)} = 0 \tag{D.6}$$

for all odd n, and the only coefficient required in order to determine the CCM ground–state energy is $z \equiv s_2^{(2)}$. In the SUB-2 approximation, the equations (D.3) then reduce to

$$z^3 - \frac{\omega_0}{4g} z^2 - \frac{\omega(\omega+\omega_0)}{16g^2} z - \frac{\omega}{16g} = 0 . \tag{D.7}$$

For $g \to 0$ at scaled resonance ($\omega = \omega_0 = 1$), equation (D.7) has one real root corresponding to a positive, and two real roots corresponding to a negative ground–state energy. One of the latter roots describes the exact ground state at $g = 0$, and the other gives a spurious solution with lower energy. As the coupling g is increased, these two roots meet and form a complex conjugate pair at

$$g_c^{(2)} = 3\left(20 + 14\sqrt{7}\right)^{-1/2} = 0.3972 . \tag{D.8}$$

Thus the physical even–parity SUB-2 solution terminates at this point, above which there exist only a single real root corresponding to an unphysical positive ground–state energy, and a pair of complex conjugate roots corresponding to a complex ground–state energy. This behaviour is illustrated in Figure D.1. In the even–parity SUB-N approximation, it may be shown using *Mathematica* [Mat] that the CCM equations (D.3) may always be reduced to a polynomial of order $N+1$ in z, and for all $N/2$ odd behaviour similar to

that in the SUB-2 case is observed. In the case $N/2$ even, there is no unphysical negative root for $s_2^{(2)}$ which, together with the physical root, can form a complex pair at finite coupling, and the physical solution therefore does not terminate. In this case, however, the CCM ground–state energy corresponding to the physical root peels off the exact ground–state energy in the same coupling region where the $N/2$ odd solution terminates.

Figure D.1: *The behaviour of the three roots for the single CCM coefficient* $s_2^{(2)}$ *in the even–parity SUB-2 NCCM Scheme I analysis of the scaled resonant* ($\omega = \omega_0 = 1$) *Rabi Hamiltonian. The termination point at* $g = g_c^{(2)} = 0.3972$, *where the physical and unphysical negative roots meet to form a complex conjugate pair, is indicated by the symbol* $\otimes$.

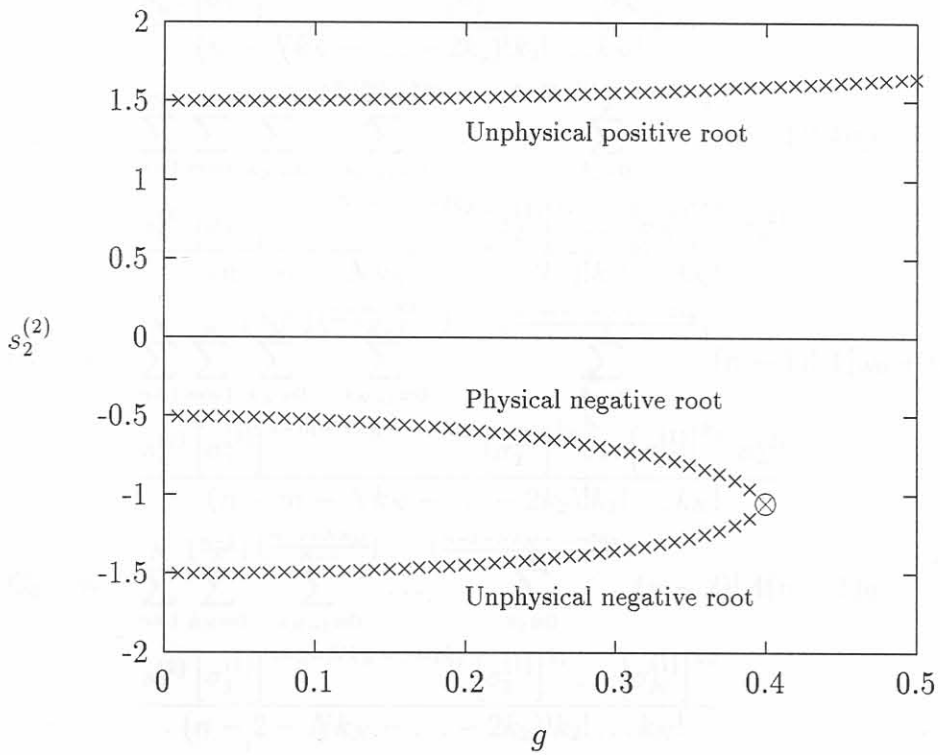

D.2 ECCM Scheme I

The similarity transform $e^{-S}H_{\text{Rabi}}e^{S}$ has the same form as for the NCCM, but the functional $\overline{H}$ in the ECCM SUB-N approximation is now given by

$$\overline{H} = \langle\Phi|e^{\Sigma}e^{-S}H_{\text{Rabi}}e^{S}|\Phi\rangle = \sum_{i=1}^{11} C_i \tag{D.9}$$

with

$$C_1 = -\frac{1}{2}\omega_0$$

$$C_2 = 4g\,\sigma_1^{(2)}$$

$$C_3 = \sum_{n=1}^{N}\sum_{k_N=0}^{\lfloor\frac{n}{N}\rfloor}\sum_{k_{N-1}=0}^{\lfloor\frac{n-Nk_N}{N-1}\rfloor}\cdots\sum_{k_2=0}^{\lfloor\frac{n-Nk_N-\ldots-3k_3}{2}\rfloor} n!\,n\omega \frac{s_n^{(1)}\left[\sigma_1^{(1)}\right]^{n-Nk_N-\ldots-2k_2}\left[\sigma_2^{(1)}\right]^{k_2}\cdots\left[\sigma_N^{(1)}\right]^{k_N}}{(n-Nk_N-\ldots-2k_2)!k_2!\ldots k_N!}$$

$$C_4 = \sum_{n=1}^{N}\sum_{m=1}^{n}\sum_{k_N=0}^{\lfloor\frac{n-m}{N}\rfloor}\sum_{k_{N-1}=0}^{\lfloor\frac{n-m-Nk_N}{N-1}\rfloor}\cdots\sum_{k_2=0}^{\lfloor\frac{n-m-Nk_N-\ldots-3k_3}{2}\rfloor} (n-1)!\,4ng \frac{s_n^{(1)}\left[\sigma_1^{(1)}\right]^{n-m-Nk_N-\ldots-2k_2}\left[\sigma_2^{(1)}\right]^{k_2}\cdots\left[\sigma_N^{(1)}\right]^{k_N}\sigma_m^{(2)}}{(n-m-Nk_N-\ldots-2k_2)!k_2!\ldots k_N!}$$

$$C_5 = \sum_{n=1}^{N}\sum_{m=1}^{n}\sum_{k_N=0}^{\lfloor\frac{n-m}{N}\rfloor}\sum_{k_{N-1}=0}^{\lfloor\frac{n-m-Nk_N}{N-1}\rfloor}\cdots\sum_{k_2=0}^{\lfloor\frac{n-m-Nk_N-\ldots-3k_3}{2}\rfloor} (n-1)!\,4\left[\omega_0+(n-1)\omega\right] \frac{s_n^{(2)}\left[\sigma_1^{(1)}\right]^{n-m-Nk_N-\ldots-2k_2}\left[\sigma_2^{(1)}\right]^{k_2}\cdots\left[\sigma_N^{(1)}\right]^{k_N}\sigma_m^{(2)}}{(n-m-Nk_N-\ldots-2k_2)!k_2!\ldots k_N!}$$

$$C_6 = \sum_{n=1}^{N}\sum_{k_N=0}^{\lfloor\frac{n-2}{N}\rfloor}\sum_{k_{N-1}=0}^{\lfloor\frac{n-2-Nk_N}{N-1}\rfloor}\cdots\sum_{k_2=0}^{\lfloor\frac{n-2-Nk_N-\ldots-3k_3}{2}\rfloor} (n-2)!\,4(n-1)g \frac{s_n^{(2)}\left[\sigma_1^{(1)}\right]^{n-2-Nk_N-\ldots-2k_2}\left[\sigma_2^{(1)}\right]^{k_2}\cdots\left[\sigma_N^{(1)}\right]^{k_N}}{(n-2-Nk_N-\ldots-2k_2)!k_2!\ldots k_N!}$$

$$C_7 = \sum_{n=1}^{N}\sum_{k_N=0}^{\lfloor\frac{n}{N}\rfloor}\sum_{k_{N-1}=0}^{\lfloor\frac{n-Nk_N}{N-1}\rfloor}\cdots\sum_{k_2=0}^{\lfloor\frac{n-Nk_N-\ldots-3k_3}{2}\rfloor} n!\,4g$$

$$\frac{s_n^{(2)}\left[\sigma_1^{(1)}\right]^{n-Nk_N-\ldots-2k_2}\left[\sigma_2^{(1)}\right]^{k_2}\ldots\left[\sigma_N^{(1)}\right]^{k_N}}{(n-Nk_N-\ldots-2k_2)!k_2!\ldots k_N!}$$

$$C_8 = \sum_{n,n'=1}^{N}\sum_{k_N=0}^{\lfloor\frac{n+n'-2}{N}\rfloor}\sum_{k_{N-1}=0}^{\lfloor\frac{n+n'-2-Nk_N}{N-1}\rfloor}\cdots\sum_{k_2=0}^{\lfloor\frac{n+n'-2-Nk_N-\ldots-3k_3}{2}\rfloor}(n+n'-2)!\;4ng$$
$$\frac{s_n^{(1)}s_{n'}^{(2)}\left[\sigma_1^{(1)}\right]^{n+n'-2-Nk_N-\ldots-2k_2}\left[\sigma_2^{(1)}\right]^{k_2}\ldots\left[\sigma_N^{(1)}\right]^{k_N}}{(n+n'-2-Nk_N-\ldots-2k_2)!k_2!\ldots k_N!}$$

$$C_9 = -\sum_{n,n'=1}^{N}\sum_{m=1}^{Min[n+n'-2,N]}\sum_{k_N=0}^{\lfloor\frac{n+n'-m-2}{N}\rfloor}\sum_{k_{N-1}=0}^{\lfloor\frac{n+n'-m-2-Nk_N}{N-1}\rfloor}\cdots$$
$$\cdots\sum_{k_2=0}^{\lfloor\frac{n+n'-m-2-Nk_N-\ldots-3k_3}{2}\rfloor}(n+n'-3)!\;16(n-1)g$$
$$\frac{s_n^{(2)}s_{n'}^{(2)}\left[\sigma_1^{(1)}\right]^{n+n'-m-2-Nk_N-\ldots-2k_2}\left[\sigma_2^{(1)}\right]^{k_2}\ldots\left[\sigma_N^{(1)}\right]^{k_N}\sigma_m^{(2)}}{(n+n'-m-2-Nk_N-\ldots-2k_2)!k_2!\ldots k_N!}$$

$$C_{10} = -\sum_{n,n'=1}^{N}\sum_{m=1}^{Min[n+n',N]}\sum_{k_N=0}^{\lfloor\frac{n+n'-m}{N}\rfloor}\sum_{k_{N-1}=0}^{\lfloor\frac{n+n'-m-Nk_N}{N-1}\rfloor}\cdots$$
$$\cdots\sum_{k_2=0}^{\lfloor\frac{n+n'-m-Nk_N-\ldots-3k_3}{2}\rfloor}(n+n'-1)!\;16g$$
$$\frac{s_n^{(2)}s_{n'}^{(2)}\left[\sigma_1^{(1)}\right]^{n+n'-m-Nk_N-\ldots-2k_2}\left[\sigma_2^{(1)}\right]^{k_2}\ldots\left[\sigma_N^{(1)}\right]^{k_N}\sigma_m^{(2)}}{(n+n'-m-Nk_N-\ldots-2k_2)!k_2!\ldots k_N!}$$

$$C_{11} = -\sum_{n,n',n''=1}^{N}\sum_{m=1}^{Min[n+n'+n''-2,N]}\sum_{k_N=0}^{\lfloor\frac{n+n'+n''-2-m}{N}\rfloor}\sum_{k_{N-1}=0}^{\lfloor\frac{n+n'+n''-2-m-Nk_N}{N-1}\rfloor}\cdots$$
$$\cdots\sum_{k_2=0}^{\lfloor\frac{n+n'+n''-2-m-Nk_N-\ldots-3k_3}{2}\rfloor}(n+n'+n''-3)!\;16ng\;s_n^{(1)}s_{n'}^{(2)}s_{n''}^{(2)}$$
$$\frac{\left[\sigma_1^{(1)}\right]^{n+n'+n''-m-2-Nk_N-\ldots-2k_2}\left[\sigma_2^{(1)}\right]^{k_2}\ldots\left[\sigma_N^{(1)}\right]^{k_N}\sigma_m^{(2)}}{(n+n'+n''-2-m-Nk_N-\ldots-2k_2)!k_2!\ldots k_N!}\,. \qquad \text{(D.10)}$$

The $4N$ ECCM Scheme I equations are

$$\frac{\partial\overline{H}}{\partial s_k^{(1)}}=0=\frac{\partial\overline{H}}{\partial s_k^{(2)}}\,,\quad \frac{\partial\overline{H}}{\partial\sigma_k^{(1)}}=0=\frac{\partial\overline{H}}{\partial\sigma_k^{(2)}}\quad .\qquad k=1,2,\ldots,N\,. \quad \text{(D.11)}$$

D.2.1 The SUB-1 case

Here the ECCM equations above are analytically soluble, and yield the trivial (even–parity) solution

$$\begin{aligned} s_1^{(1)} &= s_1^{(2)} = \sigma_1^{(1)} = \sigma_1^{(2)} = 0 \\ E_0 &= -\frac{1}{2}\omega_0 \end{aligned} \tag{D.12}$$

for $g \leq \sqrt{\omega\omega_0}/4$, and the doubly–degenerate (odd–parity) solution

$$\begin{aligned} s_1^{(1)} &= \sigma_1^{(1)} = \pm\frac{\sqrt{256g^2 - \omega^2\omega_0^2}}{8g\omega} \\ s_1^{(2)} &= \mp\frac{1}{2}\sqrt{\frac{16g^2 - \omega\omega_0}{16g^2 + \omega\omega_0}} \\ \sigma_1^{(2)} &= \mp\frac{\sqrt{256g^2 - \omega^2\omega_0^2}}{64g^2} \\ E_0 &= -\frac{4g^2}{\omega} - \frac{1}{4}\omega_0 \end{aligned} \tag{D.13}$$

for $g > \sqrt{\omega\omega_0}/4$.

D.3 NCCM Scheme II

The similarity transformed Hamiltonian is given by

$$\begin{aligned} e^{-S} H_{\text{Rabi}} e^{S} &= \frac{1}{2}\omega_0 F\left(c^\dagger\right)\sigma^z + \omega c^\dagger c + 2g\left(c^\dagger + c\right) \\ &\quad + \omega\sum_{n=1}^{\infty} n\, s_n \left(c^\dagger\right)^n + 2g\sum_{n=1}^{\infty} n\, s_n \left(c^\dagger\right)^{n-1} \end{aligned} \tag{D.14}$$

with $c^\dagger = b^\dagger\sigma^x$, $\left[c, c^\dagger\right] = \left[b, b^\dagger\right] = 1$ and

$$F\left(c^\dagger\right) \equiv \exp\left[G\left(c^\dagger\right)\right], \qquad G\left(c^\dagger\right) \equiv -2\sum_{n=1}^{\infty} s_{2n-1}\left(c^\dagger\right)^{2n-1}. \tag{D.15}$$

Using the overlap form (3.7) of the CCM equations, we obtain the following set of simultaneous equations for $\{s_k;\ k = 1, 2, 3, \ldots\}$ (see also Appendix B):

$$0 \ = \ 2g\delta_{k,1} + \omega k k!\ s_k + 2g(k+1)k!\ s_{k+1} - \frac{1}{2}\omega_0 \langle \Phi | F^{(k)}\left(c^\dagger\right) | \Phi \rangle \ . \quad \text{(D.16)}$$

We have used *Mathematica* [Mat] to evaluate the functional derivative

$$F^{(k)}\left(c^\dagger\right) \equiv \frac{\partial^k F\left(c^\dagger\right)}{\partial \left(c^\dagger\right)^k} = \frac{\partial^k}{\partial \left(c^\dagger\right)^k}\left\{e^{G\left(c^\dagger\right)}\right\} \quad \text{(D.17)}$$

and the form of the equations is greatly simplified by the fact that $\langle \Phi | c^\dagger = 0$.

D.3.1 Analytics for the SUB-1 and SUB-2 cases

In the SUB-1 approximation, one obtains the solution $s_1 = -2g/(\omega + \omega_0)$, valid for all coupling, with corresponding ground–state energy

$$E_0 = -\frac{1}{2}\omega_0 - \frac{4g^2}{\omega + \omega_0} \ . \quad \text{(D.18)}$$

In the SUB-2 case, one finds the analytic solution

$$\begin{aligned} s_1 &= \frac{-\omega\left(\omega + \omega_0\right) + \sqrt{\omega^2\left(\omega + \omega_0\right)^2 - 16g^2\omega\omega_0}}{4g\omega_0} \\ s_2 &= \frac{\omega_0}{2\omega} s_1^2 \end{aligned} \quad \text{(D.19)}$$

with corresponding ground–state energy

$$E_0 = -\frac{1}{2}\omega_0 - \frac{\omega\left(\omega + \omega_0\right)}{2\omega_0} + \frac{\sqrt{\omega^2\left(\omega + \omega_0\right)^2 - 16g^2\omega\omega_0}}{2\omega_0} \quad \text{(D.20)}$$

below $g_c^{(2)} = \frac{1}{4}\sqrt{\frac{\omega}{\omega_0}}\left(\omega + \omega_0\right)$. Above this value of the coupling, there are no physical solutions to the SUB-2 NCCM Scheme II equations. At resonance ($\omega = \omega_0 = 1$), the SUB-2 NCCM Scheme II solution (which is always of even–parity) thus terminates at $g_c^{(2)} = 0.5$.

D.4 NCCM Scheme III

For Scheme III, the similarity transformed Hamiltonian $e^{-S}H_{\rm Rabi}e^{S}$ assumes the form

$$e^{-S}H_{\rm Rabi}e^{S} = \frac{1}{2}\omega_0 F\left(c^\dagger\right)\sigma^z + \omega c^\dagger c - \frac{4g^2}{\omega} + \omega\sum_{n=1}^{\infty} n\, s_n \left(c^\dagger\right)^n \qquad \text{(D.21)}$$

with $c^\dagger = b^\dagger\sigma^x + 2g/\omega$, $\left[c, c^\dagger\right] = \left[b, b^\dagger\right] = 1$ and

$$F\left(c^\dagger\right) \equiv \exp\left[G\left(c^\dagger\right)\right], \quad G\left(c^\dagger\right) \equiv \sum_{n=1}^{\infty} s_n \left\{\left(\frac{4g}{\omega} - c^\dagger\right)^n - \left(c^\dagger\right)^n\right\}. \qquad \text{(D.22)}$$

The energy functional $\overline{H}$ is given by

$$\begin{aligned}\overline{H} &= \langle\Phi|\tilde{S}e^{-S}H_{\rm Rabi}e^{S}|\Phi\rangle \\ &= -\frac{1}{2}\omega_0 e^{-8g^2/\omega^2}\sum_{n=1}^{\infty}\tilde{s}_n\left\{\sum_{k=0}^{n} C(n,k)\left(\frac{4g}{\omega}\right)^{n-k}\langle\Phi|F^{(k)}\left(c^\dagger\right)|\Phi\rangle\right\} \\ &\quad -\frac{1}{2}\omega_0 e^{-8g^2/\omega^2}\exp\left\{\sum_{n=1}^{\infty}\left(\frac{4g}{\omega}\right)^n s_n\right\} - \frac{4g^2}{\omega} + \omega\sum_{n=1}^{\infty} nn!\, s_n\tilde{s}_n \qquad \text{(D.23)}\end{aligned}$$

where $C(n,k)$ denotes the binomial coefficient $\frac{n!}{k!(n-k)!}$ and

$$F^{(k)}\left(c^\dagger\right) \equiv \frac{\partial^k F\left(c^\dagger\right)}{\partial\left(c^\dagger\right)^k}. \qquad \text{(D.24)}$$

The CCM equations (3.14) for $\{s_k;\ k = 1,2,3,\ldots\}$ (see also Appendix B) are given by

$$\begin{aligned}0 &= -\frac{1}{2}\omega_0 e^{-8g^2/\omega^2}\sum_{n=0}^{k} C(k,n)\left(\frac{4g}{\omega}\right)^{k-n}\langle\Phi|F^{(n)}\left(c^\dagger\right)|\Phi\rangle \\ &\quad + \omega kk!\, s_k\,, \qquad \text{(D.25)}\end{aligned}$$

and those for $\{\tilde{s}_k;\ k = 1,2,3,\ldots\}$ by

$$\begin{aligned}0 &= -\frac{1}{2}\omega_0 e^{-8g^2/\omega^2}\sum_{n=1}^{\infty}\tilde{s}_n\left\{\sum_{m=0}^{n} C(n,m)\left(\frac{4g}{\omega}\right)^{n-m}\frac{\partial}{\partial s_k}\left[\langle\Phi|F^{(n)}\left(c^\dagger\right)|\Phi\rangle\right]\right\} \\ &\quad -\frac{1}{2}\omega_0 e^{-8g^2/\omega^2}\exp\left\{\sum_{n=1}^{\infty}\left(\frac{4g}{\omega}\right)^n s_n\right\}\left(\frac{4g}{\omega}\right)^k + \omega kk!\,\tilde{s}_k\,, \qquad \text{(D.26)}\end{aligned}$$

so that the expectation value of σ^z assumes the form

$$\langle\sigma^z\rangle^{\mathrm{NCCM,III}} = -e^{-8g^2/\omega^2}\sum_{n=1}^{\infty}\tilde{s}_n\left\{\sum_{k=0}^{n}C(n,k)\left(\frac{4g}{\omega}\right)^{n-k}\langle\Phi|F^{(k)}\left(c^\dagger\right)|\Phi\rangle\right\}$$
$$-e^{-8g^2/\omega^2}\exp\left\{\sum_{n=1}^{\infty}\left(\frac{4g}{\omega}\right)^n s_n\right\}. \qquad \text{(D.27)}$$

In (D.25), (D.26) and (D.27) we have again used *Mathematica* [Mat] to evaluate the derivatives explicitly, and as before $\langle\Phi|c^\dagger = 0$. For Scheme III, it is not possible to solve even the SUB-1 CCM equations analytically.

D.5 NCCM Scheme IV

Here the similarity transformed Hamiltonian

$$\begin{aligned} H_{\mathrm{sim}} &\equiv e^{-S}H_{\mathrm{Rabi}}e^{S} \\ &= \frac{1}{2}\omega_0 F\left(b^\dagger\right)\sigma^z + \omega b^\dagger b + 2g\left(b^\dagger + b\right)\sigma^x \\ &\quad +\omega\sum_{n=1}^{\infty} n\, s_n\left(b^\dagger\sigma^x\right)^n + 2g\sum_{n=1}^{\infty} n\, s_n\left(b^\dagger\sigma^x\right)^{n-1} \end{aligned} \qquad \text{(D.28)}$$

with

$$F\left(b^\dagger\right) \equiv \exp\left[G\left(b^\dagger\right)\right], \qquad G\left(b^\dagger\right) \equiv -2\sum_{n=1}^{\infty} s_{2n-1}\left(b^\dagger\right)^{2n-1}\sigma^x \qquad \text{(D.29)}$$

obviously has the same form as for Scheme II.

In this section, all expectation values refer to the model state

$$|\Phi\rangle = |\Psi_+^{\mathrm{PBV2}}(x_{\mathrm{opt}}, v_{\mathrm{opt}})\rangle \qquad \text{(D.30)}$$

(see (4.38)) of Scheme IV, *i.e.* $\langle A\rangle = \langle\Phi|A|\Phi\rangle$ for arbitrary A. Note also that the optimal values x_{opt} and v_{opt} of the variational parameters are predetermined via (C.7) and (C.8) at each value of the coupling g.

The Hermitian conjugate $c = b\sigma^x$ of $c^\dagger = b^\dagger\sigma^x$ does not annihilate the model state $|\Phi\rangle$. However, since

$$c^2|\Phi\rangle = b^2|\Phi\rangle = x_{\rm opt}^2|\Phi\rangle \ , \tag{D.31}$$

it follows that

$$\begin{aligned} c^m|\Phi\rangle &= x_{\rm opt}^m|\Phi\rangle \ , \qquad\qquad m = 2,4,6,\ldots \\ c^m|\Phi\rangle &= x_{\rm opt}^{m-1}c|\Phi\rangle = x_{\rm opt}^{m-1}b\sigma^x|\Phi\rangle \qquad m = 1,3,5,\ldots \ . \end{aligned} \tag{D.32}$$

This, together with the fact that $\left[c, c^\dagger\right] = \left[b, b^\dagger\right] = 1$, allows us to set up the equations for $\{s_k;\ k = 1,2,3,\ldots\}$ by constructing, for $m = 2,4,6,\ldots$, the overlaps

$$\begin{aligned} \langle c^m H_{\rm sim}\rangle &= \left\langle b^m E_0^{\rm NCCM,IV}\right\rangle = x_{opt}^m E_0^{\rm NCCM,IV} \\ &= \langle H_{\rm sim} b^m\rangle + \sum_{r=1}^{m} C(m,r)\left\langle H_{\rm sim}^{(r)} b^{m-r}\right\rangle \\ &= x_{opt}^m E_0^{\rm NCCM,IV} + \sum_{\substack{r=2 \\ r\ \text{even}}}^{m} C(m,r) x_{\rm opt}^{m-r}\left\langle H_{\rm sim}^{(r)}\right\rangle \\ &\qquad + \sum_{\substack{r=1 \\ r\ \text{odd}}}^{m-1} C(m,r) x_{\rm opt}^{m-r-1}\left\langle H_{\rm sim}^{(r)} b\right\rangle \ , \end{aligned} \tag{D.33}$$

and, for $m = 1,3,5,\ldots$, the overlaps

$$\begin{aligned} \langle c^m H_{\rm sim}\rangle &= \left\langle b^{m-1} b\sigma^x E_0^{\rm NCCM,IV}\right\rangle = x_{opt}^{m-1} E_0^{\rm NCCM,IV}\langle b\sigma^x\rangle \\ &= \sum_{r=0}^{m} C(m,r)\left\langle \sigma^x H_{\rm sim}^{(r)} b^{m-r}\right\rangle \\ &= x_{\rm opt}^{m-1}\langle\sigma^x H_{\rm sim} b\rangle + \sum_{\substack{r=2 \\ r\ \text{even}}}^{m-1} C(m,r) x_{\rm opt}^{m-r-1}\left\langle \sigma^x H_{\rm sim}^{(r)} b\right\rangle \\ &\qquad + \sum_{\substack{r=1 \\ r\ \text{odd}}}^{m} C(m,r) x_{\rm opt}^{m-r}\left\langle \sigma^x H_{\rm sim}^{(r)}\right\rangle \ . \end{aligned} \tag{D.34}$$

Here $E_0^{\mathrm{NCCM,IV}}$ is the NCCM Scheme IV ground–state energy (6.3), and

$$
\begin{aligned}
H_{\mathrm{sim}}^{(r)} &\equiv \frac{\partial^r H_{\mathrm{sim}}}{\partial \left(b^\dagger\right)^r} \\
F^{(r)} &\equiv \frac{\partial^r F\left(b^\dagger\right)}{\partial \left(b^\dagger\right)^r} \\
\left\langle H_{\mathrm{sim}}^{(r)} \right\rangle &= \frac{1}{2}\omega_0 \left\langle F^{(r)}\sigma^z \right\rangle \\
&\quad + \omega \sum_{\substack{n=r+1 \\ n \text{ odd}}}^{\infty} \frac{nn!}{(n-r)!} x_{\mathrm{opt}}^{n-r-1} \left\langle b\sigma^x \right\rangle \; s_n \\
&\quad + \omega \sum_{\substack{n=r \\ n \text{ even}}}^{\infty} \frac{nn!}{(n-r)!} x_{\mathrm{opt}}^{n-r} \; s_n \\
&\quad + 2g \sum_{\substack{n=r+1 \\ n \text{ odd}}}^{\infty} \frac{n!}{(n-r-1)!} x_{\mathrm{opt}}^{n-r-1} \; s_n \\
&\quad + 2g \sum_{\substack{n=r+2 \\ n \text{ even}}}^{\infty} \frac{n!}{(n-r-1)!} x_{\mathrm{opt}}^{n-r-2} \left\langle b\sigma^x \right\rangle \; s_n \; , \qquad r \in \{2,4,6,\ldots\} \\
\left\langle H_{\mathrm{sim}}^{(r)} b \right\rangle &= \frac{1}{2}\omega_0 \left\langle F^{(r)} b\sigma^z \right\rangle + \left\{ \omega x_{\mathrm{opt}}^2 + 2g \left\langle b\sigma^x \right\rangle \right\} \delta_{r,1} \\
&\quad + \omega \sum_{\substack{n=r \\ n \text{ odd}}}^{\infty} \frac{nn!}{(n-r)!} x_{\mathrm{opt}}^{n-r} \left\langle b\sigma^x \right\rangle \; s_n \\
&\quad + \omega \sum_{\substack{n=r+1 \\ n \text{ even}}}^{\infty} \frac{nn!}{(n-r)!} x_{\mathrm{opt}}^{n-r-1} \left\langle b^\dagger b \right\rangle \; s_n \\
&\quad + 2g \sum_{\substack{n=r+2 \\ n \text{ odd}}}^{\infty} \frac{n!}{(n-r-1)!} x_{\mathrm{opt}}^{n-r-2} \left\langle b^\dagger b \right\rangle \; s_n \\
&\quad + 2g \sum_{\substack{n=r+1 \\ n \text{ even}}}^{\infty} \frac{n!}{(n-r-1)!} x_{\mathrm{opt}}^{n-r-1} \left\langle b\sigma^x \right\rangle \; s_n \; , \qquad r \in \{1,3,5,\ldots\} \\
\left\langle \sigma^x H_{\mathrm{sim}}^{(r)} b \right\rangle &= \frac{1}{2}\omega_0 \left\langle F^{(r)} b\sigma^x\sigma^z \right\rangle \\
&\quad + \omega \sum_{\substack{n=r+1 \\ n \text{ odd}}}^{\infty} \frac{nn!}{(n-r)!} x_{\mathrm{opt}}^{n-r-1} \left\langle b^\dagger b \right\rangle \; s_n \\
&\quad + \omega \sum_{\substack{n=r \\ n \text{ even}}}^{\infty} \frac{nn!}{(n-r)!} x_{\mathrm{opt}}^{n-r} \left\langle b\sigma^x \right\rangle \; s_n
\end{aligned}
$$

$$
\begin{aligned}
&+ 2g \sum_{\substack{n=r+1 \\ n \text{ odd}}}^{\infty} \frac{n!}{(n-r-1)!} x_{\text{opt}}^{n-r-1} \langle b\sigma^x \rangle \; s_n \\
&+ 2g \sum_{\substack{n=r+2 \\ n \text{ even}}}^{\infty} \frac{n!}{(n-r-1)!} x_{\text{opt}}^{n-r-2} \left\langle b^\dagger b \right\rangle \; s_n \;, \qquad r \in \{2,4,6,\ldots\} \\
\left\langle \sigma^x H_{\text{sim}}^{(r)} \right\rangle &= \frac{1}{2}\omega_0 \left\langle F^{(r)} \sigma^x \sigma^z \right\rangle + \{\omega \langle b\sigma^x \rangle + 2g\} \, \delta_{r,1} \\
&+ \omega \sum_{\substack{n=r \\ n \text{ odd}}}^{\infty} \frac{nn!}{(n-r)!} x_{\text{opt}}^{n-r} \; s_n \\
&+ \omega \sum_{\substack{n=r+1 \\ n \text{ even}}}^{\infty} \frac{nn!}{(n-r)!} x_{\text{opt}}^{n-r-1} \langle b\sigma^x \rangle \; s_n \\
&+ 2g \sum_{\substack{n=r+2 \\ n \text{ odd}}}^{\infty} \frac{n!}{(n-r-1)!} x_{\text{opt}}^{n-r-2} \langle b\sigma^x \rangle \; s_n \\
&+ 2g \sum_{\substack{n=r+1 \\ n \text{ even}}}^{\infty} \frac{n!}{(n-r-1)!} x_{\text{opt}}^{n-r-1} \; s_n \;, \qquad r \in \{1,3,5,\ldots\} \\
\langle \sigma^z \rangle &= \frac{v_{\text{opt}}^2 - 1}{v_{\text{opt}}^2 + 1} \\
\left\langle b^\dagger b \right\rangle &= \frac{x_{\text{opt}}^2}{1 + v_{\text{opt}}^2} \left(\tanh x_{\text{opt}}^2 + v_{\text{opt}}^2 \coth x_{\text{opt}}^2 \right) \\
\langle b\sigma^x \rangle &= \frac{2 x_{\text{opt}} v_{\text{opt}}}{1 + v_{\text{opt}}^2} \left(1 - \exp\left[-4 x_{\text{opt}}^2 \right] \right)^{-1/2} \\
\langle b\sigma^x \sigma^z \rangle &= \frac{2 x_{\text{opt}} v_{\text{opt}} \exp\left[-2 x_{\text{opt}}^2 \right]}{1 + v_{\text{opt}}^2} \left(1 - \exp\left[-4 x_{\text{opt}}^2 \right] \right)^{-1/2} \;. \qquad \text{(D.35)}
\end{aligned}
$$

We have again used *Mathematica* [Mat] to set up the derivatives $F^{(r)}$ as a function of the set $\left\{ G^{(k)}; k = 0, 1, 2, \ldots \right\}$ with

$$
G^{(k)} \equiv \frac{\partial^k G\left(b^\dagger\right)}{\partial \left(b^\dagger\right)^k} = \begin{cases} -2 \sum_{\substack{n=k+1 \\ n \text{ odd}}}^{\infty} \frac{n!}{(n-k)!} \left(b^\dagger\right)^{n-k-1} b^\dagger \sigma^x \; s_n & k \in \{0,2,4,\ldots\} \\ -2 \sum_{\substack{n=k \\ n \text{ odd}}}^{\infty} \frac{n!}{(n-k)!} \left(b^\dagger\right)^{n-k} \sigma^x \; s_n & k \in \{1,3,5,\ldots\} \end{cases} \qquad \text{(D.36)}
$$

One may readily prove the identity

$$
\langle \Phi | \exp\left[G\left(b^\dagger\right) \right] = \langle \Phi | \cosh \alpha - \langle \Phi | \left(\frac{\sinh \alpha}{x_{\text{opt}}} \right) b^\dagger \sigma^x \qquad \text{(D.37)}
$$

with

$$\alpha \equiv \sum_{n=0}^{\infty} 2\, s_{2n+1}\, x_{\text{opt}}^{2n+1}\,, \tag{D.38}$$

which is the final element required in order to set up the CCM equations (D.33) and (D.34).

Appendix E

Acronyms and Abbreviations

Acronym/abbrevation	Explanation	Relevant chapters
CCM	Coupled cluster method	1,3,5,6,8
CI	Configuration–interaction	1,4,7
ECCM	Extended coupled cluster method	1,3,5
JT	Jahn–Teller	1,2,7,8
PJT	Pseudo Jahn–Teller	1,2,7,8
LMG	Lipkin–Meshkov–Glick	1,5
NCCM	Normal coupled cluster method	1,3,5,6,8
PAV	Projection after variation	4
PBV	Projection before variation	4
RPJT	Resonant pseudo Jahn–Teller	1,2,7,8
RWA	Rotating–wave approximation	1, 4
TIPT	Time–independent perturbation theory	1,4

Bibliography

[Abr] M. Abramowitz and I. A. Stegun (Eds.), *Handbook of Mathematical Functions* (National Bureau of Standards, Washington, 1964).

[Al69] J. S. Alper and R. Silbey, J. Chem. Phys. **51**, 3129 (1969).

[An94] K. An, J. J. Childs, R. R. Dasari and M. S. Feld, Phys. Rev. Lett. **73** 3375 (1994).

[Ar82] J. Arponen, J. Phys. G **8**, L129 (1982).

[Ar83a] J. Arponen, Ann. Phys. (NY) **151**, 311 (1983).

[Ar83b] J. Arponen and J. Rantakivi, Nucl. Phys. A **407**, 141 (1983).

[Ar87] J. Arponen, R. F. Bishop and E. Pajanne, Phys. Rev. A **36**, 2519 (1987); J. Arponen, R. F. Bishop and E. Pajanne, Phys. Rev. A **36**, 2539 (1987).

[Ar90] J. Arponen and R. F. Bishop, Phys. Rev. Lett. **64**, 111 (1990).

[Ba96] S. J. Baker, R. F. Bishop and N. J. Davidson, Phys. Rev. D **53**, 2610 (1996).

[Ba77] H. Barentzen and O. E. Polansky, Chem. Phys. Lett. **49**, 121 (1977).

[Ba78] H. Barentzen and O. E. Polansky, J. Chem. Phys. **68**, 4398 (1978).

[Bar78] R. J. Bartlett and G. D. Purvis,
Int. J. Quantum Chem. **14**, 561 (1978).

[Bar89] R. J. Bartlett, J. Chem. Phys. **93**, 1697 (1989).

[Bera] I. B. Bersuker, *The Jahn–Teller Effect and Vibronic Interactions in Modern Chemistry* (Plenum Press, New York, 1984).

[Berb] I. B. Bersuker and V. Z. Pollinger, *Vibronic interactions in molecules and crystals* (Springer-Verlag, New York, 1989).

[Bi78] R. F. Bishop and K. H. Lührmann, Phys. Rev. B **17**, 3757 (1978);
R. F. Bishop and K. H. Lührmann, Phys. Rev. B **26**, 5523 (1982).

[Bi87] R. F. Bishop and H. G. Kümmel, *Physics Today*, March 1987, p. 52.

[Bi91a] R. F. Bishop, Theor. Chem. Acta **80**, 95 (1991).

[Bi91b] R. F. Bishop, J. B. Parkinson and Y. Xian,
Phys. Rev. B **43** 13782 (1991);
R. F. Bishop, J. B. Parkinson and Y. Xian,
Theor. Chem. Acta **80**, 181 (1991).

[Bi93] R. F. Bishop, A. S. Kendall, L. Y. Wong and Y. Xian,
Phys. Rev. D **48**, 887 (1993).

[Bi96] R. F. Bishop, N. J. Davidson, R. M. Quick and D. M. van der Walt,
Phys. Rev. A **54**, R4657 (1996).

[Bi97] R. F. Bishop, N. J. Davidson, R. M. Quick and D. M. van der Walt, *"The Coupled Cluster Method in Quantum Optics"*, to be published in the Proceedings of the XXI International Workshop on Condensed Matter Theories, Luso, Portugal, September 1997.

[Bi98] R. F. Bishop, N. J. Davidson, R. M. Quick and D. M. van der Walt, *"Quantum Optics Meets Quantum Many–Body Theory: Coupled Cluster Studies of the Rabi Hamiltonian"*, in *Recent Progress in Many–Body Theories*, Proceedings of the 9th International Conference, Sydney, Australia, July 1997, p. 163 (World Scientific, Singapore, 1998).

[Bi99a] R. F. Bishop, N. J. Davidson, R. M. Quick and D. M. van der Walt, Phys. Lett. A **254**, 215 (1999).

[Bi99b] R. F. Bishop, N. J. Davidson, R. M. Quick and D. M. van der Walt, *"Simple accurate CCM results for the linear $E \otimes e$ pseudo Jahn–Teller effect"*,
article to be submitted for publication in J. Chem. Phys. (1999).

[Bl96] R. Blatt, *Physics World*, June 1996, p. 25.

[Bl40] F. Bloch and A. Siegert, Phys. Rev. **57**, 522 (1940).

[Bor] M. Born and K. Huang, *Dynamical Theory of Crystal Lattices* (Oxford University Press, New York, 1954).

[Bo27] M. Born and R. Oppenheimer, Ann. Phys. **84**, 457 (1927).

[Ca87] M. C. Cambiaggio and J. Dukelsky, Phys. Lett. B **197**, 479 (1987).

[Ca68] P. Carruthers and M. M. Nieto, Rev. Mod. Phys. **40**, 411 (1968).

[Ci98] O. Civitarese and M. Reboiro, Phys. Rev. C **57**, 3055 (1998).

[Ci66] J. Čižek, J. Chem. Phys. **45**, 4256 (1966);
J. Čižek, Adv. Chem. Phys. **14**, 35 (1969).

[Co60] F. Coester and H. Kümmel, Nucl. Phys. **17**, 477 (1960).

[Co58] F. Coester, Nucl. Phys. **7**, 421 (1958).

[Coh] C. Cohen–Tannoudji, J. Dupont–Roc, G. Grynberg,
Photons and Atoms (Wiley, New York, 1989).

[Cr91] M. D. Crisp, Phys. Rev. A **43**, 2430 (1991).

[Ei86] J. Eidson and R. F. Fox, Phys. Rev. A **34**, 3288 (1986).

[Em81] K. Emrich, Nucl. Phys. A **351**, 379 (1981).

[Em84] K. Emrich and J. G. Zabolitzky, Phys. Rev. B **30**, 2049 (1984).

[Fu61] R. L. Fulton and M. Gouterman, J. Chem. Phys. **35**, 1059 (1961).

[Fu87] M. Funke, U. Kaulfuss and H. Kümmel, Phys. Rev. D **35**, 621 (1987).

[Fe96] I. D. Feranchuk, L. I. Komarov and A. P. Ulyanenkov,
J. Phys. A **29**, 4035 (1996).

[Fe39] R. P. Feynman, Phys. Rev. **56**, 340 (1939).

[Ge90] J. Gea–Banacloche, Phys. Rev. Lett. **65**, 3385 (1990).

[Gr84a] R. Graham and M. Höhnerbach, Phys. Lett. **101A**, 61 (1984).

[Gr84b] R. Graham and M. Höhnerbach, Z. Phys. B **57**, 233 (1984).

[Hak] H. Haken, *Quantum Field Theory of Solids* (North–Holland, Amsterdam, 1976).

[He35] H. Hellmann, Acta Physicochimica USSR **I(6)**, 913 (1935).

[Hu57] N. M. Hugenholtz, Physica **23**, 481 (1957).

[Hu98] P. Huai and H. Zheng, Phys. Lett. A **240**, 341 (1998).

[Hua] K. Huang, *Quantum Field Theory*, (Wiley, New York, 1998).

[Ja37] H. A. Jahn and E. Teller, Proc. R. Soc. Ser. A **161**, 220 (1937).

[Ja63] E. T. Jaynes and F. W. Cummings, Proc. IEEE **51**, 89 (1963).

[Ju77] B. R. Judd, J. Chem. Phys. **67**, 1174 (1977).

[Ju79] B. R. Judd, J. Phys. C **12**, 1685 (1979).

[Kol] D. S. Koltun and J. M. Eisenberg, *Quantum mechanics of many degrees of freedom*, (Wiley, New York, 1988).

[Ko96] V. A. Kostelecký and B. Tudose, Phys. Rev. A **53**, 1978 (1996).

[Ku85] M. Kuś, Phys. Rev. Lett. **54**, 1343 (1985).

[Le87] A. J. Leggett, S. Chakravarty, A. T. Dorsey, M. P. A. Fisher, A. Garg and W. Zwerger, Rev. Mod. Phys. **50**, 1 (1987).

[Le93] C. H. Llewellyn–Smith and N. J. Watson, Phys. Lett. B **302**, 463 (1993).

[Le98] C. R. Leonard, *The Coupled Cluster Method in Hamiltonian Lattice Gauge Theory*, Ph.D. thesis, University of Melbourne (1998).

[Li65] H. J. Lipkin, N. Meshkov and A. J. Glick, Nucl. Phys. **62**, 188, 199, 211 (1965).

[Lo91] C. F. Lo, Phys. Rev. A **43**, 5127 (1991).

[Lo95] C. F. Lo and W. H. Wong, Phys. Rev. B **52**, 3333 (1995).

[Lo96] C. F. Lo and W. H. Wong, Chem. Phys. Lett. B **256**, 159 (1996).

[Lo98] C. F. Lo, K. L. Liu and K. M. Ng, Europhys. Lett. **42**, 1 (1998).

[Lo58] H. C. Longuet—Higgins, U. Öpik, M. H. L. Pryce and R. A. Sack, Proc. Roy. Soc. (London) **A244**, 1 (1958).

[Mah] G. D. Mahan, *Many–Particle Physics*, (Plenum Press, London, 1990).

[Man] F. Mandl and G. Shaw, *Quantum Field Theory*, (Wiley, Chichester, 1984).

[Mar] D. Marcuse, *Principles of Quantum Electronics* (Academic Press, New York, 1980).

[Mat] *Mathematica* is a licensed trademark of *Wolfram Research, Inc.*

[Mer] E. Merzbacher, *Quantum Mechanics* (Wiley, New York, 1970).

[Mi83] P. W. Milonni, J. R. Ackerhalt, and H. W. Galbraith, Phys. Rev. Lett. **50**, 966 (1983).

[Mi91] P. W. Milonni and S. Singh, Adv. At. Mol. Opt. Phys. **28**, 75 (1991).

[Mo87] H. J. Monkhorst, Phys. Rev. A **36**, 1544 (1987).

[Na88] N. Nayak, R. K. Bullough, B. V. Thompson and G. S. Agarwal, Journ. of Quant. Electron. **24**, 1331 (1988).

[No87] J. Noga and R. J. Bartlett, J. Chem. Phys. **86**, 7041 (1987).

[No88] J. Noga and R. J. Bartlett, J. Chem. Phys. **89**, 3401 (E) (1988).

[Pei] R. Peierls, *Surprises in Theoretical Physics* (Princeton University Press, Princeton, 1979).

[Ph89] S. J. D. Phoenix, J. Mod. Opt. **36**, 1163 (1989).

[Pu82] G. D. Purvis and R. J. Bartlett, J. Chem. Phys. **76**, 1910 (1982).

[Qi98] G. Qin, K.–L. Wang, T.–Z. Li, R.–S. Han and M. Feng, Phys. Lett. A **239**, 272 (1998).

[Ra37] I. I. Rabi, Phys. Rev. **51**, 652 (1937).

[Ra54] I. I. Rabi, N. F. Ramsey and J. Schwinger, Rev. Mod. Phys. **26**, 167 (1954).

[Re81a] H. G. Reik and H. Nusser, Solid State Commun. **40**, 943 (1981).

[Re81b] H. G. Reik, L. A. Amarante Ribeiro and H. Nusser, Solid State Commun. **39**, 95 (1981).

[Re81c] H. G. Reik, L. A. Amarante Ribeiro and M. Blunck, Solid State Commun. **38**, 503 (1981).

[Re82] H. G. Reik, H. Nusser and L. A. Amarante Ribeiro, J. Phys. A **15**, 3491 (1982).

[Re86] H. G. Reik and M. Doucha, Phys. Rev. Lett. **57**, 787 (1986).

[Re87] H. G. Reik, P. Lais, M. E. Stützle, and M. Doucha, J. Phys. A **20**, 6327 (1987).

[Ro89] N. I. Robinson, R. F. Bishop and J. Arponen, Phys. Rev. A **40**, 4256 (1989).

[Ro90] M. Roger and J. H. Hetherington, Phys. Rev. B **41**, 200 (1990).

[Sc92] F. G. Scholtz, H. B. Geyer and F. J. W. Hahne, Ann. Phys. **213**, 74 (1992).

[Sh93] B. W. Shore and P. L. Knight, J. Mod. Opt. **40**, 1195 (1993).

[Sz96] M. Szopa, G. Mys and A. Ceulemans, J. Math. Phys. **37**, 5402 (1996).

[Sz97] M. Szopa and A. Ceulemans, J. Phys. A **30**, 1295 (1997).

[Th68] W. Thorson and W. Moffit, Phys. Rev. **168**, 168 (1968).

[Tho] D. J. Thouless, *The quantum mechanics of many–body systems*, (Academic Press, New York, 1961).

[Wo94] W. H. Wong and C. F. Lo, Phys. Rev. B **50**, 17615 (1994).

[Wo96a] W. H. Wong and C. F. Lo, Phys. Lett. A **223**, 123 (1996).

[Wo96b] W. H. Wong and C. F. Lo, Phys. Rev. B **54**, 12859 (1996).

[Za88] K. Zaheer and M. S. Zubairy, Phys. Rev. A **37**, 1628 (1988).

[Za69] J. Zak, Phys. Rev. **187**, 1803 (1969).

[Zh90] H. Zheng and A. M. Jayannavar,
Solid State Commun. **74**, 1137 (1990).